

https://dspace.org/

# Evaluation of the effect of acid-base properties of Ruthenium on Mn-Al2O3 catalyst for FTS

**Mavundla, Xongotelo Eudorah**

**2020**

https://hdl.handle.net/10539/30206

Downloaded from a DSpace repository. https://dspace.org/

# Evaluation of the effect of acid-base properties of Ruthenium on Mn-$Al_2O_3$ catalyst for FTS




By

Xongotelo Eudorah Mavundla (1787619)

Supervisor: Dr John Moma (WITS)

Co-Supervisors: Dr Pheladi Mohlala (Sasol) & Jacobus Visagie (Sasol)

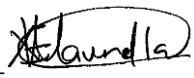
A dissertation submitted to the Faculty of Science at The University of the Witwatersrand, Johannesburg

In fulfilment of the requirements for the degree of

Masters of Science

# Declaration

I declare that this dissertation is my own, unaided work. It is being submitted for the Master of Science Degree at the University of the Witwatersrand, Johannesburg. It has not been submitted before for any degree or examination at any other University.

____ _____

(Xongotelo E Mavundla)

____10th_____Day of__February__2020___at__University of Witwatersrand_____

# Acknowledgements

*"Being confident of this very thing, that He who has begun a good work in you will complete it until the day of Jesus Christ" Philippians 1:6*

To God my father and my saviour Jesus Christ. I stand in awe of all the things you have brought me through. Indeed I am a testament that you are alive and that all things work together for good. This document could have not been possible if it wasn't for you.

To my supervisors Dr John Moma, Dr Pheladi Mohlala, Jacobus Visagie (The legend). Much thanks for the support and the guidance you gave me through this journey. You made the journey bearable and I believe I am a better chemist after this exercise. Thank you for your patience. I take this to be the greatest gift to have worked with seasoned scientists like you.

To my manager Dr Alta Ferreira, I have no words. Thank you for always believing in me and always seeing the best in me even when I could not see. Your support through my lowest and darkest period of my MSc is much appreciated.

My mentor and technical coach Dr Denzil Moodley. I remember very well when I asked you to mentor me. You have been the pillar in this journey and you came through where and when it mattered the most. I appreciate your part in my career growth and development.

Rhirhandzu book club ladies, thank you for all the love and support. For giving me the necessary laughter to get me through this journey one day at a time. Dr Pheladi Mohlala, Dr Zandile Chonco, Dr Boitumelo Makume, Nangamso Sosibo (my Attorney), Linky Baloyi and lastly Sis Letty Maluleke. You are an inspiration in my life. Indeed I am the company I keep.

To Sasol for funding and giving me the time to complete this work. All the Sasol crew that helped with the analysis and training on analytical techniques. For your tireless efforts and patience I am grateful. Dr Thabiso Phadi, Harry Moloto, Marietjie du Toit, Dr Esna du Plessis, Gerda de Jager, Moses Leakwe, Bafana Mazibuko, Dr Stanley Manzini, Dr Matthew Coombes, Thabo Mogopodi, Godfrey Kupi, Dr Wonga Hexana and my peer reviewer Dr Roxy Gostynski.

To my husband Mr Ditaba Mavundla. Doing this life with you is a bliss. Thank you for your continued support and encouragement. My sister in law Dikeledi, Ausi waka ke a leboha, for taking care of my daughter when I couldn't, for allowing me to pursue this dream while you became a mother to Oarona. My mom aka "Mother", it is finally done. You can finally come

to WITS for my graduation. Thank you for being a loving and supportive mother to me. Thank you for all the prayers, for I know they carried me even in the darkest of times. Thank you for single handily raising me and my brother. This one is for you. I live to make you proud. I don't see how I could have done all this without your support and encouragement.

To My late father Tirhani Maswanganyi, I wish you were around to see me winning in this game of life.

# Publications and Poster presentations arising from this work

**Presentations**

1. CATSA Conference 2018, Limpopo, South Africa

Characterisation: Evaluation of the effect of acid-base properties of Ruthenium on Mn-$Al_2O_3$ catalyst for FTS

2. CATSA Conference 2019, Cape Town, South Africa

FT Testing: Evaluation of the effect of acid-base properties of Ruthenium on Mn-$Al_2O_3$ catalyst for FTS

# Abstract

The effect of acid-base properties as a result of calcination temperature of alumina was investigated on manganese modified supports for ruthenium Fischer-Tropsch catalysts. The process of high temperature calcination is one of the methods used to make material with specific low surface areas and a distinct α-alumina phase. Support modification and catalyst preparation were performed by applying the incipient wetness impregnation method and resulted in supports containing 4, 6 and 10 wt% Mn. Selected support samples have in addition been impregnated with 2 wt% Ru. The support modification and catalyst preparation was conducted on calcined Puralox (PuCal) and on uncalcined Puralox (Pu) alumina support. The adjusted Pu and PuCal supports as well as the corresponding catalysts were characterized by $N_2$ adsorption, $H_2$ chemisorption, x-ray diffraction, IPA & $CO_2$ TPD and evaluated in a slurry reactor at 25 bar, 230 ± 0,5 °C and $H_2/CO$ = 2,1 for Fischer Tropsch synthesis.

It was established that a support calcination temperature of around 1100 °C led to the support material consisting of a mixture of both γ-alumina and ɵ-alumina (PuCal). For the Pu support, only γ-alumina was detected. Elevated calcination temperatures resulted in half the surface areas of the starting material, smaller pore volumes and increased pore diameter. The uncalcined Pu support's surface area and pore volume was around 162 $m^2/g$ and 0.5 $cm^3/g$ and the support decreased to 97 $m^2/g$ and 0.38 $cm^3/g$ respectively indicating a collapse of pore structure and a decreased surface area due to harsh temperature treatment of the support material. A further decrease in surface area was observed upon addition of manganese and the Ru metal to form Mn-modified Ru catalysts on both PuCal and Pu supports.

The effect of total acid and base properties of the materials as a function of calcination, Mn addition and subsequently Ru addition was determined using temperature programed desorption (TPD) techniques. Between the Pu and the PuCal systems, the effect Mn per support surface area due to calcination was also determined. Results indicated that Mn made the support more basic, as an effect of increased basicity resulted in a decrease in Brønsted acidity. However the influence of Mn per surface area between the Pu and the PuCal system indicated similar yields of both the basic and acidic sites. The influence of Ru addition on the acid-base properties, shifted the Brønsted acidity peaks to lower temperatures, meaning that Ru occupies the stronger acid sites and on the basicity sites an increase in peak intensity was observed. From Fischer Tropsch synthesis, on Ru based catalysts on Mn modified supports Mn seemed to

promoted selectivity towards highly oxygenated products on both systems. With regards to catalysts activity, Mn played a role as a poison on the Pu catalyst system and an activity promoter on the PuCal catalysts system.

PuCal/6wt%Mn/Ru was the most active catalyst, with the lowest methane selectivity of all the catalysts prepared. Thus this implies that there should also be an optimum Mn loading, and other surface properties to in order to obtain the desire activity and selectivity.

# Contents

**Declaration**

**Acknowledgements……i**

**Presentations and Publications ……iii**

**Abstract ……...iv**

**List of Figures ……ix**

**List of Appendix Figures……...xii**

**List of Tables ……xiii**

**List of abbreviations ……xv**

**1. Introduction**.....*1*

***1.1 Background***.....**1**

***1.2 Objectives and aims***…….....***3***

***1.3 Outline of the study***…….....***5***

***Reference***.....**7**

**2. Literature review**…….....**9**

***2.1 History and background***.....***9***

***2.2 Three main steps in the FT process***.....***12***

***2.3 The Fischer-Tropsch Synthesis (FTS)***.....***13***

***2.4 The Fischer Tropsch reactor***…….....***15***

2.4.1 Reactors.....15

2.4.2 The Effect of Fischer-Tropsch synthesis conditions……...……....18

***2.5 Fischer Tropsch reactions***…….....……...***18***

***2.6 FT process product distribution***……..***19***

**2.7 The Fischer Tropsch catalysts**…….....**20**

**2.8 Supported FT catalysts**…….....**21**

2.8.1 The effect of thermal treatment of Alumina .....22

2.8.2 Effect of support modification.....24

**2.9 Synthesis of Fischer Tropsch ……**.....**24**

2.9.1 Impregnation Method.....25

**2.10 Acid base properties of Fischer-Tropsch catalyst**.....**26**

***Reference*** .....**29**

*3. Experimental ……*.....*32*

**3.1 Support preparations**.....**32**

**3.2 Reagents**…….....**32**

**3.3 Support modification…….....32**
**3.4 Support modification…….....33**
**3.5 Catalyst and support characterization…….....34**
3.5.1 Thermogravimetric analysis (TGA) .....35
3.5.2 $N_2$ Physisorption (BET)……..……..35
3.5.3 X-ray fluorescence (XRF).....36
3.5.4 X-ray diffraction spectroscopy (XRD).....36
3.5.5 Temperature programmed desorption using $CO_2$ and IPA as probe molecules.....38
3.5.6 Temperature-Programmed Reduction (TPR) .....39
3.5.7 $H_2$ chemisorption and $O_2$ titration analysis .....40
3.5.8 Scanning electron microscopy - Energy dispersive x-ray analysis (SEM- EDX)…….…...42
3.5.9. Transmission electron microscopy (TEM).....43
3.5.10 HAADF STEM imaging…….....44
**3.6 Catalyst evaluation.....44**
3.6.1 Activation of model catalysts.....45
3.6.2 Fischer-Tropsch synthesis and conditions.....45
3.6.3 GC X GC Analysis……...46
***References.*.....47**
*4. Characterization of supports and catalysts.....48*
**4.1 Introduction.....48**
**4.2 Characterization of Pu and PuCal supports.....49**
4.2.1 Preliminary results: TG-DTA-MS.....49
4.2.2 Textural and structural properties of the supports.....50
4.2.3 IPA-Temperature programmed desorption.....51
4.2.4 $CO_2$-Temperature programmed desorption…….....53
**4.3. Characterization of Mn-modified Pu and PuCal supports.....54**
4.3.1 Scanning electron microscopy-energy dispersive X-ray (SEM-EDX).....55
4.3.2 IPA-Temperature programmed desorption.....56
4.3.3 $CO_2$-Temperature programmed desorption…….....58
4.3.4 Summary of the characterization results of the Pu and PuCal Mn-modified supports.....61
**4.4 Characterization of the prepared Ru catalysts.....61**
4.4.1 Metal loading by XRF spectroscopy ……....62
4.4.2 Textural and structural properties of the catalysts ……...62
4.4.3 SEM-EDX for catalysts systems ……...64
4.4.4 IPA-Temperature programmed desorption ……..64
4.4.5 CO2-Temperature programmed desorption ……67
4.4.6 TEM-Elemental mapping ……69

4.4.7 Temperature Programed Reduction of catalysts (TPR) & In-Situ XRD ……70
4.4.8 H2-chemisorption ……74
4.4.9 Summary of the characterization results of the calcined and uncalcined Ru-based FTS catalyst……...74
***Reference*……...76**
*5. Fischer-Tropsch synthesis performance of the model catalysts……77*
5.1 FTS behaviour of model catalysts ……...78
5.2 Selectivities of model catalysts ……...82
5.3 GC-GC results ……86
5.4 Concluding remarks ……87
***Reference*** ……..88
6 Conclusions and Summary .....*90*
7 Appendix……*92*

# List of Figures

## Chapter 1

**Figure 1. 1** Acid base properties of aluminium hydroxide as a function of temperature [12].... 3
**Figure 1. 2** Illustration of proposed FTS process for Mn-modified Ru catalysts ..... 4
**Figure 1. 3** Summary of the objectives..... 5

## Chapter 2

**Figure 2.1** Variation in the price of crude oil from 1970 to 2000[6]..... 10
**Figure 2.2** Three main steps of the FTS process[9,10] ..... 13
**Figure 2.3** FT stepwise growth process[6]..... 14
**Figure 2. 4** High- and low-temperature Fischer Tropsch process [12] ..... 15
**Figure 2. 5** Overview of Fischer–Tropsch technology with reactors (figure microchannel reactor: courtesy of the Oxford Catalysts Group)..... 16
**Figure 2. 6** An Anderson-Schulz-Flory product distribution[15] ..... 20
**Figure 2. 7** Thermal transformation of alumina..... 23
**Figure 2. 8** Concept of catalyst design[26]..... 25
**Figure 2.9** A schematic representation of the catalyst impregnation process[19] ..... 26
**Figure 2.10** Illustration of a typical results obtained from $NH_3$-TPD analysis[30] ..... 28

## Chapter 3

**Figure 3.1** Summary of experimental plan ..... 34
**Figure 3. 2** DTA curve of the membrane ground powder; specific surface area (SSA) of the membrane heated powders, temperature ranges and transition temperatures of the aluminas.[2]..... 35
**Figure 3.3** Schematic illustration of powder XRD, showing the nature of the crystallite size measurement. All Bragg orientations are measured by scanning the X-ray source and detector to measure all the grains in all the particles[3] ..... 37
**Figure 3. 4** AutoChem 2920 (Micromeritics, USA coupled to a Cirrus Mass Spectrometer (MKS Instruments) ..... 40
**Figure 3.5** a) Process for SEM resin preparation and (b) Sputter coater instrument ..... 42
**Figure 3.6** Schematic illustration of the STEM mechanism. The electron beam is scanned across the sample so that a projection of the particle is traced in the image plane[3] ..... 43

## Chapter 4

**Figure 4. 1** A summary of all the materials being characterised and their names ..... 48
**Figure 4. 2** TG, DTG and DTA profiles of the Puralox support sample..... 49
**Figure 4. 3** Dehydration and hydration representation of alumina [3] ..... 51

**Figure 4. 4** The schematic showing amine reacting with acid sites to decompose..... 52
**Figure 4. 5** MS data of evolved propylene on Pu and PuCal supports support ..... 53
**Figure 4. 6** MS data of evolved $CO_2$ on Pu and PuCal supports support..... 54
**Figure 4. 7** SEM-Backscatter of Mn modified alumina support (6wt%Mn/Pu)..... 55
**Figure 4. 8** EDX- spectra of Mn alumina support..... 56
**Figure 4. 9** MS data of evolved propylene on Mn-modified Pu supports ..... 57
**Figure 4. 10** MS data of evolved propylene on Mn-modified PuCal supports..... 58
**Figure 4. 11** MS data of evolved $CO_2$ on Pu-Mn modified support ..... 59
**Figure 4. 12** MS data of evolved $CO_2$ on PuCal-Mn modified support ..... 60
**Figure 4. 13** SEM-back scatter of Pu/6wt%Mn/Ru ..... 64
**Figure 4. 14** MS data of evolved propylene on Pu support system ..... 65
**Figure 4. 15** MS data of evolved propylene on PuCal and Pu support ..... 66
**Figure 4. 16** MS data of evolved $CO_2$ on Pu catalysts system ..... 67
**Figure 4. 17** MS data of evolved $CO_2$ on PuCal catalysts system ..... 68
**Figure 4. 18** (a) PuCal/6wt%Mn/Ru; (b) Pu/10wt%Mn/Ru before reduction..... 69
**Figure 4. 19** (a) PuCal/6%Mn/Ru before reduction; (b) PuCal/6%Mn/Ru after reduction.... 70
**Figure 4. 20** TPR profiles of the Pu system..... 70
**Figure 4. 21** TPR profiles of the PuCal system ..... 71
**Figure 4. 22** In-situ XRD results of Pu/Ru catalysts system ..... 73
**Figure 4. 23** In-situ XRD results of PuCal/6wt% Mn/Ru catalysts system..... 73

# Chapter 5

**Figure 5. 1** FTS Activity (mole CO/g-cat/s) with TOL of Pu system..... 79
**Figure 5. 2** FTS Activity (mole CO/g-cat/s) with TOL of PuCal system ..... 80
**Figure 5. 3** A summary of FTS Activity (mole CO/g-cat/s) with TOL for all the catalysts .. 81
**Figure 5. 4** Methane selectivity with TOL for all the catalysts ..... 83
**Figure 5. 5** Summary of FTS reaction performances for all the catalysts at approx. 200 h TOL..... 84
**Figure 5. 6** GCXGC spectra of Pu/Ru catalyst ..... 86
**Figure 5. 7** GCXGC spectra of PuCal/6wt%Mn/Ru catalyst ..... 87

# APPEDIX

**Figure A.1** Schematic diagram of reactor rig layout used FTS testing ..... 92

**Figure B.1** SEM-Backscatter 6wt% Mn/Pu support ..... 92
**Figure B.2** SEM-Backscatter 10wt% Mn/Pu support ..... 93
**Figure B.3** SEM-Backscatter 4wt% Mn/PuCal support ..... 93

**Figure C.1** SEM-Backscatter Ru/Pu catalyst ..... 93
**Figure C.2** SEM-EDX Ru/6wt%/Pu catalyst ..... 94
**Figure C.3** SEM-EDX Ru/10wt%/Pu catalyst ..... 94
**Figure C.4** SEM-Backscatter Ru/PuCal catalyst ..... 94
**Figure C.5** SEM-Backscatter Ru/4wt%/PuCal catalyst ..... 95
**Figure C.6** SEM-backscatter Ru/6wt%/PuCal catalyst ..... 95

# List of Tables

## Chapter 2

**Table 2.1** An overview of the current commercial operations using FTS technology[2] ..... 11
**Table 2.2** Differences of the Fischer Tropsch reactors ..... 17
**Table 2.3** Effect of process conditions on Fischer-Tropsch synthesis product selectivity (adapted from Mabaso et al.[14]) ..... 18
**Table 2.4** Findings on the performance and characterisation of $Ru/Al_2O_3$ and $Ru/SiO_2$[20] .. 22
**Table 2.5** Summary on the effect of manganese salts on catalytic activity and stability[25] ... 24

## Chapter 3

**Table 3.1** Drying profile for the Mn impregnated Puralox material ..... 33
**Table 3. 2** Drying profile for ruthenium impregnated catalysts ..... 33
**Table 3. 3** Summarized $H_2$-Chemisorption analysis conditions ..... 41
**Table 3.4** HAADF STEM mode and EDS mapping beam settings ..... 44
**Table 3.5** Activation of model catalysts conditions ..... 45
**Table 3.6** Fischer-Tropsch synthesis conditions for model catalysts ..... 46

## Chapter 4

**Table 4. 1** XRD and BET results of Pu and PuCal supports ..... 51
**Table 4. 2** Brønsted acidity of Pu vs PuCal supports ..... 53
**Table 4. 3** Basicity results of Pu vs the PuCal supports ..... 54
**Table 4. 4** A list of Mn modified supports with their corresponding surface areas ..... 55
**Table 4. 5** Brønsted acidity results for Mn-modified Pu supports ..... 57
**Table 4. 6** Brønsted acidity results for Mn-modified PuCal supports ..... 58
**Table 4. 7** Summary of Basicity as a function of Mn addition on both the Pu and PuCal systems ..... 60
**Table 4. 8 A list of synthesized Ru-based** ..... 62
**Table 4. 9** XRF analysis for the %Ru & Mn loading on catalyst materials ..... 62
**Table 4. 10** The composition and textural properties of the Pu and the PuCal catalysts systems ..... 63
**Table 4. 11** Summary of BAS of Ru on Mn modified catalysts for Pu system ..... 65
**Table 4. 12** Summary of BAS of Ru on Mn modified catalysts for PuCal system ..... 66
**Table 4. 13** Summary of Basicity of Ru on Mn modified catalysts for Pu system ..... 68
**Table 4. 14** Summary of Basicity of Ru on Mn modified catalysts for PuCal system ..... 68
**Table 4. 15** $H_2$-chemisorption results of the prepared catalysts systems ..... 74

## Chapter 5

**Table 5. 1** A summary of acid-base properties of prepared catalysts ..... 82

**Table 5. 2** A summary of acid-base properties of Mn-modified supports..... 83
**Table 5. 3** Summary of FTS reaction performances for all the catalysts at approx. 200 h TOL
..... 85

# List of abbreviations

FT: Fisher Tropsch

FTS: Fisher Tropsch Synthesis

GTL: Gas to Liquid

CTL: Coal to Liquid

LPG: Liquefied petroleum gas

LTFT: Low Temperature Fisher Tropsch

HTFT: High Temperature Fisher Tropsch

CO: Carbon monoxide

$H_2$: Hydrogen

Ru: Ruthenium

Mn: Manganese

Co: Cobalt

Fe: Iron

Ni: Nickel

WGS: Water Gas Shift

BET: Brunnauer-Emmett-Teller

TPR: Temperature Programmed Reduction

TGA: Thermogravimetric Analysis

TG-DTG: Thermogravimetric- Derivative Thermogravimetry

EDX: Energy Dispersion X-ray analysis

IPA: Iso-propyl-amine

TPD: Temperature Programmed Desorption

NMR: Nuclear Magnetic Resonance

TPO: Temperature Programmed Oxidation

XPS: X-ray Photoelectron Spectroscopy

FTIR: Fourier Transform Infrared Spectroscopy

BAS: Brønsted acid sites

BASF: Badishe Anilin und Soda Fabrik

OPEC: Organization of petroleum exporting countries

CFB: Circulating Fixed Bed reactor

GHSV: Gas Hourly Space Velocity

ASF: Anderson-Schulz-Flory

# Chapter 1

## Introduction

### *1.1 Background*

Catalysis plays an important role in society by providing fuels, commodities and fine chemicals for everyday use. It is a phenomenon by which chemical reactions are accelerated by a small quantity of foreign substances called catalysts which takes part in the chemical reaction however are not used up by this chemical reaction. Catalysts are known to lower the activation energy for both the forward and the reverse reactions. A catalyst is a surface active material i.e. catalysis occurs on the material surface and therefore the activity of the catalyst depends greatly on the nature of the surface.

In 1902 Sabatier and Senderens carried out the first catalytic experiments on the hydrogenation of carbon monoxide. The experiments involved the synthesis of methane over a cobalt or nickel catalyst from a mixture of hydrogen and carbon monoxide[1,2,3]. Around the 1920‘s a proposal of a ‘synthol process’ was introduced by two scientists named Frans Fischer and Hans Tropsch, in Germany. The process involved the production of oxygen containing products under high pressure (>100 bar) and at lower pressure (~ 7 bars) where the products consisted of mainly olefinic and paraffinic hydrocarbons[4]. The latter process became known as the Fischer-Tropsch synthesis (FTS).

The Fischer-Tropsch synthesis carried out a substantial part of German fuel production at the beginning of the Second World War. Germany generated mid-distillates at low pressure from direct hydrogenation of carbon-derived CO over promoted cobalt catalysts in fixed-bed reactors. Group 8-10 transition metals such as ruthenium (Ru), nickel (Ni), cobalt (Co) and iron (Fe) have shown significant activity for the Fischer-Tropsch synthesis, cobalt and iron being the mostly studied metals due to their commercial importance[4]. Ni on the other hand is known to catalyse the methanation reaction. The disadvantage of using ruthenium is its limited availability which results in relatively high price[5]. These disadvantages preclude its use at an industrial scale.

Ru was first investigated by Fischer in 1925. Ru-based catalysts show great potential for FTS by providing the highest catalytic activity, selectivity and stability[6]. Ru catalyst improves

middle distillate yields and increases wax formation, the latter of which can be cracked into middle distillates in the presence of effective additives and supports on the catalyst. It can also operate as a pure metal without any promoter added to stabilize its activity and can also be used at low reaction temperatures of between 180 °C - 190 °C[7].

Supported catalysts are desired in heterogeneous catalysis for high dispersion of the active metal [6]. A good metal-support interface can provide active sites which can lead to improved activity and selectivity. Alumina is commonly used as a FT catalyst support due to its high surface area, crystalline structure, high porosity, mechanical strength and acid/base properties[8]. Interaction of the support with the metal, changes its electronic properties and, concomitantly, its activity or selectivity [9]. High surface area supports are of interest and are of importance due to the following reasons:

(i) Metal loading or dispersion becomes a parameter which can be adjusted in order to study structure sensitivity of the reaction.
(ii) Metal sintering can be reduced.
(iii) Some of the catalytic metal species are sufficiently expensive that high dispersions and low loadings are an economic necessity[9].
(iv) Support may interact with the active component deposited therein and form a new complex that may have a better catalytic and selective function than that of the support or active component.

The catalytic applications of alumina are based on its surface acid-base properties and these applications have been extensively reviewed and reported. Previous studies have shown that the surface acid-base properties of supports have a significant impact on the FTS reaction with regards to catalytic activity and selectivity[10]. The surface acid-base properties of a support could be influenced by calcination temperature[11] of the support and modification with other metals. Lewis and Brønsted acidity in aluminium hydroxide may be generated by subjecting it to heat treatment for example in Figure 1.1[12]. On the hydroxylated surface of aluminium oxides, the surface hydroxyl groups may ionize as Brønsted acid or base sites in appropriate circumstances[12].

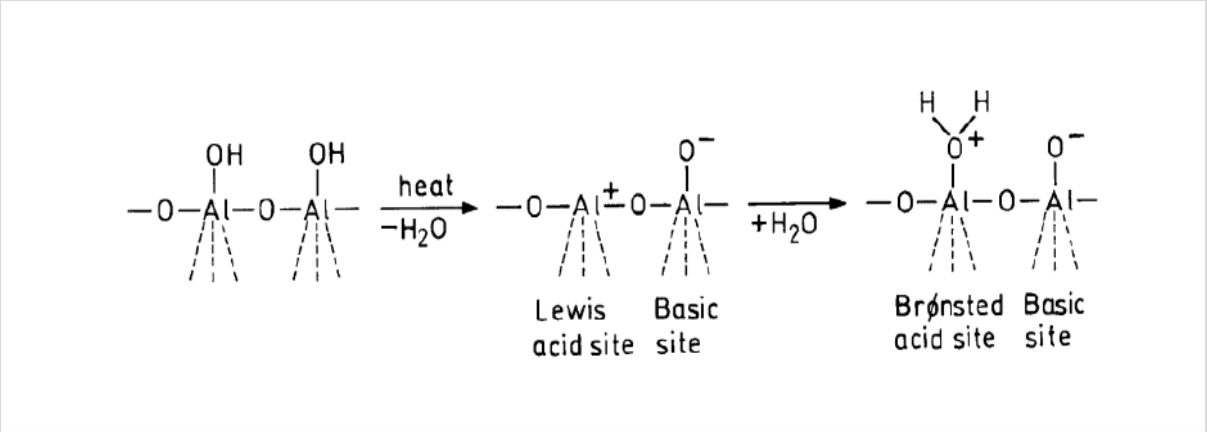



**Figure 1. 1** Acid-base properties of aluminium hydroxide as a function of temperature [12]

Manganese can be used as a modifier or a promoter depending on when it is impregnated on the support. Its addition can aid in catalyst stability, resistance to deactivation and improves CO adsorption on Ru-based catalysts[13].

## 1.2 Aims and Objectives

Catalyst activity and selectivity are the key concepts for performance in FT catalysis and a lot of research has gone in establishing the right catalyst properties with a combination of right operation condition. There is a need to optimize the amount of basic sites in Fischer Tropsch catalysts for optimum activity and selectivity. In the Fischer-Tropsch synthesis, a higher surface basicity correlates with a lower methane selectivity,[14] while excess basicity favours the methane reaction. Optimized basicity via Mn addition can improve the CO adsorption on the catalyst surface leading to improved activity and selectivity. Figure 1.2 below is a high-level schematic of the FTS process for Mn-modified Ru catalyst which will be used in this study.

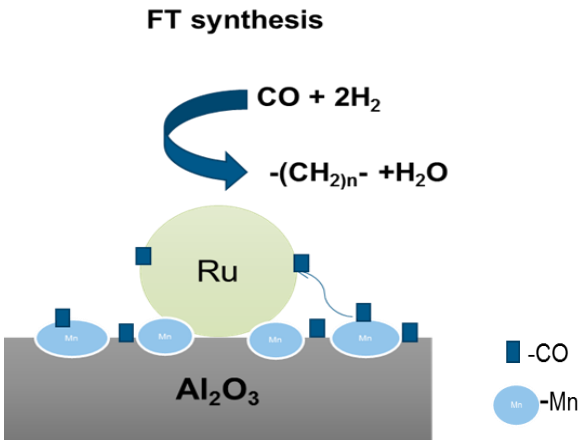



**Figure 1. 2** Illustration of proposed FTS process for Mn-modified Ru catalysts

This study will cover the investigation of the acid-base properties of ruthenium based FT catalysts as influenced by (i) calcination temperatures of the alumina support, and (ii) support modification with manganese addition. The aim is that optimisation of the above-mentioned parameters can improve the CO adsorption on the catalyst surface, leading to improved activity and selectivity.

The objectives of this work, which are graphically presented in Figure 1.3, are to determine the relationship between the acidic-basic properties of ruthenium based catalysts and their catalytic performance in FTS. The main technique used to reveal the acidic-basic properties of solid materials in this work is temperature programed desorption (TPD). Compared to other analytical techniques, TPD analysis provides information closely related to catalytic properties and was commonly used in the adsorption – desorption kinetics research for the supported catalyst.[15].

This will be achieved by:

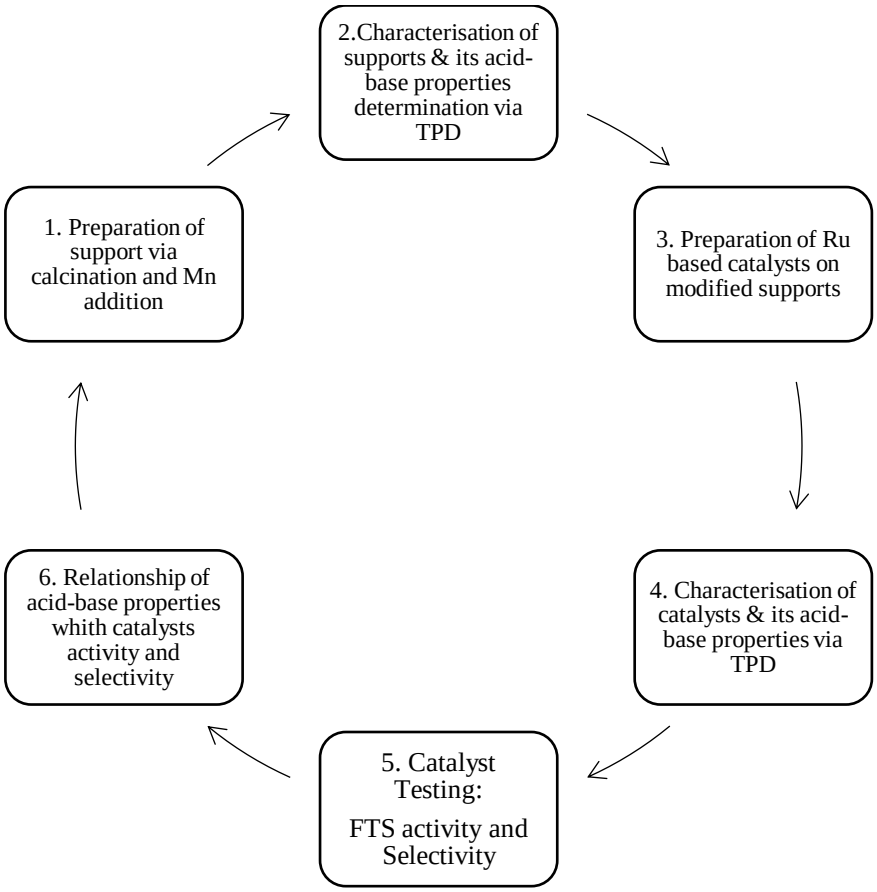



**Figure 1. 3** Summary of the objectives

## 1.3 Outline of the dissertation

Heterogeneous catalysis involves specific chemical interactions between the surface of a solid and the reacting gas (or liquid phase) molecules. The catalytic cycle is generally composed of adsorption steps, surface reaction processes (such as dissociation and coupling), and desorption steps. The energetics of these surface chemical events plays an important role in determining the catalytic properties of the surface. The techniques that are used for the study of these interactions are Fourier transform infrared spectroscopy (FTIR), X-ray photoelectron spectroscopy (XPS), temperature-programmed oxidation (TPO), temperature-programmed reduction (TPR), temperature-programmed desorption (TPD) and nuclear magnetic resonance (NMR). TPD is used to measure the number and strengths of sites found on solid base catalysts.

Having this in mind the work done in this thesis can be outlined as:

Chapter 1 gives a detailed background of the study, as well as to point out the research questions that will be addressed, giving the aims as well as the objectives of the study. This will also cover the outline of the rest of the dissertation.

Chapter 2 covers a detailed literature review, related to the use of supports in the FTS process and the effect of modifications on the support caused by thermal treatment and doping of other metals. An evaluation of prior work on Ru based FTS catalyst is also given.

Chapter 3 presents all the experimental techniques and procedures that were used to carry out the study. The focus of this dissertation is on investigating the surface acid-base properties of supports and catalyst materials by temperature programmed desorption techniques and correlation of these properties with activity and selectivity patterns in the FTS reaction.

Characterisation of the support material and the prepared Ru catalyst is covered in Chapter 4. The effect of calcination on the acid-base properties and textural properties of the support was investigated and determined. After modification with Mn, the supports were further monitored and the change in the acid-base properties as an influence of Mn was established. Ru impregnation was done for the final catalysts synthesis, and the acid-base properties of the catalysts were determined as a function of Ru addition.

Chapter 5 looks into the FT activity and selectivity of Ru based catalysts as a function of modified acid-base properties of the catalyst as a function of calcination and Mn modifications.

The general conclusions on the effect of acid-base properties as a function of calcination and manganese on the activity and the selectivity of ruthenium based FT catalysts are presented in Chapter 6. This chapter sums up all the effects caused by the above mentioned modifications and conclusions reached from each chapter are contextualised.

# *References*


(1) Leckel, D. Diesel Production from Fischer−Tropsch: The Past, the Present, and New Concepts. *Energy & Fuels* **2009**, *23* (6), 2342–2358.

(2) King, B. F.; Shutt, E.; Thornson, A. I. Ruthenium Catalyst Systems for the Production of Hydrocarbons from Coal. **1985**, No. 4, 146–154.

(3) VanderWiel, D. P.; Pruski, M.; King, T. S. A Kinetic Study on the Adsorption and Reaction of Hydrogen over Silica-Supported Ruthenium and Silver-Ruthenium Catalysts during the Hydrogenation of Carbon Monoxide. *J. Catal.* **1999**, *188* (1), 186–202.

(4) Van de Loosdrecht, J.; Botes, F. G.; Ciobica, I. M.; Ferreira, A.; Gibson, P.; Moodley, D. J.; Saib, A. M.; Visagie, J. L.; Weststrate, C. J.; Niemantsverdriet, J. W. *Fischer-Tropsch Synthesis: Catalysts and Chemistry*; Elsevier Ltd., 2013; Vol. 7.

(5) Khodakov, A. Y.; Chu, W.; Fongarland, P. Advances in the Development of Novel Cobalt Fischer-Tropsch Catalysts for Synthesis of Long-Chain Hydrocarbons and Clean Fuels. *Chem. Rev.* **2007**, *107* (5), 1692–1744.

(6) Smith, K. J.; Everson, R. C. Fischer-Tropsch Reaction Ruthenium Studies with Supported Catalysts. *J. Catal.* **1986**, *99*, 349–357.

(7) Schulz, H. Short History and Present Trends of Fischer–Tropsch Synthesis. *Appl. Catal. A Gen.* **1999**, *186* (1–2), 3–12.

(8) Samain, L.; Jaworski, A.; Edén, M.; Ladd, D. M.; Seo, D.; Garcia-garcia, F. J.; Häussermann, U. Journal of Solid State Chemistry Structural Analysis of Highly Porous γ -Al 2 O 3. *J. Solid State Chem.* **2014**, *217*, 1–8.

(9) King, D. L. A Fischer-Tropsch Study of Supported Ruthenium Catalysts. *J. Catal.* **1978**, *51* (3), 386–397.

(10) Naturwissenschaften, D. Der. Characterization of Acidic and Basic Properties of Heterogeneous Catalysts by Test Reactions. **2004**.

(11) Komeili, S.; Takht Ravanchi, M.; Taeb, A. Influence of Calcination Parameters on the Properties of Alumina as a Catalyst Support. *Sci. Iran.* **2017**, *23* (3), 1128–1135.

(12) Yang, X.; Sun, Z.; Wang, D.; Forsling, W. Surface Acid-Base Properties and Hydration/Dehydration Mechanisms of Aluminum (Hydr)Oxides. *J. Colloid Interface Sci.* **2007**, *308* (2), 395–404.

(13) Nurunnabi, M.; Murata, K.; Okabe, K.; Inaba, M.; Takahara, I. Effect of Mn Addition on Activity and Resistance to Catalyst Deactivation for Fischer-Tropsch Synthesis over Ru/Al2O3 and Ru/SiO2 Catalysts. *Catal. Commun.* **2007**, *8* (10), 1531–1537.

(14) Dry, M. E.; Oosthuizen, G. J. The Correlation between Catalyst Surface Basicity and Hydrocarbon Selectivity in the Fischer-Tropsch Synthesis. *J. Catal.* **1968**, *11* (1), 18–24.

(15) Lin, H.; Chen, Y. The Kinetics of H 2 Adsorption on Supported Ruthenium Catalysts. **2004**, *419* (October 2003), 283–290.

# Chapter 2

## Literature Review

### *2.1 History and background*

The conversion of gas to liquid product was first reported by Losanitsch and Jovitschitsch in 1897 on electric discharge[1]. In 1902, Sabatier and Senderens discovered that methane could be synthesized at atmospheric pressure from syngas, nickel or cobalt catalysts[2]. The production of liquid products was documented by BASF (Badische Anilin UND Soda Fabrik) using a cobalt catalyst in 1913[3]. In the 1920's two researchers Franz Fischer and Hans Tropsch, working at the Kaiser Wilhelm Institute discovered what would take the world of research by storm. Their work involved the reaction of syngas over alkalised iron and many other catalysts to produce a mixture of hydrocarbons and oxygenated compounds (diesel fuels, gasoline, lower olefins etc.)[4]. In 1934, Ruhrchemie A.-G began commercialization of the Fischer-Tropsch (FT) technology by undertaking industrial development of the process[4]. This process is known as the gas-to-liquid (GTL) production engine technology. The reaction entails the conversion of syngas (a mixture of hydrogen and carbon monoxide) into hydrocarbon products. At ambient conditions these hydrocarbon products are mostly in liquid form, but some can be in a gaseous state or even in solid state[5].

The first Fischer-Tropsch industrial plant operation was in Germany in 1936, with over 1 million tons of FTS liquid being produced annually till the 1940's. The Carthage Hydrocol Fischer-Tropsch plant in 1940-1950 was an example of an earlier iron-based high temperature (HTFT) process developed in the United States of America[4,6].

In South Africa, the initial process utilised coal, and saw its first coal-based construction plant in Sasolburg in 1952. This was due to the large coal reserves in the country that was very cheap to mine. The oil embargo by OPEC (Organization of the Petroleum Exporting Countries) in the early 1970's led to a huge increase in the price of oil and, hence, the economics of the FTS in South Africa improved dramatically which led to the construction of two new and much larger Sasol coal-to-liquid (CTL) plants which came on stream in 1980 and 1982 in Secunda (from Latin meaning second or following), South Africa[2]. The economic viability of the FT

process obviously depends on the price of crude oil and as this has varied considerably over the past 30 years as represented in Figure 2.1, the decision to construct an FT complex became an advantage for Sasol because by the time the two plants come on-line for operation in 1980 and 1982, the price of crude exceeded US$ 30 per barrel.

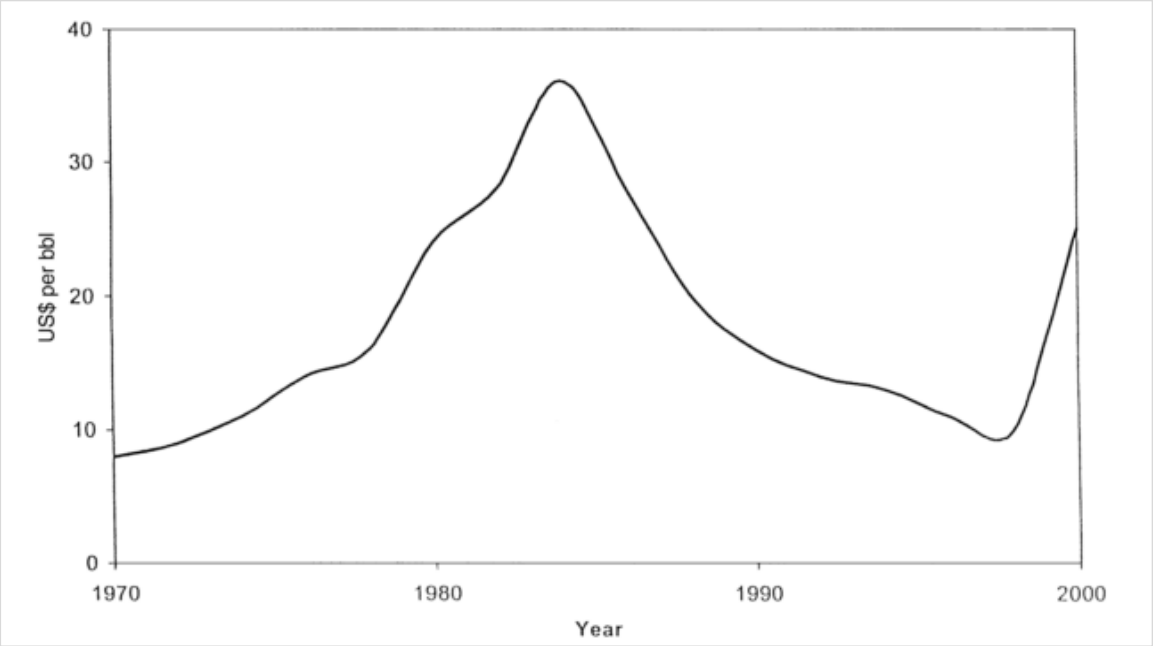



**Figure 2.1** Variation in the price of crude oil from 1970 to 2000[6]

The oil crises also saw an increase in interest in the FTS process from companies such as Shell, Gulf, BP, Statoil and Exxon Mobil. In the last two decades to date, the technology has received great attention which led to the development of new commercial GTL plants by PetroSA (South Africa; 1993), Shell (Malaysia; 1992), Sasol-Qatar Petroleum, represented in Table 2.1[2]. The technology has also been seen as one of the options that focus on the production of clean fuels and chemicals.[7] Not mentioned in the table below is recent development of large CTL plants in China. CTL and SNG have been paid great attention recently in China and a summary of their government approved CTL/SNG projects is listed in an article by Jian Xu *et al.* [8]

**Table 2.1** An overview of the current commercial operations using FTS technology[2]

| Company | Location | Carbon feed stock | Catalyst type | Reactor type | Start-up date | Approximate plant capacity (barrels per day) |
|---|---|---|---|---|---|---|
| **Sasol** | Sasolburg, South Africa | Initially coal, currently natural gas | Fused Fe/K | HTFT circulating fluidized bed | 1955-1985 | 5000 |
| | | | Precipitated Fe/K | LTFT multi-tubular fixed bed | 1955 | |
| | | | Precipitated Fe/K (spray dried) | LTFT slurry phase | 1993 | |
| **Sasol** | Secunda, South Africa | Mostly coal, now supplemented by natural gas | Fused Fe/K | HTFT circulating fluidized bed<br>HTFT SAS reactor [a] | 1980-1999<br>1995 | 160 000 |
| **Shell** | Bintulu, Malaysia | Natural gas | $Co/SiO_2$<br>$Co/TiO_2$ | LTFT multi-tubular fixed bed | 1992 | 14500 |
| **PetroSA** | Mosselbay, South Africa | Natural gas | Fused Fe/K | HTFT circulating fluidized bed (Sasol technology) | 1993 | 22000 |
| **Sasol-QP (Oryx)** | Ras Laffan, Qatar | Natural gas | $Co/Al_2O_3$ | LTFT slurry phase | 2007 | 34000 |
| **Shell (Pearl)** | Ras Laffan, Qatar | Natural gas | $Co/TiO_2$ | LTFT multi-tubular fixed bed | 2011 | 140000 |
| **Chevron-Sasol** | Escravos, Nigeria | Natural gas | $Co/Al_2O_3$ | LTFT slurry phase | 2013 | 34000 |

[a] ***SAS: Sasol Advanced Synthol, fixed fluidised bed***

### *2.2 Three main steps in the FT process*

The application of Fischer Tropsch technology usually involves a complex integration of reaction steps. These consist of three main basic steps that are inevitable, depicted in Figure 2.2 namely:

- Synthesis gas production
- FT synthesis
- Product upgrading

The initial reactants (syngas) used in the Fischer-Tropsch process are hydrogen gas ($H_2$) and carbon monoxide (CO). These chemicals are usually produced by one of two methods; the partial combustion of a hydrocarbon (e.g. $CH_4$) or the gasification of coal, biomass, or natural gas. The Fischer-Tropsch process is generally operated in the temperature range of 180- 350 °C. The primary upgrade of liquid products typically starts with the removal of light hydrocarbons and dissolved gases to make the hydrocarbons suitable for storage at atmospheric pressure. A number of possible processes for FT products are: wax hydrocracking, distillate hydrotreating, catalytic reforming, naphtha hydrotreating, alkylation and isomerisation etc.

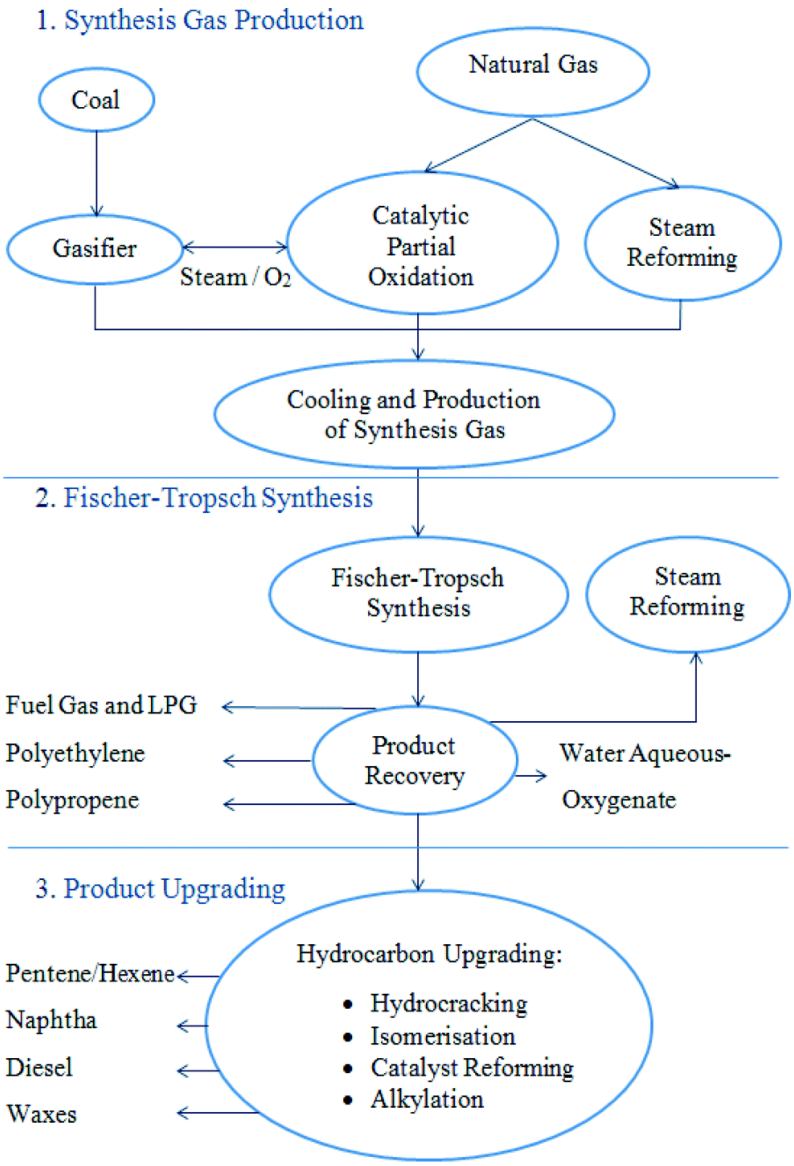



**Figure 2.2** Three main steps of the FTS process[9,10]

### *2.3 The Fischer-Tropsch Synthesis (FTS)*

The FTS reaction is a polymerisation reaction, whereby the bonds formed from carbon atoms are as a result of the reaction of carbon monoxide and hydrogen gas in the presence of a metal catalyst. The process involves adsorption, chain initiation and chain growth with termination as illustrated in Figure 2.3[6]. The hydrogenation of CO leads to the formation of active $CH_2$ units which are taken as the "monomers" in the propagation step. All this happens on the surface of the catalyst. These adsorbed species can either desorb or be hydrogenated further to form primary FT products or another monomer unit can add to the chain to continue the chain growth. If it is assumed that the probability of chain growth (α) is independent of the chain

length then it is a simple matter to calculate the product distribution for various values of $\alpha$[6]. Alternative mechanistic pathways have been proposed, but all of them involve initiation, propagation and termination steps.

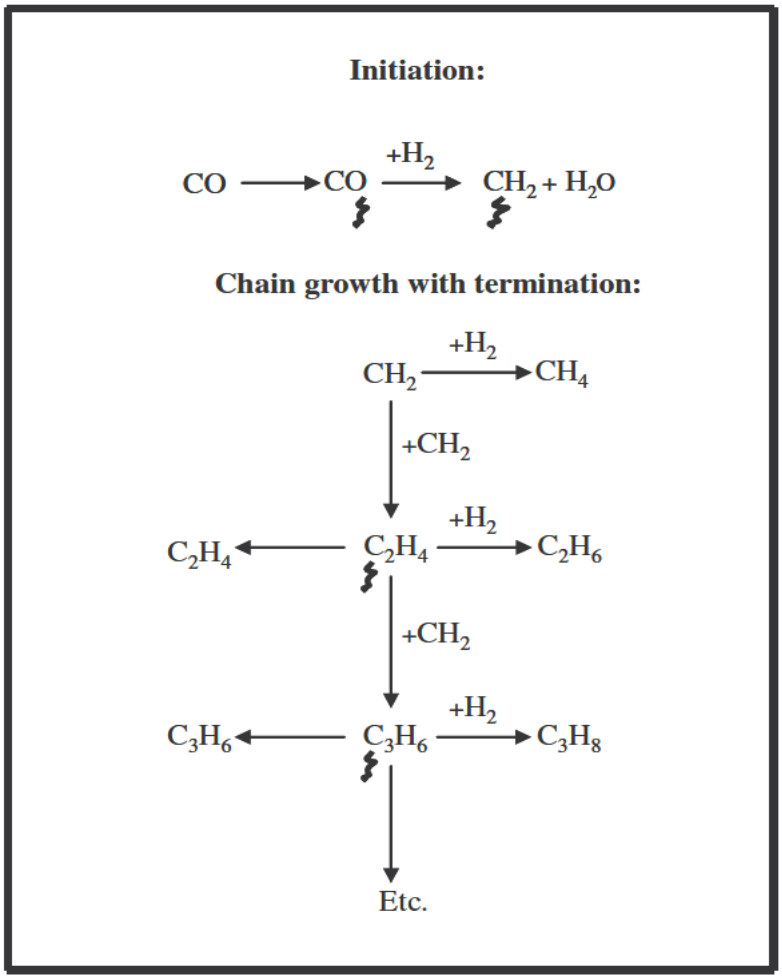



**Figure 2.3** FT stepwise growth process[6]

A range of products are then obtained, which depend on the reaction conditions, the reactor and the type of catalyst used. There are currently two modes of operation for FT technologies i.e. low temperature Fischer-Tropsch (LTFT) process with operation temperatures around 180 - 200 °C, and the high temperature Fischer-Tropsch (HTFT) process with operating temperatures around 330 - 350 °C[6]. Figure 2.4 depicts the overall FT process scheme as well as its product slate reported by Khodakov[11].

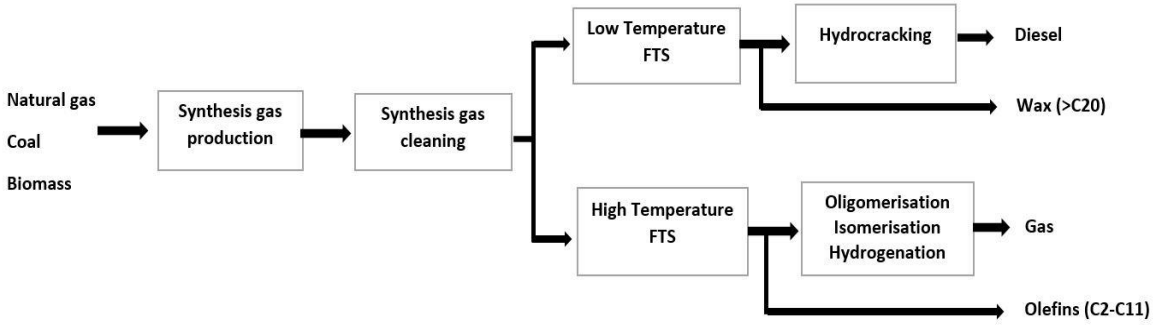



**Figure 2. 4** High- and low-temperature Fischer Tropsch process[12]

### *2.4 The Fischer Tropsch reactors*

Since the FT reactions are highly exothermic it is important to rapidly remove the heat of reaction from the catalyst particles in order to avoid overheating of the catalyst which would otherwise result in an increased rate of deactivation due to sintering and fouling and also in the undesirable high production of methane.

#### *2.4.1 Reactors*

There are four types of Fischer-Tropsch (FT) reactors which were known for commercial use. Presently only three are in use, with the fixed bed reactor no longer being used. The four types of reactor are:

- Circulating fluidized bed (CFB) reactor
- Fluidized bed reactor- Not in use
- Multi-Tubular fixed bed reactor
- Slurry phase reactor

The FTS operates in two modes, or can broadly be classified in two classes, namely two-phase or three-phase reactors, and moving or stationary catalyst bed reactors as indicated in Figure 2. 5. Iron based catalysts can operate at high-temperature (300 - 350 ºC) for the production of gasoline and linear low molecular mass olefins. Originally, this process was operated in circulating fluidized bed reactors and more recently in fixed fluidized bed reactors[12]. The low temperature (200 - 240 ºC) mode with either iron or cobalt catalysts is used for the production of high molecular mass linear waxes.[6] Cobalt catalysts would typically be used toward the

lower half of the quoted temperature range. The heavy product spectrum extends well into the domain of waxes, which are liquid under reaction conditions. Originally, only fixed-bed reactors operating in a trickle bed mode were employed for this synthesis. More recently, slurry bubble-column reactors have been developed to overcome some of these drawbacks.

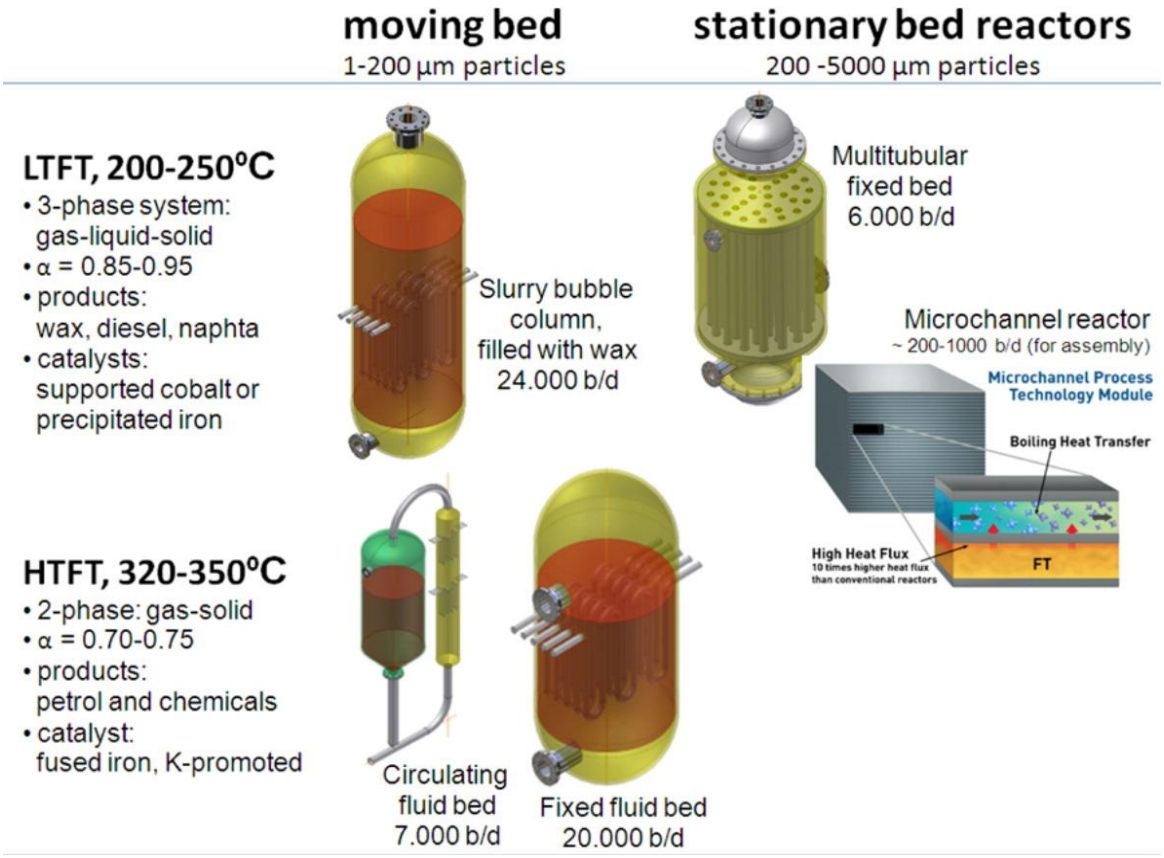



**Figure 2. 5** Overview of Fischer–Tropsch technology with reactors (figure microchannel reactor: courtesy of the Oxford Catalysts Group).

**Table 2.2** Differences of the Fischer Tropsch reactors

| **1. Fixed Bed Reactors** | | **2. Fluidized Bed Reactors** | **3. Slurry Reactors** | |
|---|---|---|---|---|
| ***Sasol fixed bed***<br>➢ Used pre WWII till recently<br>➢ Challenges associated with removal of heat<br>➢ Catalyst placed in tubes with small diameters<br>➢ T = 200 – 250 °C, lifetime up to 350 days.<br>➢ High wax production.<br>➢ Improving isothermicity by:<br>– Large empty reactor volume<br>– Tube wall reactors. | ***Shell fixed bed***<br>➢ Was used from 1992<br>➢ The intraparticle diffusion resistance is very high<br>➢ Uses a tubular fixed bed reactor containing a proprietary cobalt-based catalyst with mild recycle.<br>➢ LTFT operation<br>➢ High quality synthetic oil products and specialty chemicals, which are paraffinic | ➢ Used from 1989 to present.<br>➢ Better temperature control.<br>➢ High yields for gasoline and light products.<br>➢ T = 320 – 360 °C, catalyst lasts about 40 days.<br>➢ High yields and high throughput.<br>➢ SASOL Advanced Synthol design | ***ExxonMobil Slurry reactor***<br>➢ Merge between Mobil and Exxon<br>➢ Uses AGC-21 FTS process<br>➢ Uses $Co/TiO_2$ catalyst<br>➢ Products are heavy hydrocarbons, mostly linear paraffin<br>➢ The isothermal reactor design enables high selectivity. | ***SASOL Slurry Phase Distillate reactor***<br>➢ Was used from 1993 to present.<br>➢ Small catalyst particles suspended in a liquid with low vapour pressure.<br>➢ Low reaction temperature.<br>➢ High wax selectivity.<br>➢ Most flexible design |

### *2.4.2 The Effect of Fischer-Tropsch synthesis conditions*

Synthesis conditions i.e. synthesis gas ratio, temperature, total pressure, and reaction time on stream (TOS) can affect the FT product selectivity and composition but can be controlled. The selectivity of the material is determined by the ability of the catalyst to facilitate chain propagation over chain termination. Fischer-Tropsch selectivities have previously been reported to rely heavily on CO conversion. The conversion of CO can be controlled by changing the reactor partial pressure, space velocity and reactor temperature[13]. A review of the effect of increasing these process conditions in the Fischer-Tropsch synthesis was published by Mabaso *et al.*[14] as summarized in Table 2.3. Although he stated that there is no clear effect of increase in $H_2$: CO ratio on chain branching, high hydrogen pressures (resulting in higher hydrogenation activity) normally decreases this parameter[15].

**Table 2.3** Effect of process conditions on Fischer-Tropsch synthesis product selectivity (adapted from Mabaso et al.[14])

| **Parameters** | **Temperature↑** | **Pressure↑** | **$H_2$:CO↑** |
|---|---|---|---|
| Methane Selectivity | + | - | + |
| Olefin selectivity | * | * | - |
| Oxygenate selectivity | - | + | - |
| Chain growth | - | + | - |
| Chain branching | + | - | * |
| Carbon deposition | + | * | - |

*+ Increase with increasing parameter*

*- Decrease with increasing parameter*

** No clear effect*

### *2.5 Fischer Tropsch reactions*

The most important FT reactions are those resulting in the formation of alkanes (paraffins) and alkenes (olefins) as products of interest[10]. Most of the alkanes produced tend to be straight-chain, suitable for diesel fuel production although some branched alkanes are also formed. Other competing reactions results in the production of alkenes as well as alcohols and other oxygenated hydrocarbons given in some equations below. These can be described by chemical equations (1) and (2) respectively. The main by-products are water and/or carbon dioxide, that is, due to the water-gas shift (WGS) reaction equation (3). The reaction is highly exothermic and generates large amounts of heat.

$$\text{Alkane Production: } (2n+1)H_2 + nCO \rightarrow C_nH_{(2n+2)} + nH_2O \quad (1)$$

$$\text{Alkene Production: } 2nH_2 + nCO \rightarrow C_nH_{(2n)} + nH_2O \quad (2)$$

$$\text{WGS: } CO + H_2O \rightleftarrows H_2 + CO_2 \quad (3)$$

where 'n' is a positive integer.

Process conditions and catalyst composition impacts the kind of product output expected from the process. Usually higher order reactions (n>1) are favored and thus minimize methane formation. Most of the alkanes produced tend to be straight-chain, although some branched alkanes are also formed.

The other side reactions taking place during FT are those producing alcohols (equation 4) and the Boudouard reaction (equation 5). The Boudouard reaction is known for disproportionation of CO that leads to the formation of $CO_2$ and carbon. The produced carbon is undesired as it can cause catalyst deactivation.

$$\text{Alcohols: } 2nH_2 + nCO \rightarrow C_nH_{2n}+ 2O + (n-1)\,H_2O \quad (4)$$

$$\text{Boudouard reaction: } 2CO \rightarrow C + CO_2 \quad (5)$$

### *2.6 FT process product distribution*

The resulting FTS hydrocarbon products follow an arithmetical distribution identified as the Anderson–Schulz–Flory (ASF) distribution. At the chemistry level, the FT synthesis is both a CO hydrogenation reaction and a polymerization reaction. In the Anderson–Schulz–Flory relationship, it is widely accepted that chain growth occurs one carbon atom at a time via a polymerization mechanism represented by the following equation:

$$W_n = n(1-\alpha)\alpha^{2n-1} \quad (6)$$

where $W_n$ is the weight percent of a product containing $n$ carbon atoms and, α(or Pg), is the chain growth probability. The probability for growth, determines the competition between chain growth (yielding a surface intermediate with one higher carbon number) and chain termination (yielding a desorbed final product). A product distribution that follows this model is represented graphically in Figure 2.6[16]. Irrespective of operating conditions the FT synthesis always produces a wide range of olefins, paraffins and oxygenated products (alcohols, aldehydes, acids and ketones). The distribution and composition of the products are however

dependent on the reaction variables, such as, temperature, pressure and feed gas composition[14]. Synthesis over cobalt catalysts generally yields more methane and $C_{5+}$ and less $C_2$-$C_3$ than ASF kinetics would predict.

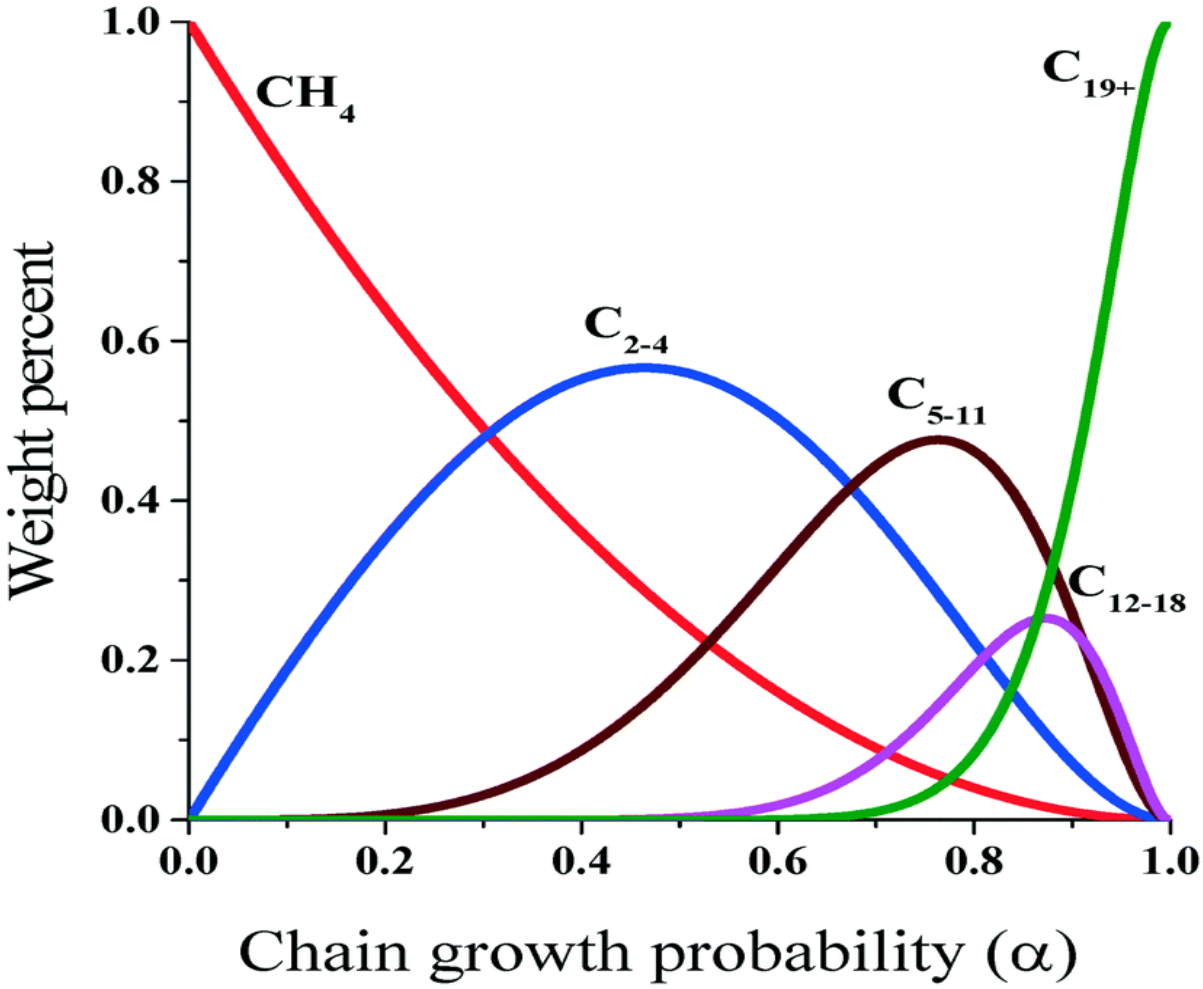



**Figure 2. 6** An Anderson-Schulz-Flory product distribution[16]

### *2.7 The Fischer Tropsch catalysts*

Catalysts play a major role in the FT process. They are also used to catalyse processes such as the methanol production, ammonia synthesis, etc. Metal choice is dictated by the balance of bond-breaking and bond-forming processes on the metal surface. In the periodic table, transition metals to the left can quickly dissociate CO, but the products, i.e. surface carbon and oxygen, are too closely bound to the surface to block subsequent hydrogenation and carbon binding reactions.

On the other hand, transition metals to the right of the periodic table are not sufficiently active to dissociate CO. The ideal metals are those that can facilitate CO dissociation, together with a balanced degree of hydrogenation of surface carbon and carbon coupling to create longer chain hydrocarbon products. The transitional metals usually used are Iron (Fe), Cobalt (Co), Nickel (Ni) and Ruthenium (Ru). Fe and Co being the most studied out of the four because of their commercial importance. Nickel in FT has a disadvantage due to high methanation activity and formation of volatile sub-carbonyls [4].

Ruthenium, on the other hand, has been recorded to be the most active metal but has its disadvantages of being too expensive and scarce. This is one of the reasons why it has never been used commercially in the FT process. Regardless of this disadvantage, Ru has a number of advantages. One of these advantages is that Ru can be used purely without any promoters, thus performing the chain growth reaction in its cleanest mode.[8] Claeys and van Steen reported ruthenium to be active in the presence of excess water, where the addition of water during Fischer–Tropsch synthesis can lead to an increase in catalyst activity and indicated significant changes in product composition.[17] It was also observed that addition of water during FT synthesis can decrease methane selectivity and improve chain growth. Anderson (1956) reported on yields of high average molecular weight products and a large $C_{5+}$ fraction even at atmospheric conditions[18]. H. Schulz (1999) reported Ru metal to be most stable having the simplest product spectra which makes it easy to interpret the activity and selectivity trends.[8] Ruthenium catalysts can also be operated over a wide range of operation conditions i.e. temperatures and pressures.

### *2.8 Supported FT catalysts*

Supported catalysts are preferred catalysts because they provide a high dispersion of the active phase on the support and a high degree of thermal stability of the catalytic component[19]. It is very important to select a good support for FT catalysts. Research has proved that supported catalysts exhibit better characteristics than unsupported ones[20]. Supports can include metal oxides such as $TiO_2$, $ZrO_2$, $SiO_2$ and $Al_2O_3$. Metal-support interactions are important for catalyst activity and stability. A good support is required to have the following characteristics: inertness, resistance towards attrition, hardness, compressive strength & stability under reaction conditions, regeneration conditions, high surface area, porosity and low expense. There is quite a diversity of supports which can be used, but only a few possess these

characteristics. Alumina, silica and activated carbon are most widely used ones[19]. A study by Nurunnabi *et al.* investigated the effects of different supports on ruthenium based catalysts, which also included heat-treated alumina support (more on heat treatment of supports is discussed in section 1.8.1) and the findings are reported in Table 2.4.

**Table 2.4** Findings on the performance and characterisation of $Ru/Al_2O_3$ and $Ru/ SiO_2$[21]

| **Research title** | *Performance and characterisation of $Ru/Al_2O_3$ and $Ru/ SiO_2$* |
|---|---|
| **Variable investigated** | $\alpha$-$Al_2O_3$, $\Upsilon$-$Al_2O_3$ and $SiO_2$ supports |
| | ✓ $\Upsilon$-$Al_2O_3$ catalysts showed high catalytic activity and high $C_{5+}$ selectivity.<br>✓ Showed a high resistance to catalyst deactivation which is due to the addition of Mn.<br>✓ Although $SiO_2$ and $\alpha$-$Al_2O_3$ promotes a highly dispersed Ru on the surface, moderate particle size and pore diameter (8 nm) on the $\Upsilon$-$Al_2O_3$ was found to be more active. |

### *2.8.1 The effect of thermal treatment of Alumina*

High mechanical strength and hardness, good wear resistance, low electric conductivity, low refractoriness and high corrosion resistance are all the favourable qualities of alpha alumina ($\alpha$-$Al_2O_3$, corundum) which is one of the most widely used ceramic materials in a broad range of chemical environments[22]. The slurry phase Fischer-Tropsch process favours several of these properties. When aluminum hydroxides or oxide hydroxides are heated in air at atmospheric pressure, they undergo a series of compositional and structural changes before ultimately being converted to $\alpha$-$Al_2O_3$ as shown in Figure 2. 7. The thermal transformation, at ambient pressure, of $\Upsilon$-AlO(OH) and the trihydroxides to $\alpha$-$Al_2O_3$ requires considerably more structural rearrangements and is generally not completed until the temperature reaches at least 1375 – 1400 °C.

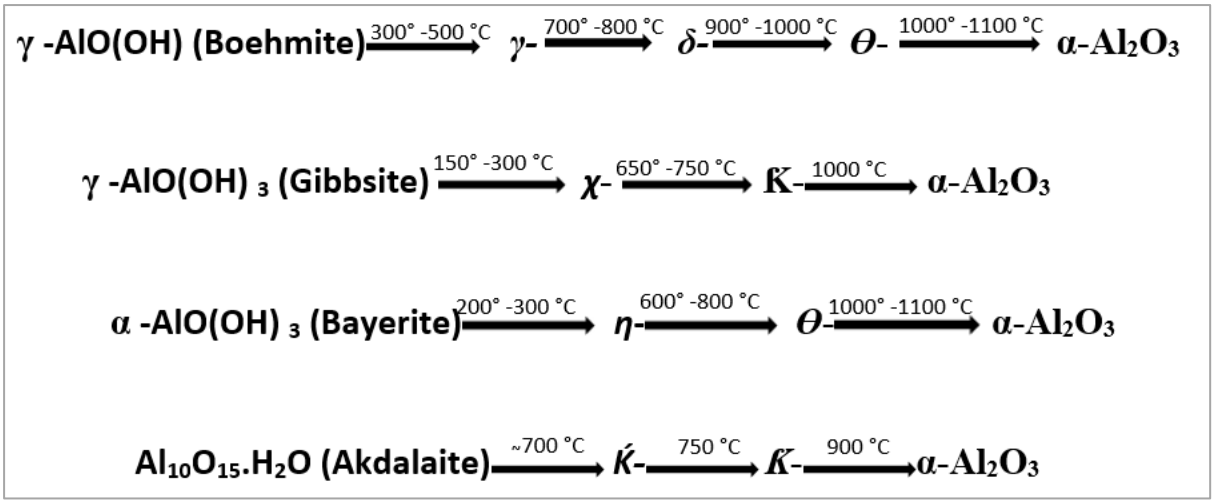



**Figure 2. 7** Thermal transformation of alumina

The first step in the reaction sequence is the diffusion of protons to adjacent OH groups and the subsequent formation of water. This process begins at a temperature near 475 °C. If this water cannot diffuse rapidly out of larger trihydroxide particles, hydrothermal conditions may develop locally, resulting in the formation of ϒ-AlO(OH). With increasing loss of water, a large internal porosity develops. Nanosized α- $Al_2O_3$ powders are being sought as a thermally stable alternative to widely used transition aluminas, which undergo phase transformations during high temperature use and thus suffer loss of surface area.[23] The hexagonally close packed α-$Al_2O_3$ is the only stable oxide in the $Al_2O_3$-$H_2O$ system and can be synthesized by several high temperature methods. When aluminium hydroxides or oxide hydroxides are heated in air at atmospheric pressure, they undergo a series of compositional and structural changes before ultimately being converted to α-$Al_2O_3$. The high temperature calcination procedure is used as one of the means to prepare alpha alumina which yields support materials with a low specific surface area. It was found that cobalt or rhenium catalysts supported on low surface area aluminas resulted in lower metal dispersion and reduced activity. The collapse of pore structure can be counteracted by introducing a 2-valent metal in the support material that forms an aluminate spinel phase during high-temperature treatment. Previous reports also suggest that a $\gamma$-$Al_2O_3$ support is more effective in presence of Mn for FT synthesis[21,24].

### *2.8.2 Effect of support modification*

The development of catalysts for the Fischer–Tropsch synthesis is one of the key technologies required for the GTL process. The common problem in the FT synthesis is the possibility of hotspots forming on the catalyst surface during the reaction since FT synthesis is known to be an exothermic reaction.This can also lead to undesirable activity and selectivity due to catalyst damage as well as catalyst deactivation[12]. There is therefore, a need to develop catalyst with high and stable activity. Mn can be effective as an additive for Fischer–Tropsch catalysts. Mn has been described as a perspective promoter, which could enhance both the carbon monoxide conversion rate and hydrocarbon selectivity[25]. Depending on when it's impregnated during catalyst preparation, Mn can play a role as either a support modifier or a catalyst promoter. Mn effect strongly depends on the supports and the preparation method to achieve better stability, activity and selectivity toward carbon chain growth probability. Many studies have been dedicated to investigate the effect of additives on FTS reaction. In recent studies done by Narunnabi *et al.*, the effect of different Mn salts on catalytic activity and stability of Ru based catalyst was investigated [22]. Table 2.5 below summarises the findings of their studies:

**Table 2.5** Summary on the effect of manganese salts on catalytic activity and stability[26]

| **Research title** | *Effect of Manganese salts on catalytic activity and stability* |
|---|---|
| **Variable investigated** | Mn $(NO_3)_2$. $6H_2O$, $MnSO_4$, $MnCl_2$ and $Mn(CH_3COO)_2$ |
| | ✓ Mn $(NO_3)_2$. $6H_2O$ gave high and stable catalytic-activity whereas other catalyst with different Mn salts deactivated.<br>✓ Moderate particle size and diameter (8 nm) on the ɣ-$Al_2O_3$ was found to be more active<br>✓ The order of activity was Mn $(NO_3)_2$. $6H_2O$> $Mn(CH_3COO)_2$ > $MnCl_2$ > $MnSO_4$ |

### *2.9 Synthesis of Fischer Tropsch catalysts*

The catalytic performance of alumina supported FT catalyst depends on the support properties and the nature of the surface species formed after catalyst preparation. The function of the support in Fischer Tropsch is to disperse the active metal and produce stable metal catalyst particles after reduction. The size of the supported metal particles could be controlled by the porous structure. For optimum catalyst performance, catalyst design should also be considered. A combination of chemical, physical and mechanical properties play a major role in this case. Anderson *et al*. defined a catalyst design concept which was adapted for Fischer Tropsch

synthesis by Farrauto and Bartholomew, as illustrated in Figure 2.8. In addition the physico-chemical properties of the active phase, specifically formulation shape, size and crystallinity of the nanoparticles are significant factors for optimisation during catalyst design.

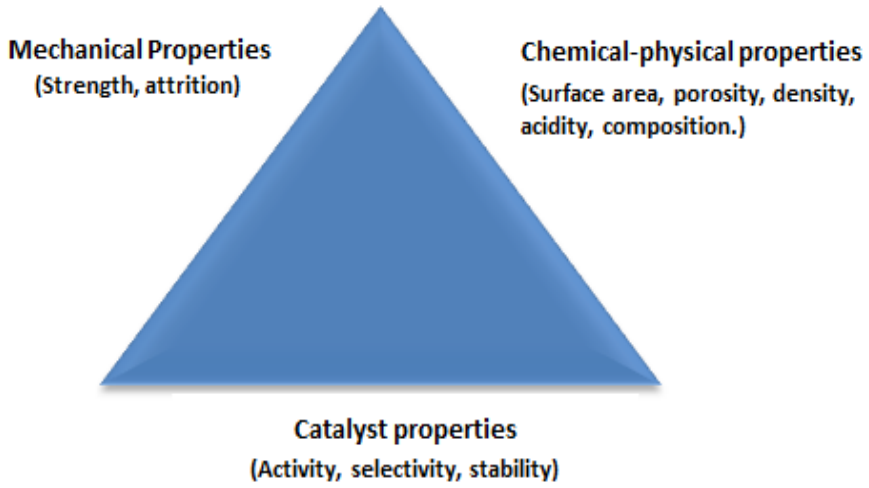



**Figure 2. 8** Concept of catalyst design[27]

Extensive studies have gone into understanding these three components and how to relate them in obtaining a catalyst with superior activity, selectivity and stability. The most common preparation methods for supported catalysts are: precipitation and impregnation methods. Ion-exchange and deposition of organometallic compounds on the support material, colloidal method, micro-emulsion technique, sol-gel method, plasma method and chemical vapour deposition are the other methods of catalyst preparation but are used less frequently[16].

### *2.9.1 Impregnation Method*

The incipient wetness impregnation method, or the pore volume impregnation method, is a common method used to prepare FT catalysts and is normally described as being the simplest practical way to impregnate an active phase onto the support. However, this is not necessarily true because the fundamental phenomena underlying impregnation and drying are extremely complex[11]. In this method a salt solution, typically a metal-nitrate is added to a dry porous support. After contact, the solution is drawn into the pores of a support by capillary action. When all pores of the support are filled with the liquid and when there is no more excess liquid required to fill the pores, then the incipient wetness process has occurred. The liquid is then

removed by drying in a rotary vapour unit, and then a calcination step resulting in the preparation of the oxidic catalyst precursor. Figure 2.9 is a schematic representation of the impregnation process from the starting material which is the support, to the thermal treatment step known as calcination.

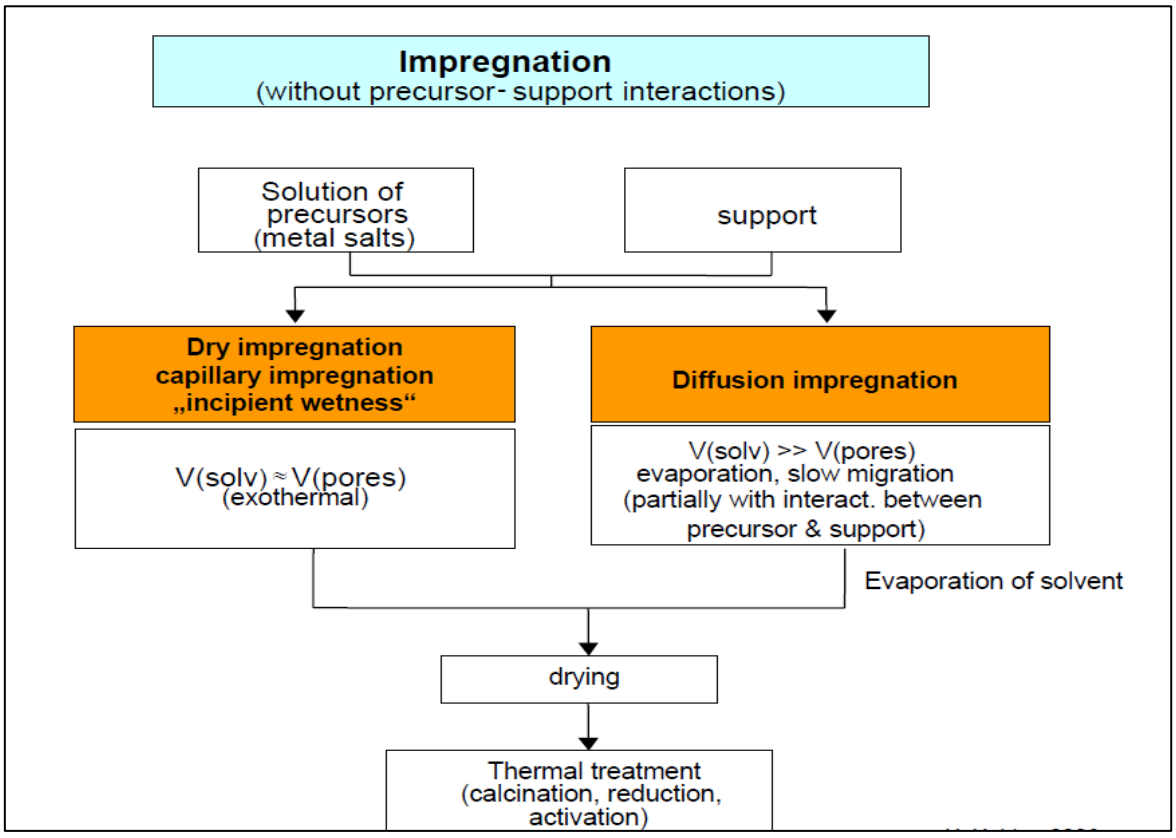



**Figure 2.9** A schematic representation of the catalyst impregnation process[20]

### *2.10 Acid-base properties of Fischer-Tropsch catalyst*

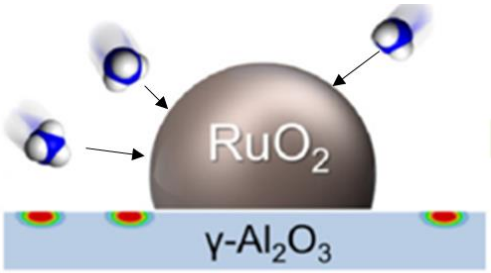
Alumina obtained from boehmite is usually used as catalyst support due to favourable properties such as large surface areas, porosities, crystalline structures and acid-basic properties[28]. Aluminium oxide is amphoteric in nature and thus shows both acidic and basic properties. Surface acid-base properties of supports significantly affects the activity and selectivity of FTS reaction[29]. The surface acid-base properties of a support can be influenced by calcination temperatures[23], and modification with other metals[30].

There are many methods used for the determination of acidic and basic properties of solids. Temperature-programmed desorption is often used apart from titration and spectroscopic techniques (FTIR, XPS, NMR). The most widely applied molecular probes are ammonia (to

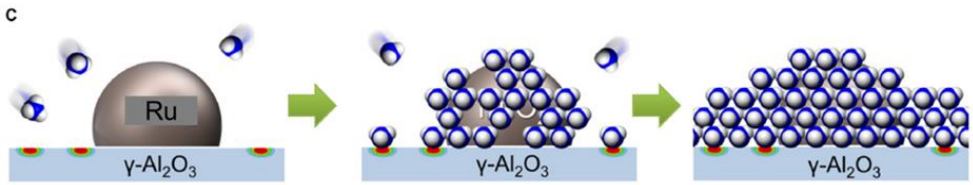
study acidic sites) and carbon dioxide (basic sites)[31]. The TPD method is used to measure the number and base strengths of sites found on solid base catalysts. Since strongly bound probe molecules have high binding energies, increased temperatures are necessary to desorb these adsorbates. Experiments are typically performed under identical experimental conditions (heating rates and sample size) so that a qualitative comparison can be made between samples. During a TPD experiment, the amount of desorbed molecules is often monitored by mass spectrometry and the surface interactions are explored with infrared spectroscopy[32]. The technique employed in the adsorption experiments involves an intermediate degassing step at 0 °C when all physically and weakly chemisorbed $CO_2$ is removed, leaving only the relatively strongly bound $CO_2$, on the surface. The technique thus to some extent provides a combined measure of both the strength and extent of the surface basicity.

Temperature programmed desorption (TPD) consist of three steps which are:

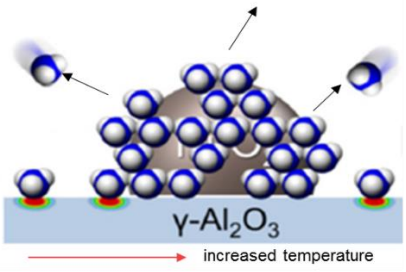
- Activation - which entails cleaning of the oxide surface of the catalyst with an inert gas such as He, Ar or $N_2$,




- Adsorption or pulse chemisorption - adsorption of the probing molecule, illustrated by the figure below.




- Desorption stage - where molecules are desorbing from the surface of the catalyst with an increase in temperature.




- An illustration of a typical results obtained from $NH_3$-TPD analysis is represented below. Five samples were analysed and two important information can be derived from the TPD profile.

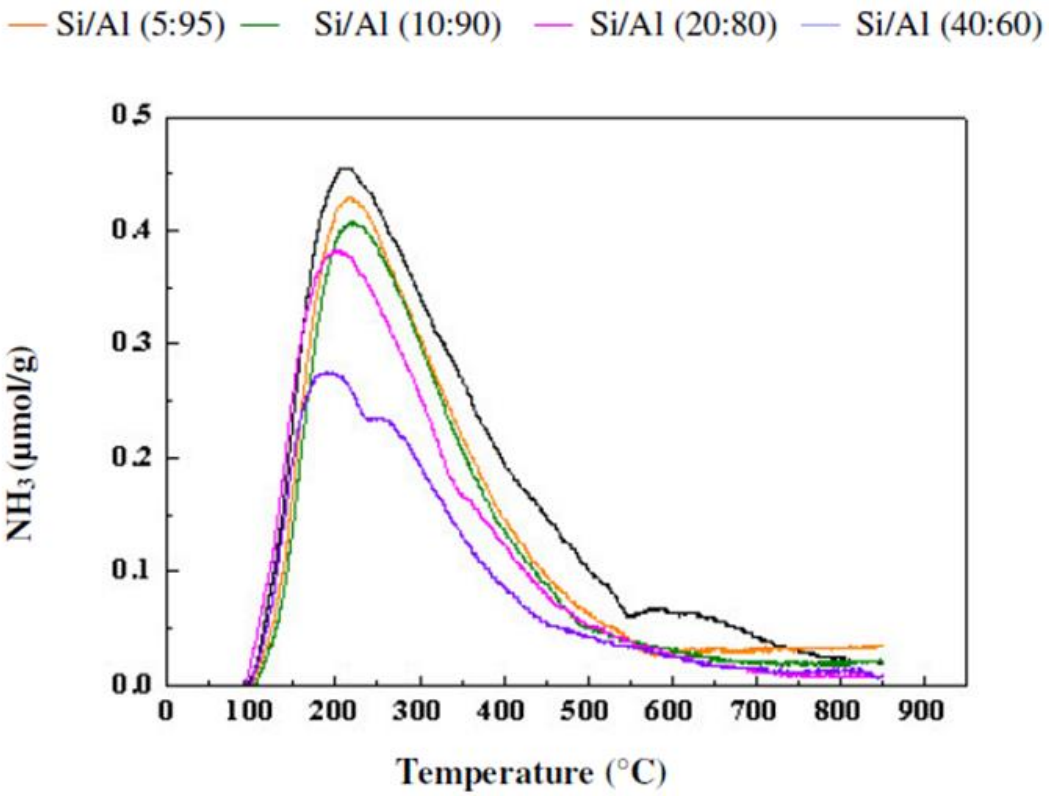



**Figure 2.10** Illustration of a typical results obtained from $NH_3$-TPD analysis[31]

1. The profile indicates two peaks, one peak at lower temperatures which indicates weak acid sites and a peak at higher temperatures which indicates the presence of strong acid sites.

The intensity of the peaks and the peak area relates to the quantity of the acid sites present on the samples.

## *References*


(1) Hexana, W. M. A Systematic Study of the Effect of Chemical Promoters on the Precipitated Fe-Based Fischer-Tropsch Synthesis Catalyst. **2009**.

(2) Van de Loosdrecht, J.; Botes, F. G.; Ciobica, I. M.; Ferreira, A.; Gibson, P.; Moodley, D. J.; Saib, A. M.; Visagie, J. L.; Weststrate, C. J.; Niemantsverdriet, J. W. *Fischer-Tropsch Synthesis: Catalysts and Chemistry*; Elsevier Ltd., 2013; Vol. 7.

(3) Bartholomew, C. H. History of Cobalt Catalysts Design for FTS. *AIChE Natl. Spring Meet.* **2003**, 83b.

(4) Leckel, D. Diesel Production from Fischer−Tropsch: The Past, the Present, and New Concepts. *Energy & Fuels* **2009**, *23* (6), 2342–2358.

(5) Steynberg, A. P. *Introduction to Fischer-Tropsch Technology*; Elsevier B.V., 2004; Vol. 152.

(6) Dry, M. E. The Fischer-Tropsch Process: 1950-2000. *Catal. Today* **2002**, *71* (3–4), 227–241.

(7) Schulz, H. Short History and Present Trends of Fischer–Tropsch Synthesis. *Appl. Catal. A Gen.* **1999**, *186* (1–2), 3–12.

(8) Xu, J.; Yang, Y.; Li, Y. W. Recent Development in Converting Coal to Clean Fuels in China. *Fuel* **2015**, *152* (March 2018), 122–130.

(9) Jahangiri, H.; Bennett, J.; Mahjoubi, P.; Wilson, K.; Gu, S. A Review of Advanced Catalyst Development for Fischer-Tropsch Synthesis of Hydrocarbons from Biomass Derived Syn-Gas. *Catal. Sci. Technol.* **2014**, *4* (8), 2210–2229.

(10) Fahim, M. A.; Alsahhaf, T. A.; Elkilani, A. Clean Fuels. *Fundam. Pet. Refin.* **2010**, 303–324.

(11) Khodakov, A. Y.; Chu, W.; Fongarland, P. Advances in the Development of Novel Cobalt Fischer-Tropsch Catalysts for Synthesis of Long-Chain Hydrocarbons and Clean Fuels. *Chem. Rev.* **2007**, *107* (5), 1692–1744.

(12) Saeidi, S.; Amiri, M. T.; Amin, N. A. S.; Rahimpour, M. R. Progress in Reactors for Higherature Fischer-Tropsch Process: Determination Place of Intensifier Reactor

Perspective. *Int. J. Chem. React. Eng.* **2014**, *12* (1), 639–664.

(13) Ramana, V.; Pendyala, R.; Jacobs, G.; Graham, U. M.; Shafer, W. D.; Martinelli, M.; Kong, L.; Davis, B. H. Fischer − Tropsch Synthesis : In Fl Uence of Acid Treatment and Preparation Method on Carbon Nanotube Supported Ruthenium Catalysts. **2017**.

(14) Mabaso, E. I. For Fischer-Tropsch Synthesis.

(15) Snel, R. Factors Affecting the Extent of Branching in Fischertropsch Synthesis Products with Iron-Based Catalysts. *J. Mol. Catal.* **1989**, *50* (1), 103–114.

(16) Phadi, T. T. Titanates and Titania Coated Titanates as Supports in the Fischer-Tropsch Synthesis By Titanates and Titania Coated Titanates as Supports in the Fischer-Tropsch Synthesis.

(17) Claeys, M.; van Steen, E. On the Effect of Water during Fischer-Tropsch Synthesis with a Ruthenium Catalyst. *Catal. Today* **2002**, *71* (3–4), 419–427.

(18) King, D. L. A Fischer-Tropsch Study of Supported Ruthenium Catalysts. *J. Catal.* **1978**, *51* (3), 386–397.

(19) Che, M.; Bennett, C. O. The Influence of Particle Size on the Catalytic Properties of Supported Metals. *Adv. Catal.* **1989**, *36* (C), 55–172.

(20) de Jong, K. P. Preparation of Supported Catalysts. *Catal. - From Princ. to Appl.* **2012**, 420–430.

(21) Nurunnabi, M.; Murata, K.; Okabe, K.; Inaba, M.; Takahara, I. Performance and Characterization of Ru/Al2O3 and Ru/SiO2 Catalysts Modified with Mn for Fischer-Tropsch Synthesis. *Appl. Catal. A Gen.* **2008**, *340* (2), 203–211.

(22) Lamouri, S.; Hamidouche, M.; Bouaouadja, N.; Belhouchet, H.; Garnier, V.; Fantozzi, G.; Trelkat, J. F. Control of the γ-Alumina to α-Alumina Phase Transformation for an Optimized Alumina Densification. *Bol. la Soc. Esp. Ceram. y Vidr.* **2017**, *56* (2), 47–54.

(23) Komeili, S.; Takht Ravanchi, M.; Taeb, A. Influence of Calcination Parameters on the Properties of Alumina as a Catalyst Support. *Sci. Iran.* **2017**, *23* (3), 1128–1135.

(24) Nurunnabi, M.; Murata, K.; Okabe, K.; Inaba, M.; Takahara, I. Effect of Mn Addition

on Activity and Resistance to Catalyst Deactivation for Fischer-Tropsch Synthesis over Ru/Al2O3 and Ru/SiO2 Catalysts. *Catal. Commun.* **2007**, *8* (10), 1531–1537.

(25) Keyser, M. J.; Everson, R. C.; Espinoza, R. L. Fischer-Tropsch Studies with Cobalt-Manganese Oxide Catalysts: Synthesis Performance in a Fixed Bed Reactor. *Appl. Catal. A Gen.* **1998**, *171* (1), 99–107.

(26) Nurunnabi, M.; Murata, K.; Hanaoka, T. Effects of Manganese Salts on Ru/Mn/Al Sub (2) O Sub (3) Catalytic Activity and Stability for Fischer-Tropsch Synthesis. *J. Japan Pet. Inst.* **2011**, *54* (1), 36–44.

(27) Perego, C.; Bortolo, R.; Zennaro, R. Gas to Liquids Technologies for Natural Gas Reserves Valorization: The Eni Experience. *Catal. Today* **2009**, *142* (1–2), 9–16.

(28) Samain, L.; Jaworski, A.; Edén, M.; Ladd, D. M.; Seo, D. K.; Javier Garcia-Garcia, F.; Häussermann, U. Structural Analysis of Highly Porous γ-Al2O3. *J. Solid State Chem.* **2014**, *217*, 1–8.

(29) Chen, L.; Tian, X.; Fu, Y.; Shen, J. The Effect of Surface Acidic and Basic Properties of Highly Loaded Co Catalysts on the Fischer-Tropsch Synthesis. *Catal. Commun.* **2012**, *28* (3), 155–158.

(30) Ragaini, V.; Carli, R.; Bianchi, C. L.; Lorenzetti, D.; Predieri, G.; Moggi, P. Fischer-Tropsch Synthesis on Alumina-Supported Ruthenium Catalysts II. Influence of Morphological Factors. *Appl. Catal. A Gen.* **1996**, *139* (1–2), 31–42.

(31) Naturwissenschaften, D. Der. Characterization of Acidic and Basic Properties of Heterogeneous Catalysts by Test Reactions. **2004**.

(32) Hattori, H. Heterogeneous Basic Catalysis. *Chem. Rev.* **1995**, *95* (3), 537–558.

# Chapter 3

## Experimental

### *3.1* Materials

The support material used in this study was the commercial Puralox B21884 obtained from Sasol Germany GmbH. The support was modified with an aqueous solution of (99.99%) Manganese (II) acetate-tetrahydrate (CAS 6156-78-1). The active metal used was (97%) Ru acetylacetonate (CAS 14284-93-6). All reagents were used as received and were supplied by Sigma-Aldrich.

### *3.2* Support preparation

The Puralox samples were calcined at different calcination temperatures ranging from 850 to 1050 ºC in order to alter the physical and chemical properties of the material. From the XRD and BET results which showed the structural and physical properties of the supports respectively, only two different supports were selected to make two catalyst systems at different calcination temperatures of the support.

### *3.3* Support Modification

The desired grams of Manganese (II) acetate-tetrahydrate was dissolved in water (80 - 100 g) and allowed to mix for 10 minutes to obtain 4, 6, 10 wt. % Mn loadings. The free flowing powder of Puralox (100 g) was added to this solution and allowed to mix for a further 10 minutes. Following this the water was removed under reduced pressure using the drying profile in Table 3.1 to obtain a free flowing powder. After the drying step, the modified support was calcined in a muffle oven to 550 °C at a heating rate of 5 °C/min and a final hold time of 5 hrs.

**Table 3.1** Drying profile for the Mn impregnated Puralox material

| Pressure ( mbar) | Temperature ( °C) | Time ( min) |
|---|---|---|
| 100 | 85 | 60 |
| 50 | 85 | 180 |

### *3.4* Catalyst preparations

2 wt% $Ru(C_5H_7O_2)_3$ was dissolved in an organic solvent (ethanol) (100 g). The modified support, Mn-Puralox (100 g) was then added to this mixture and the excess water removed under reduced pressure using the drying profile in Table 3.2 to obtain a free flowing powder.

The free flowing powder was then calcined in a fluidised bed calciner with a heating ramp rate of 1 °C/min to 250 °C with a hold time of 6 hours, using a GHSV of 2500 $Nm^3$/kg /hour.

**Table 3. 2** Drying profile for ruthenium impregnated catalysts

| Temperature (°C) | Pressure (mbar) | Time (min) |
|---|---|---|
| **60** | 250 | 15 |
| **75** | 250 | 30 |
| **85** | 250 | 30 |
| **85** | 250 -130 | 120 |
| **85** | 130 - 50 | 15 |
| **120** | 50 | 180 |

In Figure 3.1, a schematic representation of the experimental plan and how it will be executed is shown.

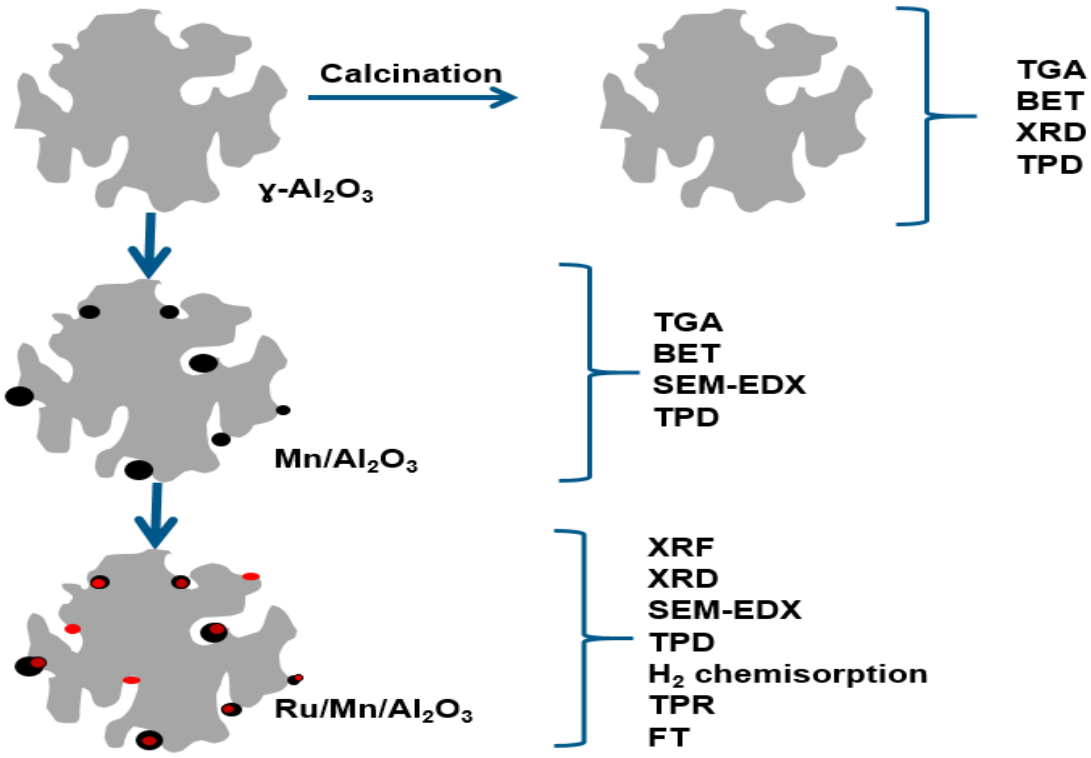



**Figure 3.1** Summary of experimental plan

### *3.5* Catalyst and support characterization

To understand both the physical and chemical properties of the catalyst, the samples were characterized by the following characterization techniques, thermogravimetric analysis (TGA), x-ray fluorescence (XRF) for elemental analysis, Brunnauer-Emmett-Teller (BET) to determine surface area and pore size, x-ray diffraction (XRD) to determine phases as influenced by calcination, scanning electron microscopy - energy dispersive x-ray analysis (SEM-EDX) for the determination of metal distribution and dispersion, transmission electron microscopy (TEM) for elemental mapping, temperature Programmed Desorption ($CO_2$, IPA) for the determination of acid base properties of the catalysts and support materials and temperature programmed reduction (TPR) to determine the temperature at which $RuO_2$ reduces. To determine the dispersion on the catalyst a $H_2$-chemisorption analysis was conducted on all the catalysts. After the characterisation results obtained, all catalyst samples were evaluated for FT synthesis to assess the effect of calcination on the activity and selectivity of the catalyst.

### 3.5.1 Thermogravimetric analysis (TGA)

Thermogravimetric analysis of the Puralox support sample was done to determine the temperature at which phase transformation takes place as a function of increased temperature. Thermal analysis was used to determine the composition of catalysts based on weight changes and thermal behaviour during thermal decomposition and reduction, to characterize the aging and deactivation mechanisms of catalysts, and to investigate the acid–base properties of solid catalysts using probe molecules[1]. A thermogravimetric-differential thermal analysis (TG-DTA-MS) instrument Netzsch STA 449 F3 Jupiter thermal analyser coupled with Cirrus Mass Spectrometer (MKS Instruments) was used in this case. Approximately 100 mg of the sample (not crushed) was placed in an open alumina crucible and heated/cooled to 30 °C at 10 °C/min under the flow of air (50 ml/min). The sample was kept isothermally at this temperature for 10 minutes to stabilize baseline and heated at 10 °C/min up to 1200 °C and under air atmosphere. Figure 3.2 is a typical profile of DTA results of alumina vs expected surface area as a function of temperature, which shows the temperature ranges and transition temperature of the alumina.

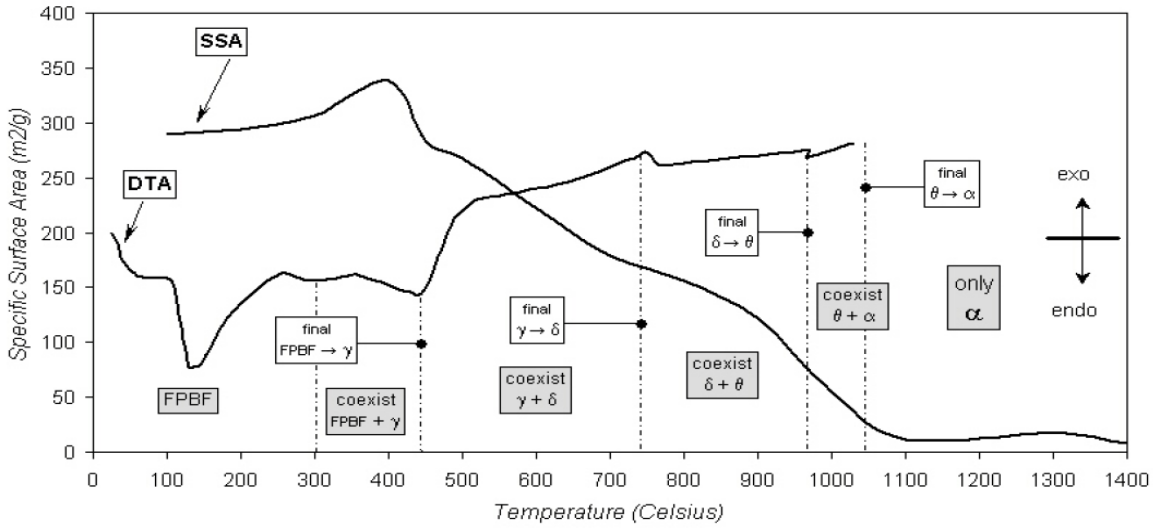



**Figure 3. 2** DTA curve of the membrane ground powder; specific surface area (SSA) of the membrane heated powders, temperature ranges and transition temperatures of the aluminas.[2]

### 3.5.2 $N_2$ Physisorption (BET)

The physicochemical properties of the Puralox support sample were determined by nitrogen physisorption analysis. The analyses were performed on a Micromeritics ASAP 2420 instrument (i.e. a six port physisorption instrument). The samples were accurately weighed (250 - 300 mg) and loaded in the glass tube and degassed under vacuum at 80 °C for a minimum

of 1 hr. Thereafter the samples were heated under vacuum at 250 °C for 4 hrs to degas. After degassing, the samples were weighed again to correct for the change in mass. Nitrogen adsorption and desorption isotherms were recorded over a nitrogen pressure range using a preset range of relative pressures, p/p0 ranging from 0.02 to 0.98.

The surface area was calculated by applying the linearized Brunauer-Emmet-Teller (BET) equation to the data between $0.05 < p/p0 < 0.30$. Total cumulative pore volume, average pore diameter, pore size distribution (PoSD) of the samples were determined by applying the Barrett-Joyner-Halenda (BJH) theory to the desorption branch of the nitrogen sorption isotherm. This theory assumes that all pores are shaped cylindrical. All calculations were performed and graphs and tables were produced using the MicroActive version 2.0 software supplied by Micromeritics.

### 3.5.3 X-ray fluorescence (XRF) spectroscopy

The ruthenium and manganese loadings of the prepared catalyst were determined by means of x-ray fluorescence (XRF) spectroscopy. A quantitative XRF method is not readily available for this sample matrix, therefore a semi-quantitative method was used. This analytical technique can be used for quantification detection of trace amounts of metals. The analyses were carried out on a Panalytical Axios Petro wavelength dispersive XRF equipped with a 2.4 kW Rh tube using the semi-quantitative SuperQ software, method IQ+. P-10 (10 % $CH_4$ in Ar) gas was used as detector gas with helium as analysis medium.

### 3.5.4 Powder X-ray diffraction (XRD)

Powder x-ray diffraction is used to analyse samples based on diffraction caused by the interaction of matter with X-rays, electrons or neutrons. The crystalline phases, relative abundances of the phases and the average crystallite sizes in the calcined support and model catalysts were determined by X-ray diffraction(XRD) using a Bruker, D8 Advanced X-ray diffractometer (Germany) with a Co-Kα radiation source ($\lambda$ = 1.78897 Å) and a position sensitive detector (Bruker Vantec) operating at 35 kV and 40 mA. For all the samples the optics were set to parallel beam geometry so as to counteract possible peak shifts due to sample height difference (sample displacement). The XRD patterns of the samples were measured in 0.0057° steps from 10° to 90° (in $2\theta$) and were identified by matching experimental patterns to entries

in the Diffrac$^{plus}$ Version 6.0 indexing software. The average crystallite sizes in nanometres (nm) were calculated using Topas Rietveld refinement software.

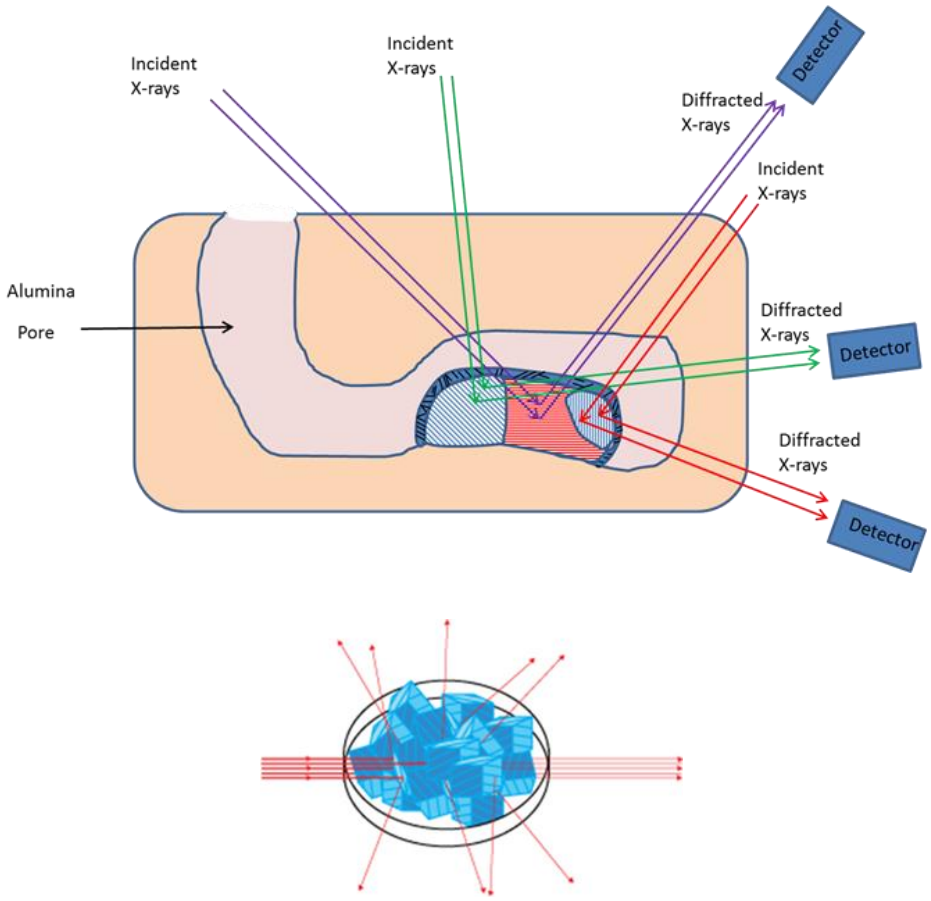


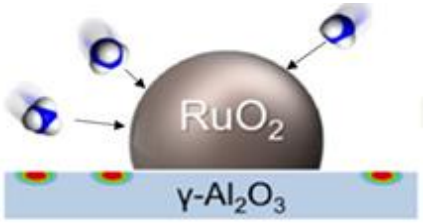

**Figure 3.3** Schematic illustration of powder XRD, showing the nature of the crystallite size measurement. All Bragg orientations are measured by scanning the X-ray source and detector to measure all the grains in all the particles[3]

### *3.5.5* Temperature programmed desorption using $CO_2$ and IPA as probe molecules

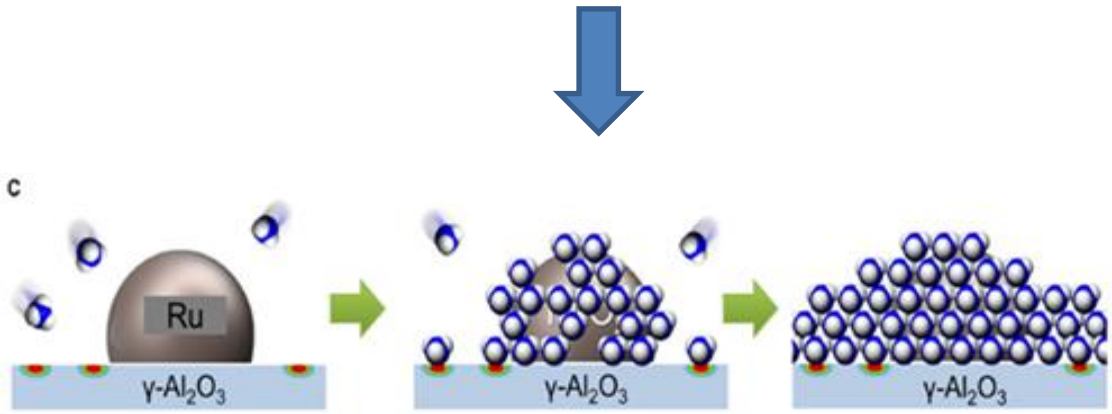
The temperature programed desorption technique is used to measure the number and strengths of base-acids sites on solid catalysts materials[4]. During a TPD experiment, the amount of desorbed molecules is often monitored by mass spectrometry with an increase in desorption temperature. The surface interactions of the probe molecule with the surface of the catalyst are explored with infrared spectroscopy in some instances depending on the research of interest.

Carbon dioxide is often used as an adsorbate for the determination of the strength and amount of basic sites. The temperature at which $CO_2$ is desorbed is then correlated with the strength of the calculated sites. The TPD of adsorbed $CO_2$ has also been used to characterize the basicity of alkali metal and alkaline earth-modified metal oxide catalysts.

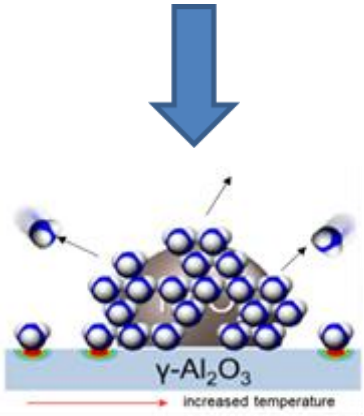
Iso-propylamine is used for the determination of Brønsted acid strength and it is illustrated by the sequence of figures below. Experiments were carried out on an AutoChem 2920 (Micromeritics, USA) instrument. The molecules desorbing were monitored on-line by Cirrus Mass Spectrometer (MKS Instruments) instrument connected directly to the reactor outlet via a heated line.




**Surface preparation** – the cleaning of the oxide surface of the catalyst with He was carried out at 550 °C using a ramp rate of 10 °C/min and held at that temperature for 30 minutes.




**Adsorption or pulse chemisorption** - adsorption of the probing molecule was done at 100 °C, using a ramp rate of 10 °C/min for 10 minutes. 15 pulses of the probe molecule was sufficient to cover the surface of the material.




**Desorption stage** – In this stage of the experiment, molecules are desorbed from the surface of the catalyst with an increased in temperatures to 550 °C, at a ramping rate of 10 °C/min and held for 120 minutes.

### *3.5.6* $H_2$-Temperature programmed reduction-Mass spectroscopy ($H_2$-TPR-MS)

Temperature programmed reduction (TPR) studies were carried out on an AutoChem 2920 (Micromeritics, USA) instrument to study the reducibility of the ruthenium catalysts. Approximately 50 mg sample was placed in quartz U-tube containing quartz wool, fitted with a thermocouple for continuous temperature measurements. The sample was dried under helium flow (50 ml/min) by increasing the temperature from room temperature, at 5 °C/min, to 120 °C where it was held constant for 10 minutes to remove moisture. The sample was then cooled to room temperature and subsequently heated to 1000 °C at 10 °C/min in a flow of 100 % $H_2$ (50 ml/min) and kept at this temperature for 10 minutes. The amount of hydrogen consumed during reduction was measured with a thermal conductivity detector (TCD) monitored on-line by Cirrus Mass Spectrometer (MKS Instruments). $H_2$ consumption and $T_{max}$ position were calculated using AutoChem II V3.05 software.




**Figure 3. 4** AutoChem 2920 (Micromeritics, USA coupled to a Cirrus Mass Spectrometer (MKS Instruments)

### 3.5.7 $H_2$ Chemisorption and $O_2$ titration analysis

Chemisorption analysis is a very useful technique that can be used to determine metal dispersion on a support, metal crystallite size, degree of reduction and the number of active adsorption sites. This process is achieved by adsorbing gaseous molecules onto activated catalyst samples. The analysis procedure can provide the number of active metal sites within the catalyst.

*$H_2$ Chemisorption*

$H_2$-Chemisorption and $O_2$-backtitration studies were carried out using a Micromeritics ASAP 2020 Unit (Micromeritics, USA). Prior to analysis, a pre-weighed catalyst sample of about 0.25 g was placed in a U-shaped quartz tube sample holder (on a bed made up of quartz wool) which was degassed at 80 °C in a Micromeritics ASAP 2020 sample degas unit until the vacuum reached an instrument base pressure, i.e. less than 5 μmHg. The sample was held under this vacuum pressure for 8 hrs. After cooling to ambient temperature, the sample tube was backfilled with a stream of He and then transferred to the analysis port where it was reduced

under the flow of pure $H_2$ (c.a. 100 ml/min) at 425 °C. The flow rate was set using a mass flow controller. After reducing the metal oxide to its metallic state, a static chemisorption was carried out using pure $H_2$ as the adsorbate molecule. Detailed information of the $H_2$-Chemisorption analysis conditions procedure is given in Table 3.3.

**Table 3. 3** Summarized $H_2$-Chemisorption analysis conditions

| Task Number | Task name | Gas | Temperature (°C) | Ramp rate (°C/min) | Time (min) |
|---|---|---|---|---|---|
| ***$H_2$ analysis:*** | | | | | |
| **1** | Evacuation | $H_2$ | 150 | 10.0 | 120 |
| **2** | Flow | $H_2$ | 425 | 5.0 | 240 |
| **3** | Flow | $H_2$ | 400 | 10.0 | 60 |
| **4** | Evacuation | | 100 | 10.0 | 300 |
| **5** | Leak | | 100 | 2.0 | |
| **6** | Analysis | $H_2$ | 100 | 2.0 | |
| ***$O_2$ back titration:*** | | | | | |
| **7** | Evacuation | | 100 | 10.0 | 120 |
| **8** | Evacuation | | 435 | 10.0 | 60 |
| **9** | Analysis | $O_2$ | | | |

*$O_2$ titration analysis*

To determine the degree of reduction (DOR), $O_2$-backtitration was performed on the reduced catalysts. After the $H_2$-Chemisorption experiment was conducted for each sample; the same sample was flushed with He and evacuated at 100 °C to remove all the adsorbed $H_2$. Evacuation then was performed at 400 °C after which $O_2$ titration was carried out using a stream of pure $O_2$ at increasing partial pressures allowing for equilibrium oxidation to occur at each pressure. This titration was carried out at 425 °C.

### 3.5.8 Scanning electron microscopy - Energy dispersive x-ray analysis (SEM- EDX)

The morphology and metal distribution of the support and calcined catalysts was determined using SEM-EDX. The samples were gently swirled in a circular motion a number of times to mix the particles. The sample was then mixed with resin (Struers EpoFix Resin and cure) at room temperature. The resin block was then allowed to cure for 24 hrs. After this time, it was placed in the oven at 70 °C for 1 – 3 hrs. The sample was then ground and polished using the Struers Tegramin-30. Imaging was performed on a Zeiss ULTRA 55 SEM instrument. An acceleration voltage of 3 kV was used as illustrated in the figure below.

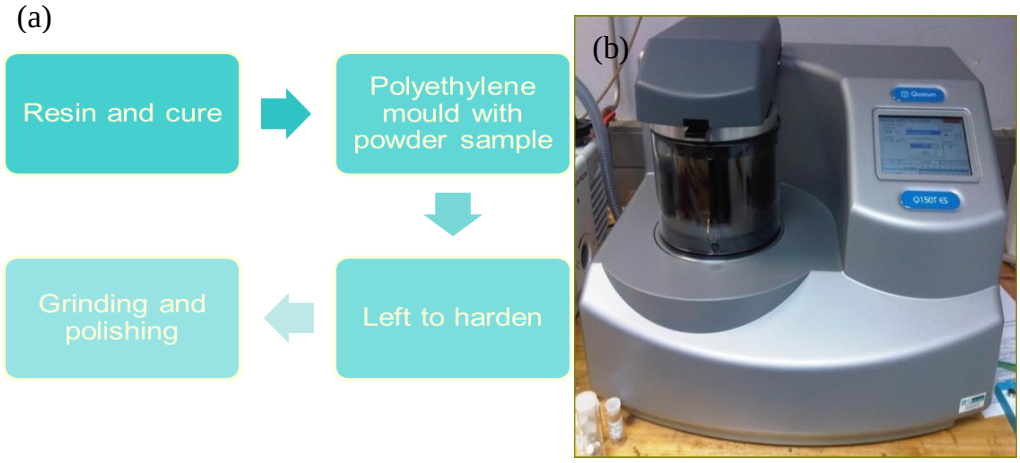



**Figure 3.5** a) Process for SEM resin preparation and (b) Sputter coater instrument

BSE imaging was performed using a Zeiss EVO 40 instrument. Imaging was done at 20 kV with the column under high vacuum. The following settings were kept constant: working distance = 11 mm, probe current 1.6 nA, filament target 2.373 A with the 30 µm aperture. Elemental identification were performed using a Bruker XFlash SDD detector that is controlled by Bruker ESPIRIT software.

Images are taken at various points on the resin block to ensure better representation of the sample. Regions that are selected for imaging are randomly selected, however, it is necessary that the images capture the various distributions present in the sample. Images are taken at 600X magnification.

### 3.5.9 Transmission electron microscopy (TEM)

The TEM is a powerful instrument that can image and analyse features on the nanometre (and sometimes even atomic) scale. It allows the visual observation of materials, which is intuitive for humans. Electrons are generated by a Field Emission Gun (FEG) filament. A series of coils accelerate the electrons down the microscope column, while a series of electromagnetic lenses reduce the size of the beam and shape it into the required form (parallel or converged). The electrons penetrate through the sample (which is required to be very thin), where they can either pass through without being affected, or can undergo various interactions such as elastic and inelastic scattering, generation of x-rays, etc. The transmitted beam or scattered electrons are then collected using a suitable detector or CCD camera.

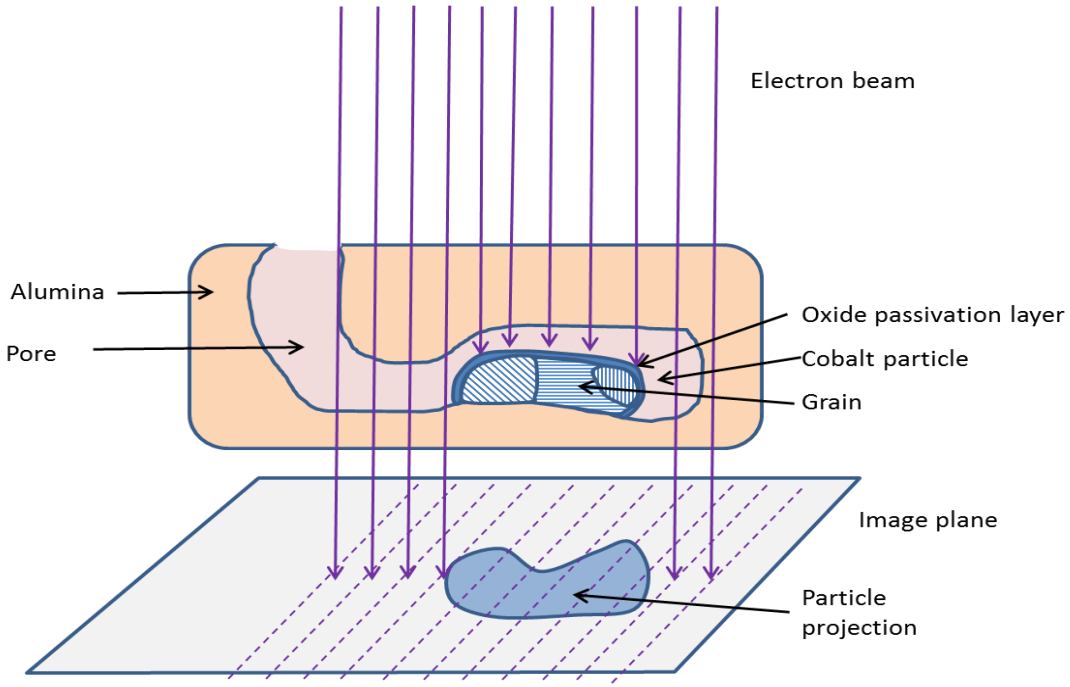



**Figure 3.6** Schematic illustration of the STEM mechanism. The electron beam is scanned across the sample so that a projection of the particle is traced in the image plane[3]

The catalyst materials were mixed inside the glass ampule using a spatula to obtain a randomly distributed sample. A small portion of the sample was then scooped and placed inside a plastic mould. Few drops of ethanol were added on the resin mould to concentrate the solid materials at the base of the mould. The mould was allowed to stand in the fume hood for 30 minutes to ensure that ethanol evaporates off. A freshly prepared TEM resin was then poured over the mould and allowed to cure in an oven set at 70 °C for 18 hrs. The hardened catalyst-resin block was then cooled to room temperature, carefully removed from the mould and transferred to a

Leica Ultramicrotomy unit for cutting. Ultrathin sections of less than 100 nm thickness of the catalyst-resin block were cut using a diamond knife and were floated onto a water surface. The suspended thin sections were then scooped and supported on copper TEM grids, dried in air and stored on TEM-grid holder.

### 3.5.10 HAADF STEM imaging

Images were obtained on the 200 kV FEI Osiris TEM system that is equipped with a Field Emission Gun (FEG) electron source. TEM images were obtained in HAADF STEM mode and EDS mapping using the following beam settings that are ideal for high image resolution;

**Table 3.4** HAADF STEM mode and EDS mapping beam settings

| Parameters | HAADF STEM | EDS mapping |
|---|---|---|
| **Condenser aperture size** | 50 µm | 70 µm |
| **Gun lens setting** | 6 | 4 |
| **Spot size selection** | 5 | 4 |

The images (acquired typically between 40 kx and 160 kx magnifications) are then used is for visual observations or utilised in the automated crystallite size distribution protocol.

## *3.6* Catalytic evaluation

The physical set-up of the rig for the Fischer-Tropsch synthesis is shown in Appendix A, Figure A.1. Gases are supplied from cylinders (Air Products, $H_2$, CO, $CO_2$, Ar) and were fed via mass flow controllers (Brooks 5850S, Brooks Instruments, The Netherlands). During normal operation, argon (used as an internal standard for the sample analysis), hydrogen ($H_2$) and carbon monoxide (CO) was fed to the system via mass flow controllers (MFC-1–3), straight to the reactor. The feed composition was measured with an on-line GC-TCD taken off the stream at sampling point SP-1. The reactor is a 1L slurry bed micro reactor (E-1), equipped with a stirrer. A back-pressure regulator (BPR) is used to maintain and control the total pressure of the system. Heavy liquid hydrocarbon products from the Fischer-Tropsch synthesis were collected in the hot wax trap (E-2). The hot wax trap temperature was set at 210 °C, to ensure efficient collection of the heavy reaction products. Samples of the reactor effluent were taken at the ampoule sampling point SP-2. The effluent was sampled using the ampoule sampling

technique and with an online-GC-TCD. Water and oil products were collected in the cold trap (E-3), at room temperature. The temperature of all the lines after the reactor to the condenser was kept at 210 ℃.

### 3.6.1 Activation of model catalysts

The catalytic performance of the prepared catalysts was tested in a stainless-steel slurry reactor with catalyst loadings of 9 to 10 grams. Before FTS testing the catalysts were activated. The activation method was done in a reduction unit using hydrogen gas, at 2000 ml GHSV, under atmospheric pressure, temperature ramp to 425 ℃, at a heating rate of 1° C/min- hold for 4hrs then cool down to room temperature. The sample was coated in hydrocarbon wax supplied by Sasol, under an inert gas to prevent oxidation. The activation conditions are summarized in Table 3.5 below.

**Table 3.5** Activation of model catalysts conditions

| **Reduction conditions** | |
|---|---|
| **Activation gas** | Hydrogen ($H_2$) |
| **Mass of catalyst** | 9 - 10 g |
| **Pressure** | Atmospheric |
| **Temperature** | 425 ℃ |
| **GHSV (mL/g cat/h)** | 2000 |

### 3.6.2 Fischer-Tropsch synthesis and conditions

After activation, the reactor was loaded with 300 g of polyalphaolefin, a hydrogenated synthetic hydrocarbon base fluid known as Durasyn and thereafter it was closed. The argon line was opened to prevent oxidation, and the temperature was set at 120 ℃. After the reactor had reached the desired temperature, the activated sample was loaded and the reactor closed to reach the Fischer-Tropsch synthesis temperature of 230 ℃. Once at reaction temperature the reactor system was pressurized to 25 bar (absolute) with Ar gas. The synthesis gases were introduced into the reactor in a $H_2$: CO ratio of 2:1. The initial space velocity was set at 8000 ml, but was adjusted to reach the desired CO conversion with time.

**Table 3.6** Fischer-Tropsch synthesis conditions for model catalysts

| **Fischer-Tropsch synthesis (FTS) conditions** | |
|---|---|
| **Mass $_{cat.}$** | 9 - 10 g |
| **H2 :CO ratio** | 2:1 |
| **Temperature** | 230 °C |
| **Pressure** | 25 bar (absolute) |
| **GHSV (mL/g cat/h)** | 8000 |
| **Internal standard gas** | Argon (Ar) |

The flow rates of hydrogen and carbon monoxide relative to the internal gas standard (Ar) were confirmed by on line gas chromatographic analysis over several consecutive feed analyses. The flow of the synthesis gas through the reactor system defined the start of the Fischer-Tropsch synthesis reaction. The progression of the reaction was monitored by regular sampling using a combination of online-TCD and offline-FID (via ampoule sampling) analytical techniques. Once the reaction was completed, the reactor was flushed with argon; thereafter, the stirring stopped and the temperature dropped to 150 °C. After 16 hrs the catalyst was allowed to settle at the bottom of the reactor, while, argon (50 ml (STP).min-1) was passed through the reactor. Once the catalyst had settled at the bottom of the reactor, the temperature was further dropped to room temperature. Thereafter, the wax embedded catalyst sample was removed from the reactor.

### 3.6.3 GC X GC Analysis

For the GC by GC analysis, 0.5 µl of sample was injected in the instrument with an offset modular temperature of 20 °C and a 2$^{nd}$ dimension separation time of 5 s. The carrier gas used was helium with a 1.0 ml/min flow rate and a split ratio of 200:1. A mass spectrometer was connected to the unit with a scan range of 20-500 m/z, the temperature source set at 250 °C and a 100 Hz scan rate. Column 1 conditions was Restek Stabilwax (30 m x 0.25 mm, 0.25 µm) with oven temperature of 40 °C, with a 1 min hold time and then ramped to 260 °C at 3°C/min, held for 5 min. Column 2 conditions was Restek Rxi-5 (2 m x 0.1mm, 0.1 µm) with oven temperature of 45 °C, with a 1 min hold time, ramped to 265 °C at 3°C/min, held for 5 min.

# *References*


(1) Zaera, F.; Ma, Z. Characterization of Heterogeneous Catalysts. *Surf. Nanomolecular Catal.* **2006**, No. May 2006, 1–38.

(2) Vieira Coelho, a. C.; Rocha, G. a.; Souza Santos, P.; Souza Santos, H.; Kiyohara, P. K. Specific Surface Area and Structures of Aluminas from Fibrillar Pseudoboehmite. *Matéria (Rio Janeiro)* **2008**, *13* (2), 329–341.

(3) Technology, G.; Dyk, B. Van; Govender, G.; Breman, B. Comparison of Crystallite Size Measurement Methods. **2015**.

(4) Naturwissenschaften, D. Der. Characterization of Acidic and Basic Properties of Heterogeneous Catalysts by Test Reactions. **2004**.

# Chapter 4

## Characterization of supports and catalysts

## 4.1. Introduction

The aim of this study is to gain a better understanding of the effect of calcination and Mn modification on the acid-base properties of the support as well as of the Ru-based catalysts. Herein, two Ru-based catalysts systems will be investigated, one prepared on base alumina Puralox B21884 (Pu) and the other on calcined Puralox B21884 alumina (PuCal). Characterization results of the alumina supports, Mn-modified supports and Ru-based, Mn-modified catalysts are discussed. A summary of the materials being characterised is represented in Figure 4.1 and the samples will be named as presented in the figure.

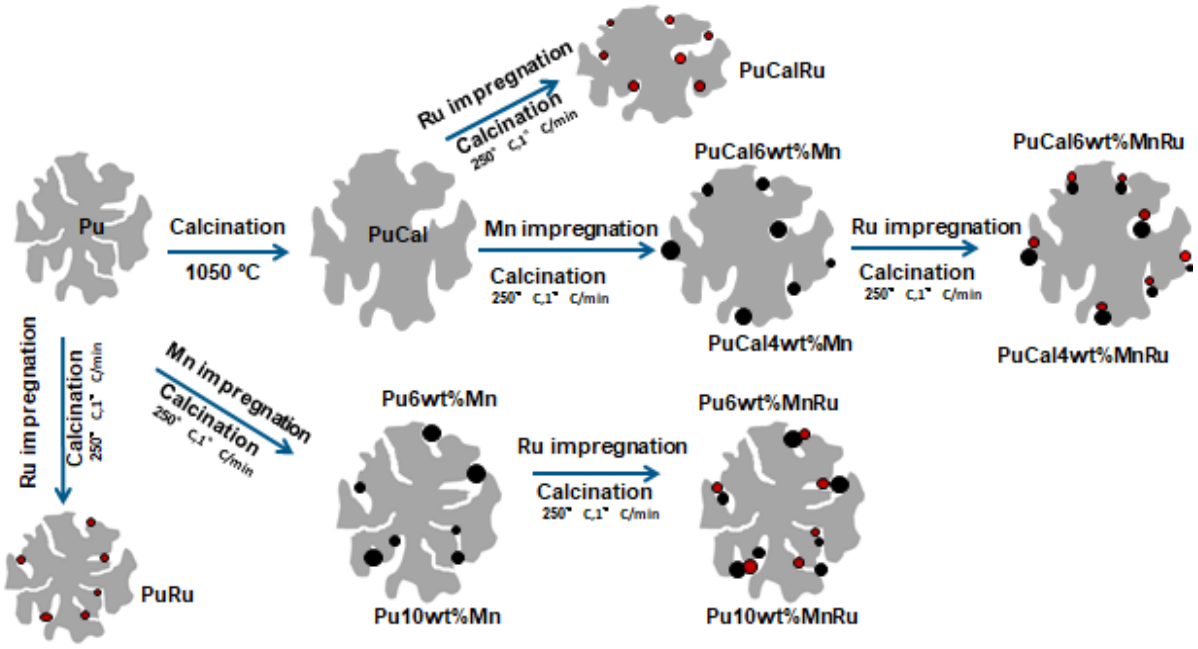



**Figure 4. 1** A summary of all the materials being characterised and their names

## 4.2. Characterization of Pu and PuCal supports

Alumina is widely used as a catalyst support and adsorbent in chemical and petrochemical processes due to its high surface area, wider pore volume, narrow pore sizes, structures, and acid-base characteristics[1]. It is known that increasing pre-treatment temperature modifies the surface area, phase composition of alumina as well as the acid-base properties[2]. High-temperature calcination is a well-known method of reducing total acidity of alumina via dehydroxylation[3].

### 4.2.1. Preliminary results: TG-DTA-MS

A thermogravimetric-derivative thermogravimetry (TG-DTG) analysis of Puralox (Pu) support sample was done to determine the mass loss and phase changes of the support upon thermal treatment as to establish the appropriate calcination temperature for the supports in order to have two support systems with different properties with respect to surface area, pore diameter and phases. Figure 4.2 indicates a total weight loss of about 7.7 % due to volatiles and water. The DTG profile indicates one major weight loss peak with a maximum temperature ($T_{max}$) of 102 °C. This could be due to the loss of physisorbed water on the surface of the support. From the DTA profile, three thermal phase changes were observed. The first phase change had an onset temperature of 156.6 °C, the second 881.9 °C and the final was 999.0 °C.

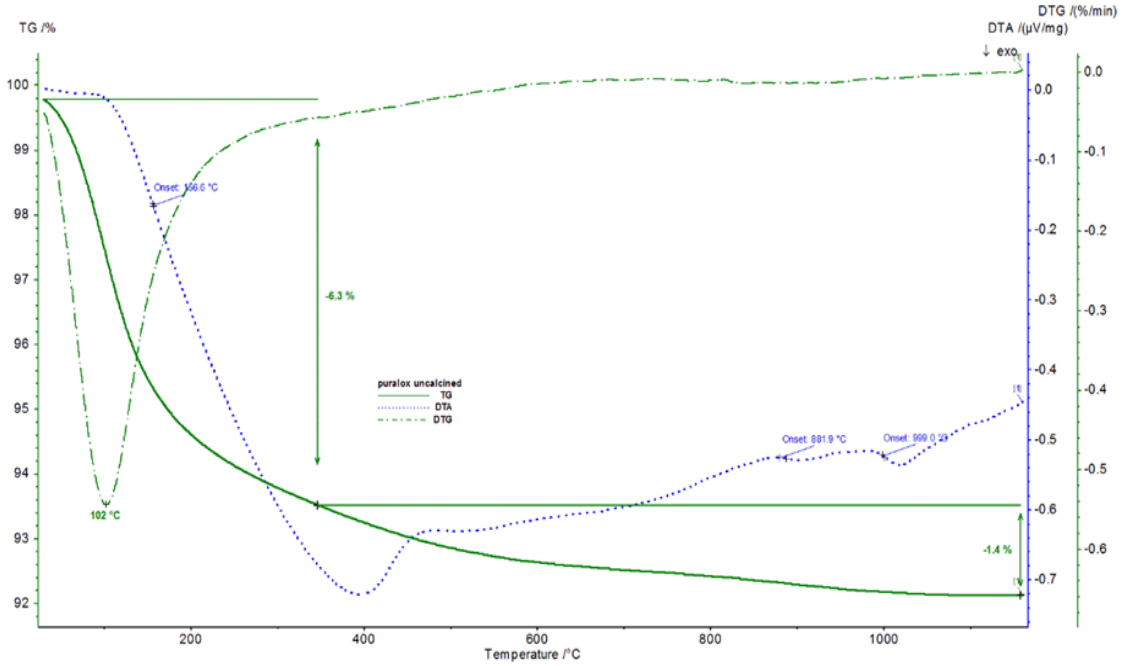



**Figure 4. 2** TG, DTG and DTA profiles of the Puralox support sample

Based on the results obtained in Figure 4.2, the Puralox sample was then calcined at 1050 ºC in a muffle oven under air, at 5 °C/min for 1 hour to ensure that a sample with ±50 % of the original surface area is obtained as determined by BET analysis, to investigate the effect of acid- base properties per surface area. The calcined sample (PuCal) was then used as system 2 to investigate the influence of acid-base properties as a function of calcination temperature, Mn modification and Ru addition. The uncalcined sample [Puralox (Pu)] with predominately ɣ-phase and SA of 162 $m^2/g$ was used as system 1. The surface area was determined using BET analysis while the phase composition was determined using XRD. Acid-base properties are also reported in the chapter by using temperature programmed desorption techniques.

### 4.2.2. Textural and structural properties of the supports

Table 4.1 is an illustration of the textural properties of the supports determined using $N_2$ physisorption (BET). The structural properties were obtained using XRD. BET results confirmed a decrease in the surface area from 162 $m^2/g$ to 97 $m^2/g$ of Pu support to PuCal as a function of temperature, a 40 % decrease in surface area. This is attributed to the changes in the crystallite size of alumina, caused by the destruction of some small pores. Sintering of particles may occur during heat treatment, which could reduce pore volume after calcination at higher temperatures. This was observed in the results, as a decrease of the pore volume from 0.5 to 0.38 $cm^3/g$ was observed. Sintering may also be responsible for decreasing the surface area and increasing the pore size, which is signified by the collapse of porous structure of the low-temperature phases and the consequent diminishing of the surface area, hence an increase in the average pore diameter was observed.

The results of the x-ray diffraction measurements indicated that the two samples represented two different common aluminium structures, as shown in Table 4.1. For the Pu sample, the predominant phase was found to be ɣ-$Al_2O_3$ with 26 % of the sample being the ɵ-$Al_2O_3$ phase. The ɣ-$Al_2O_3$ possess both cubic and tetragonal phases. The PuCal sample contains a mixture of different alumina crystalline phases having ± 50% split of both the gamma and theta alumina as a function of temperature. In terms of the acid-base properties the more aluminium-bonded hydroxyl, the stronger the surface acidity, and the more oxygen involved in the surface bonding, the stronger the surface alkalinity[3]. The Rietveld refinements of the results are in Appendix E. 1 and E.2.

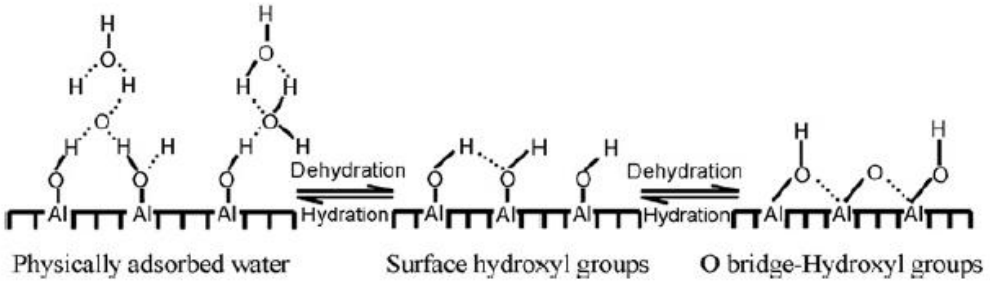



**Figure 4. 3** Dehydration and hydration representation of alumina [3]

**Table 4. 1** XRD and BET results of Pu and PuCal supports

| Sample Name | BET surface area ($m^2/g$) ±6* | BJH Cumulative pore volume ($cm^3/g$) ±0.08* | BJH Pore Diameter (nm) ±1.5* | ɣ -alumina (cubic) | ɣ -alumina (tetragonal) | Theta alumina |
|---|---|---|---|---|---|---|
| Pu | 162 | 0.5 | 8.4 | 39(2) | 34(2) | 26(1) |
| PuCal | 97 | 0.38 | 11.2 | 28(2) | 23(1) | 47(2) |

### 4.2.3. IPA-Temperature programmed desorption

Pulse chemisorption-TPD-MS studies were carried out on an AutoChem 2920 (Micromeritics, USA) instrument coupled with Cirrus Mass Spectrometer (MKS Instruments) to study the Brønsted acid sites (BAS) on the Pu and the PuCal system. When iso-propylamine (IPA) adsorption is performed on the samples, a combination of different molecules (residual amine, propylene and ammonia) desorbs from the sample surface during subsequent TPD. This makes interpretation of the TPD signal very difficult. So, to quantify the Brønsted acid sites (BAS), propylene was isolated using mass spectrometry.

Quantification of Brønsted acidic centres by IPA adsorption is based on the supposition, that Brønsted bonded IPA decomposes to propylene and ammonia at elevated temperatures via Hofmann elimination (Figure 4.4). The adsorption stoichiometry is assumed to be one IPA per acidic proton. This implicitly assumes that (i) the mobility of IPA at low temperatures is sufficiently high for IPA to saturate all surface acid sites and (ii) the chemisorption of an adsorbed molecule at one site does not prevent the adsorption of another molecule at a neighbouring acid site.

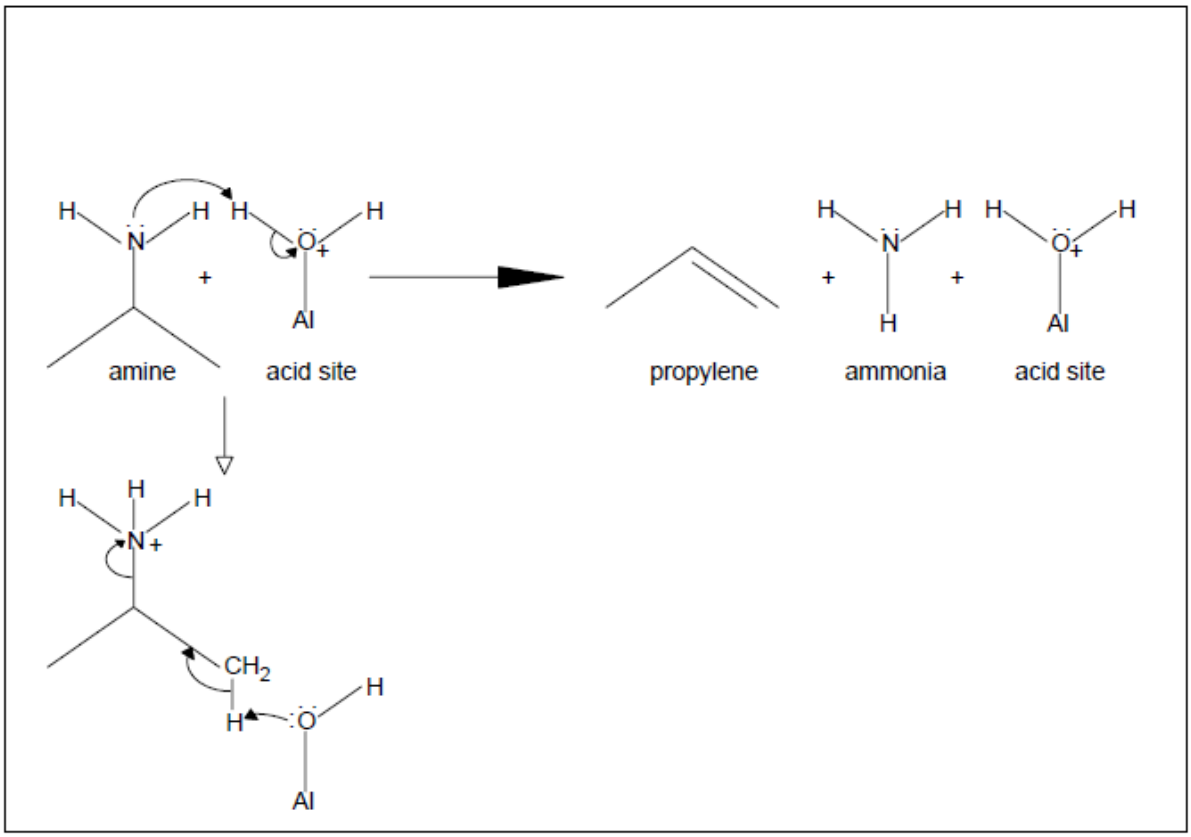



**Figure 4. 4** The schematic showing amine reacting with acid sites to decompose into propylene and ammonia *via* a mechanism analogous to Hofmann elimination[4]

Figure 4.5, is an MS detection of m/e=41, which shows the isolated propylene signal from the IPA-TPD results indicating the relative number of BAS on the support. The area of the desorption peak corresponds to the concentration of the BAS on the surface of the material. A significant difference in the amount of the BAS on these support samples was observed were the Pu sample indicated more BAS than the PuCal support. This is due to the calcination at increased temperatures which resulted in the dehydroxylation of the alumina, hence a decreased BAS is observed. A presence of strong BAS is represented by a peak at higher temperatures and weak BAS represented by a peak at lower temperatures which was observed on the two supports systems as seen in Figure 4.5. Table 4.2 is a summary comparing the BAS results between the Pu and the PuCal support were results links with what was observed in Figure 4.5. The amount of BAS per surface area, was also determined by calculation as also shown in Table 4.2 the last column.

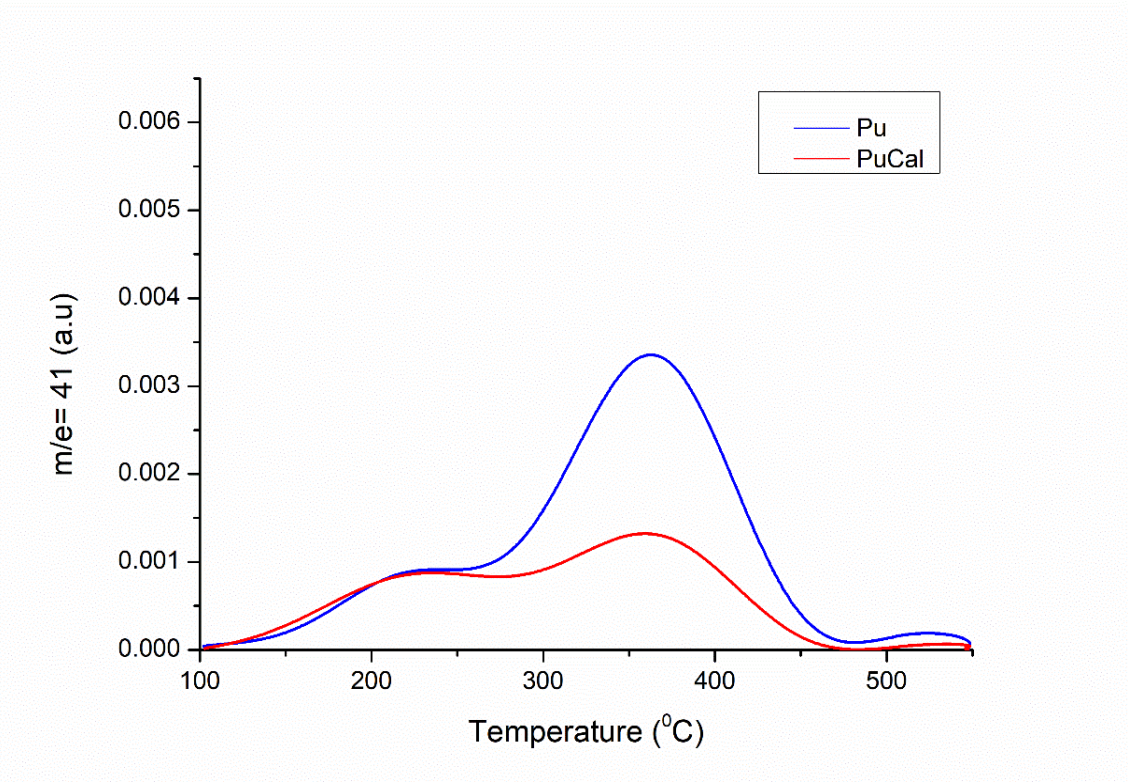



**Figure 4. 5** MS data of evolved propylene on Pu and PuCal supports support

**Table 4. 2** Brønsted acidity of Pu vs PuCal supports

| Pu system | LT-Brønsted acid sites (µmol/g) | HT-Brønsted acid sites (µmol/g) | Total-Brønsted acid sites (µmol/g) | Surface Area ($m^2/g$) | Brønsted * acid sites (µmol/$m^2$) |
|---|---|---|---|---|---|
| **Pu** | 0.91 | 3.36 | 4.27 | 167 | 0.026 |
| **PuCal** | 0.88 | 1.32 | 2.19 | 97 | 0.023 |

**Brønsted acid sites per surface area= Total Brønsted acid sites ÷ Surface area*

### 4.2.4. $CO_2$-Temperature programmed desorption

Basicity studies were carried out on an AutoChem 2920 (Micromeritics, USA) instrument coupled with Cirrus Mass Spectrometer (MKS Instruments) to study the influence of basicity as a function of calcination temperatures. Carbon dioxide (pKa= 6.37), owing to its acidic character, is commonly used to characterize the basicity of solids[5]. To quantify the basic sites, $CO_2$ was isolated using a mass spectrometry and results are shown in Figure 4.6.

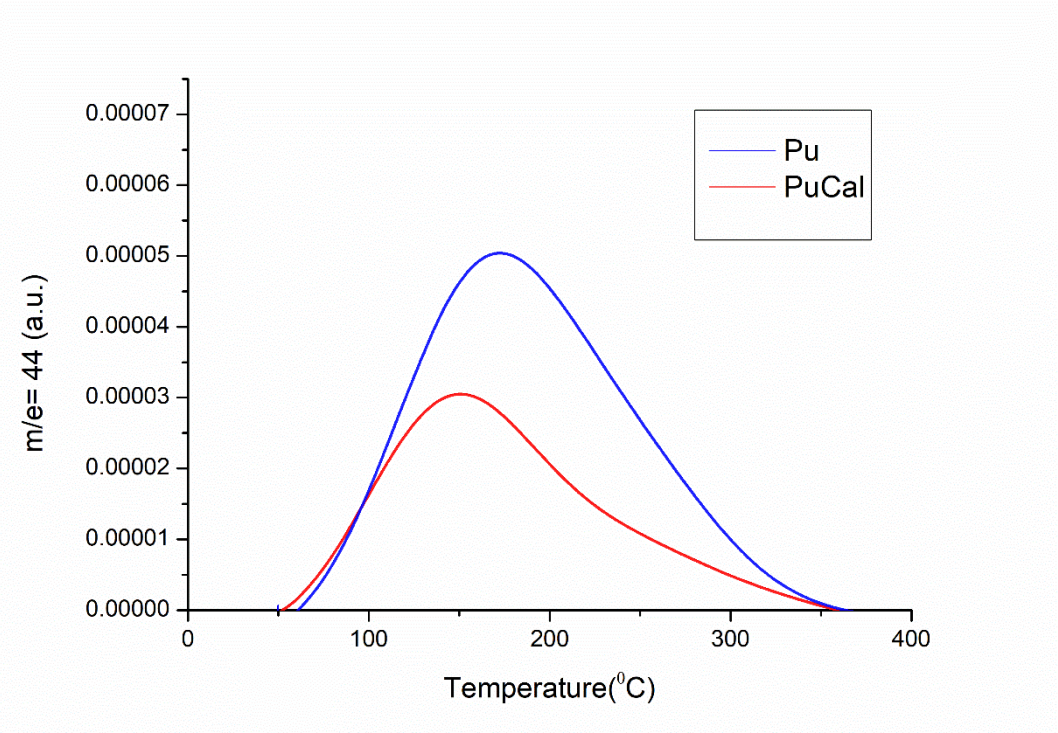



**Figure 4. 6** MS data of evolved $CO_2$ on Pu and PuCal supports support

**Table 4. 3** Basicity results of Pu vs the PuCal supports

| Catalyst systems | Basic sites (µmol/g) | Surface Area ($m^2$/g) | Basic sites* (µmol/$m^2$) |
|---|---|---|---|
| **Pu** | 0.048 | 167 | 0.00029 |
| **PuCal** | 0.030 | 97 | 0.00031 |

**Basicity sites per surface area= Total basicity sites ÷ Surface area*

From the results, both systems showed one peak at lower temperatures (both under 200 °C), which represents the presence of weak basic sites on the samples. A slight shift of the peak towards lower temperatures was observed for the PuCal sample compared to the Pu sample. A smaller peak area of the PuCal sample was obtained compared to the Pu sample, however the amount of basic sites per surface area as calculated in Table 4.3 indicates that calcination temperature does not affect the amount of basic sites on the surface. This also indicates that the change in peak area does not necessarily mean a decrease or increase in the basic sites.

## 4.3. Characterization of Mn-modified Pu and PuCal supports

Both Pu and PuCal supports were modified/impregnated with different amounts of Mn and calcined at 250 °C, at a heating rate of 1 °C/min in air to change the properties of the support. Mn was added using $Mn(acac)_3$ precursor, which is known to be basic in the form $Mn_2O_3$.

Table 4.4 represents the system of Mn addition on both Pu and PuCal supports to investigate the influence of Mn loading per surface area. From calculations the amount of Mn added on PuCal support and the Pu support should be equivalent in terms of grams of Mn per support area for both the first and the second Mn loadings.

**Table 4. 4** A list of Mn modified supports with their corresponding surface areas

| ***System 1*** | ***Surface Area*** | ***System 2*** | ***Surface Area*** |
|---|---|---|---|
| **Pu** | 162 $m^2/g$ | PuCal | 97 $m^2/g$ |
| **Pu/6wt% Mn** ***(6/162 = 0.037gMn/m²)*** | 149 $m^2/g$ | PuCal/4wt% Mn *(4/97 = 0.041gMn/m²)* | 96 $m^2/g$ |
| **Pu/10wt% Mn** ***(10/162=0.062gMn/m²)*** | 146 $m^2/g$ | PuCal/6wt% Mn *(6/97 = 0.062gMn/m²)* | 95 $m^2/g$ |

### 4.3.1. Scanning electron microscopy-energy dispersive X-ray (SEM-EDX)

SEM-EDX was used to determine the distribution of the Mn on the surface of the support as well as to confirm the elemental composition of the samples**.** SEM-backscatter of 6wt% Mn/Pu sample in Figure 4.7 indicate an even distribution of Mn on the surface of the support material. Fluctuations observed in the spectra are voids that are present on the surface of the samples.

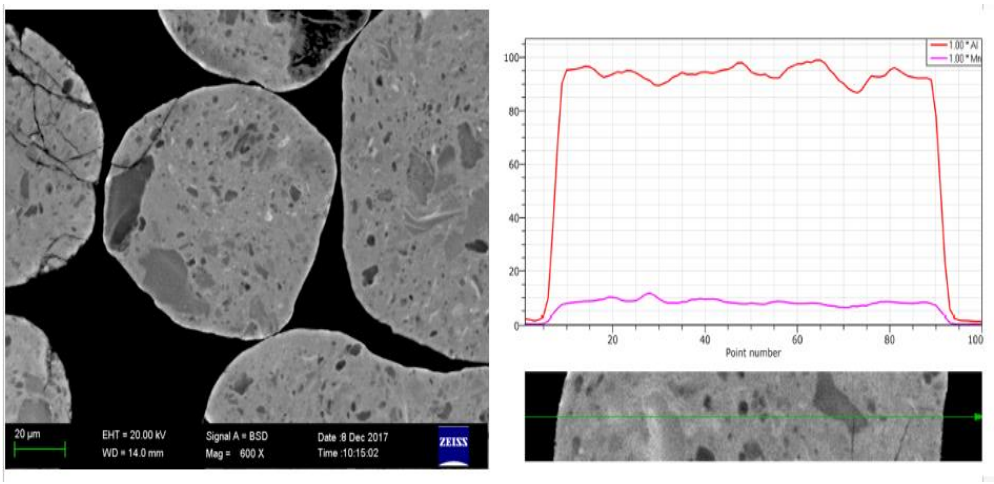



**Figure 4. 7** SEM-Backscatter of Mn modified alumina support (6wt%Mn/Pu)

Elemental identification from the EDX spectra, shows the presence of Mn, Al peaks which correlates with the addition of the precursors used to make these samples ($Mn_2O_3$, $Al_2O_3$). The Cl peak identified within the sample is usually attributed to the epoxy resin used during sample

preparation. The SEM and EDX results shown here applies to all the samples in Table 4.4, and they are also attached in Appendix B.

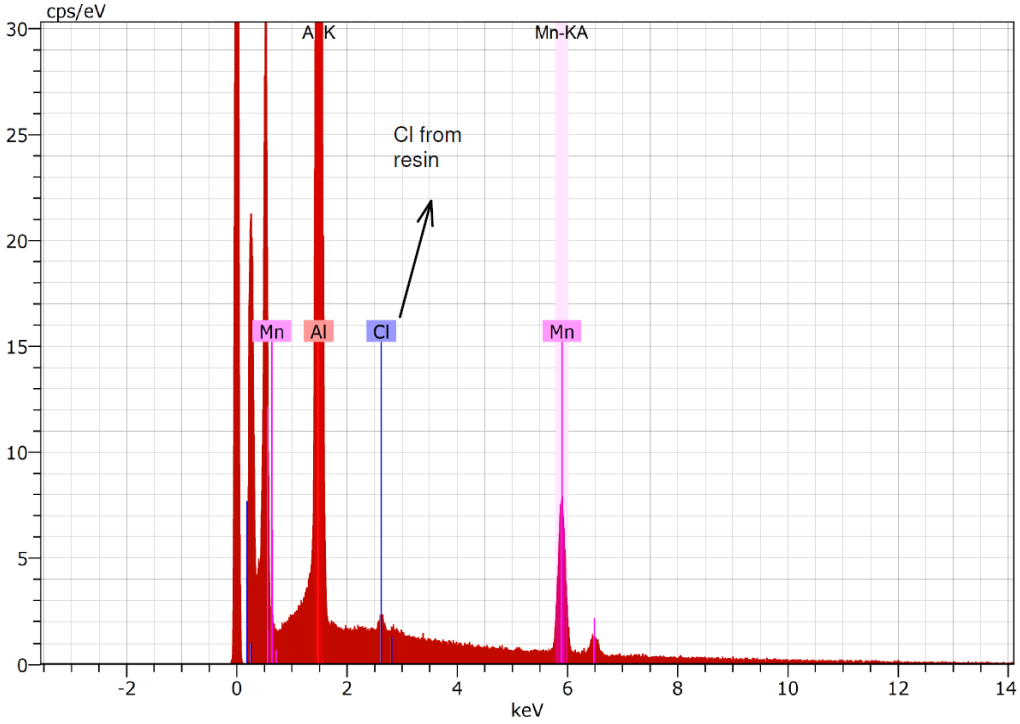



**Figure 4. 8** EDX- spectra of Mn alumina support

### 4.3.2. IPA-Temperature programmed desorption

Pulse chemisorption-TPD-MS studies were carried out on Mn-modified supports to determine the influence of Mn addition on the BAS of the supports as well as the influence of Mn per surface area. The results are discussed focusing on the Pu and the PuCal Mn modified support systems. Figure 4.9 and Figure 4.10 respectively represents the BAS results on the Pu and the PuCal systems respectively as a function of Mn modification, with 6 wt% and 10 wt% for Pu supports and 4 wt% and 6 wt% for PuCal.

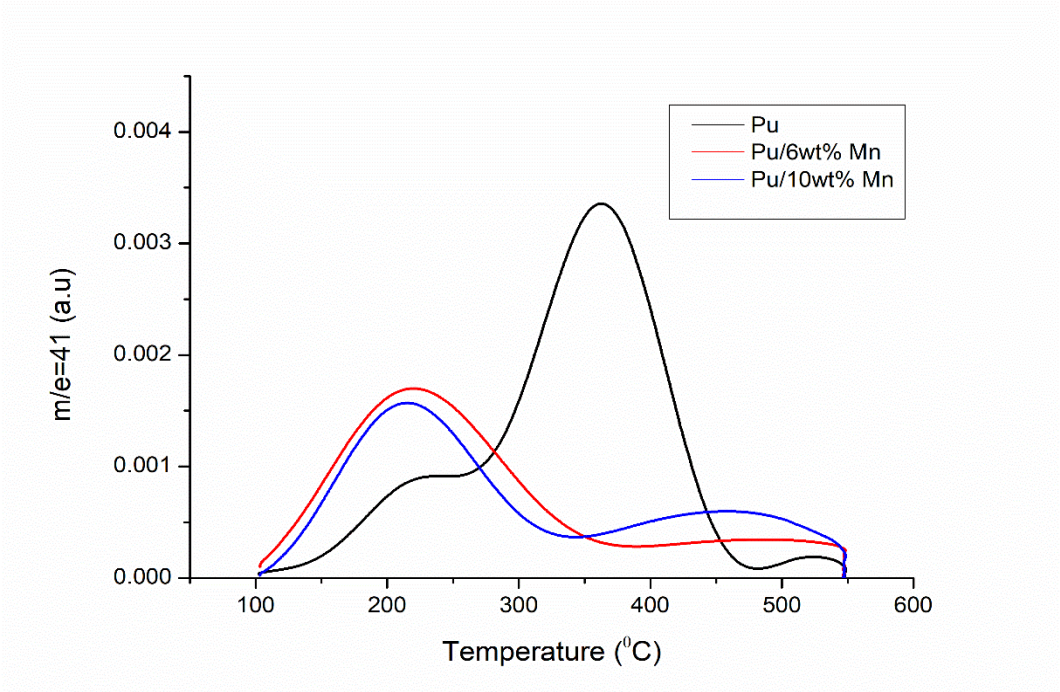



**Figure 4. 9** MS data of evolved propylene on Mn-modified Pu supports

From the results it is observed that the presence of Mn shifts the propylene peak from high temperatures to lower temperatures as a function of increased Mn loading, which implies that Mn occupies the strong BAS. An introduction of a stronger BAS was observed and represented by a broad peak at higher temperatures between 400 - 500 °C. Table 4.5 and 4.6 summarises the BAS concentrations where a decrease in the total BAS as a function of Mn is observed. Comparing the two support systems from the tables, it was observed that the amount of BAS per surface area of Mn loading are equal.

**Table 4. 5** Brønsted acidity results for Mn-modified Pu supports

| Pu system | LT-Brønsted acid sites (µmol/g) | HT-Brønsted acid sites (µmol/g) | Total-Brønsted acid sites (µmol/g) | Surface Area ($m^2$/g) | Brønsted * acid sites (µmol/$m^2$) |
|---|---|---|---|---|---|
| **Pu** | 0.91 | 3.36 | 4.27 | 167 | 0.026 |
| **Pu/6wt% Mn** | 1.7 | 0.48 | 2.18 | 147 | 0.015 |
| **Pu/10wt% Mn** | 1.6 | 0.45 | 2.05 | 146 | 0.014 |

**Brønsted acid sites per surface area= Total Brønsted acid sites ÷ Surface area*

.

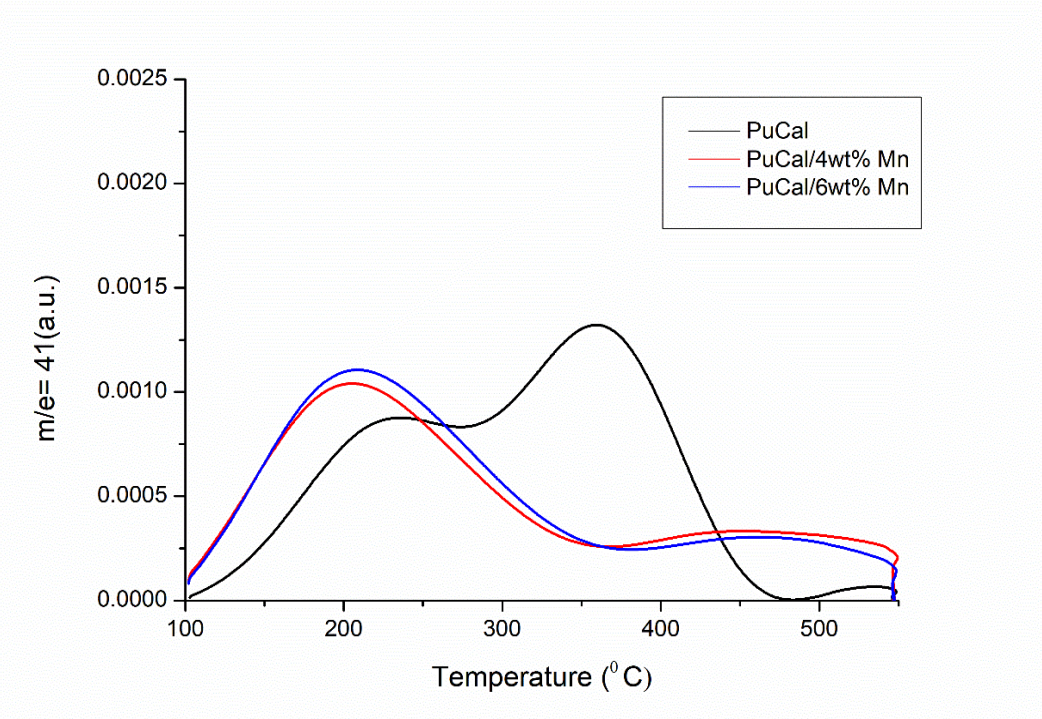



**Figure 4. 10** MS data of evolved propylene on Mn-modified PuCal supports

**Table 4. 6** Brønsted acidity results for Mn-modified PuCal supports

| PuCal system | LT-Brønsted acid sites (µmol/g) | HT-Brønsted acid sites (µmol/g) | Total-Brønsted acid sites (µmol/g) | Surface Area ($m^2/g$) | Brønsted * acid sites (µmol/$m^2$) |
|---|---|---|---|---|---|
| **PuCal** | 0.88 | 1.32 | 2.19 | 97 | 0.023 |
| **PuCal/4wt% Mn** | 1.11 | 0.30 | 1.41 | 96 | 0.015 |
| **PuCal/6wt% Mn** | 1.09 | 0.28 | 1.37 | 95 | 0.014 |

**Brønsted acid sites per surface area= Total Brønsted acid sites ÷ Surface area*

### 4.3.3. $CO_2$-Temperature programmed desorption

Basicity studies were also carried out employing the Pulse chemisorption-TPD-MS technique on Mn-modified supports to determine the influence of different Mn addition. The results are discussed focusing on both the Pu and PuCal catalysts systems.

The peak heights in Figures 4.11 and 4.12 indicates that with increase in Mn addition an increase of basic sites is observed. The amount of basicity per surface area as a function of Mn addition correlated with what observed in the Brønsted acidity results represented in Table 4.6 such that an increase in basicity resulted in a decrease in Brønsted acidity.

Yang *et.al* in the study on Surface acid–base properties and hydration/dehydration mechanisms of aluminum (hydr) oxides state that "on the hydroxylated surface of aluminum oxides, the surface hydroxyl groups may ionize as Brønsted acid or base sites in appropriate circumstances"[3] where the nature of surface sites determines the ability to bind protons, and then the concentration of these sites macroscopically presents acid–base properties. It was observed from the results that when comparing the basicity between the two support systems (Pu and PuCal), the Pu system has more basic sites than the PuCal system. It is stated in above mentioned literature that the surface of gibbsite during dehydration may involve: first the physically adsorbed water being released and then the chemically adsorbed water. Thus the Pu support will have more OH groups as a function of physisorbed water, making it basic. The more aluminum-bonded hydroxyl, the stronger the surface acidity, and the more oxygen involved in the surface bonding, the stronger the surface alkalinity. Hence for the PuCal support, as a function of heat treatment resulted in a more alumina-bounded hydroxyl group.

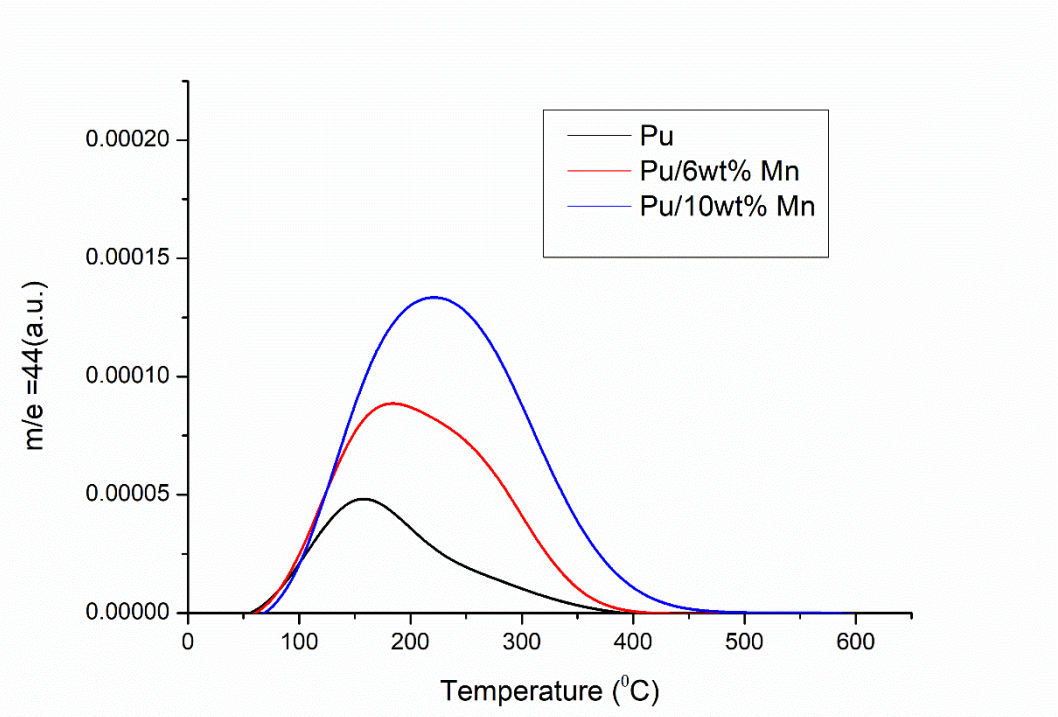



**Figure 4. 11** MS data of evolved $CO_2$ on Pu-Mn modified support

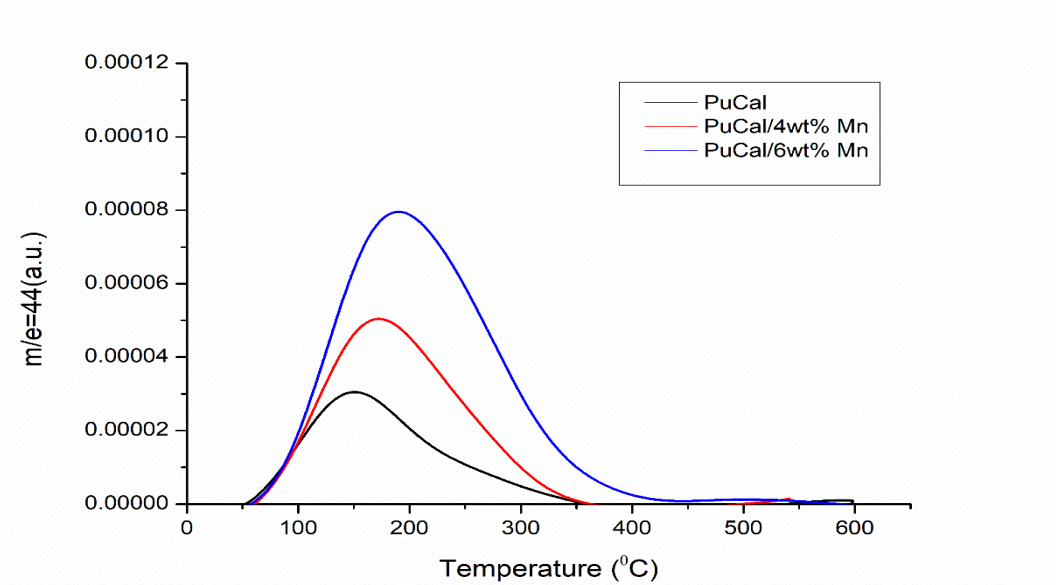



**Figure 4. 12** MS data of evolved $CO_2$ on PuCal-Mn modified support

**Table 4. 7** Summary of Basicity as a function of Mn addition on both the Pu and PuCal systems

| Samples | Surface Area ($m^2/g$) | Basic sites (µmol/g) | Basic* sites (µmol/$m^2$) | Samples | Surface Area $m^2/g$ | Basic sites (µmol/g) | Basic* sites (µmol/$m^2$) |
|---|---|---|---|---|---|---|---|
| **Pu** | 162 | 0.048 | 0.00029 | **PuCal** | 97 | 0.030 | 0.00031 |
| **Pu/6wt%Mn** | 149 | 0.089 | 0.00059 | **PuCal /4wt%Mn** | 96 | 0.050 | 0.00053 |
| **Pu/10wt%Mn** | 146 | 0.133 | 0.00091 | **PuCal /6wt%Mn** | 95 | 0.079 | 0.00084 |

**Basicity sites per surface area= Total basic sites ÷ Surface area*

### 4.3.4. Summary of the characterization results of the Pu and PuCal Mn-modified supports

The supports were successfully modified first through the calcination process and followed by Mn addition as shown by the various characterization results obtained. Characterization results from $N_2$-physisorption, XRD, TPD and SEM-EDX gave a better understanding of the physical and chemical properties of Pu support and the PuCal support system as a function of calcination temperature and Mn addition.

Characterization results from $N_2$-physisorption, indicated a decrease in the surface area and the pore volume as a function of increased calcination temperature while XRD results showed and confirmed the changes in the phases of alumina as a function of increased temperature. SEM-EDX showed that the Mn-modified supports had an even distribution of Mn on the surface. With regards to surface probing techniques, IPA-TPD indicated a shift of high temperature peaks to lower temperatures which indicated that Mn prefers to occupy the stronger acid sites on the alumina surface. However from the BAS calculations it was observed that the amount of Mn per surface area was equal for both Pu and PuCal systems. $CO_2$-TPD showed increased amount of basic sites as a function of a loss in hydroxyl groups of the alumina. The amount of basic sites per surface area for the two systems were comparable. Thus $CO_2$-TPD results complements the IPA-TPD results as Mn addition saw an increase in intensity of the basicity peak on both Pu and the PuCal systems and the actual amount of both basic and acidic sites were comparable.

## 4.4. Characterization of the prepared Ru catalysts

For the preparation of Ru catalysts, the modified Mn-$Al_2O_3$ Pu and PuCal supports were impregnated with the Ru precursor ($Ru(acac)_3$). Metallic Ru in this catalyst is the active metal necessary for the FTS synthesis. Table 4.8 represents the catalysts systems synthesised to investigate the influence of acid-base properties of Ru-based catalysts.

**Table 4. 8 A list of synthesized Ru-based**

| Pu system | PuCal system |
|---|---|
| **Pu/Ru** | PuCal/Ru |
| **Pu/6wt% Mn/Ru** | PuCal/4wt% Mn/Ru |
| **Pu/10wt% Mn/Ru** | PuCal/6wt% Mn/Ru |

### 4.4.1 Metal loading by XRF spectroscopy

The ruthenium and manganese loadings were determined by X-ray fluorescence (XRF) spectroscopy. The results of both Mn and Ru loadings are tabulated below and are based on XRF as a semi-quantitative technique.

**Table 4. 9** XRF analysis for the %Ru & Mn loading on catalyst materials

| Catalyst sample | Desired Ru loading (%) | Ru loading (%) | Desired Mn loading (%) | Mn loading (%) |
|---|---|---|---|---|
| **Pu/Ru** | 2 | 2.2 | 0 | - |
| **Pu/6wt% Mn/Ru** | 2 | 2.5 | 6 | 5.7 |
| **Pu/10wt% Mn/Ru** | 2 | 1.7 | 10 | 8.7 |
| **PuCal/Ru** | 2 | 1.8 | 0 | - |
| **PuCal/4wt% Mn/Ru** | 2 | 2.4 | 4 | 3.7 |
| **PuCal/6wt% Mn/Ru** | 2 | 1.8 | 6 | 5.6 |

### 4.4.2 Textural and structural properties of the catalysts

The textural properties of the catalysts were determined using $N_2$ physisorption (BET) as illustrated in Table 4.10 and the structural properties were by using XRD.

**Table 4. 10** The composition and textural properties of the Pu and the PuCal catalysts systems

| Sample Name | BET surface area ($m^2/g$) ±6* | BJH Cumulative pore volume ($cm^3/g$) ±0.08* | BJH Pore Diameter (nm) ±1.5* | XRD $RuO_2$ Relative abundance (%) | XRD $MnAl_2O4$ Relative abundance (%) | XRD $Mn_3O_4$ Relative abundance (%) | $RuO_2$ Area weighted ACS (nm) |
|---|---|---|---|---|---|---|---|
| **Pu/Ru** | 156 | 0.48 | 8.4 | 2(0.1) | - | - | 11(0.2) |
| **Pu/6wt% Mn/Ru** | 148 | 0.43 | 8.4 | 2(0.1) | 5(0.6) | 4(0.4) | 9(0.2) |
| **Pu/10wt% Mn/Ru** | 139 | 0.40 | 8.2 | 2(0.1) | 8(0.8) | 4(0.5) | 11(0.3) |
| **PuCal/Ru** | 102 | 0.38 | 11.4 | 3(0.1) | - | - | 6(0.2) |
| **PuCal/4wt% Mn/Ru** | 99 | 0.36 | 11.2 | 2(0.1) | 5(0.6) | 4(0.4) | 9(0.2) |
| **PuCal/6wt% Mn/Ru** | 38 | 0.14 | 10.8 | 2(0.1) | 5(0.6) | 4(0.4) | 5(0.2) |

BET results indicate a drop in surface area, pore volume as well as the pore diameter as a function of Ru and Mn addition. This effect is attributed to the pre-treatment condition of the supports via the calcination process.

From the XRD results, a consistent relative abundance of 2 % of the $RuO_2$ phase and the relative abundance of $MnAl_2O_4$ was consistent with the Mn loadings as reported by XRF. The average $RuO_2$ crystallite size results in Table 4.10 indicate no consistent trend with relation to an increased Mn addition however smaller $RuO_2$ crystallite sizes of about 5 nm were observed for the PuCal system when compared to the Pu system with an average crystallite size of 11 nm. The difference in the $RuO_2$ crystallite sizes between the two systems can be attributed to the difference in the surface area and pore volume of the support as a function of calcination. Rietveld refinement results for the catalysts are provided in Appendix E.

### 4.4.3 SEM-EDX for catalysts systems

SEM-Backscatter for catalysts systems was employed to determine the distribution of both Ru and Mn on the surface of the support and EDX to confirm the elemental composition. SEM-backscatter in Figure 4.13 indicate an even distribution of Ru and Mn on the surface of the support material as anticipated which means the catalysts were successfully synthesised. Figure 4.13 below is a representation of all catalysts synthesised in this study (refer Appendix C).

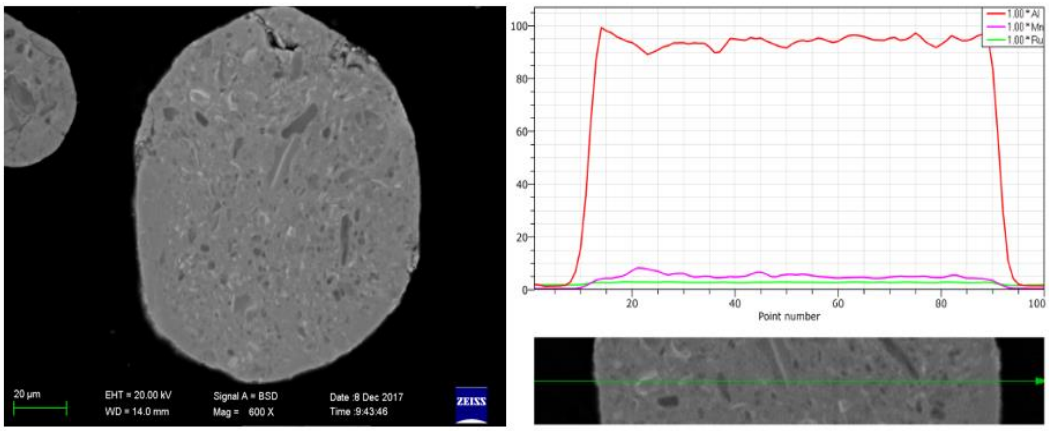



**Figure 4. 13** SEM-back scatter of Pu/6wt%Mn/Ru

### 4.4.4 IPA-Temperature programmed desorption

Figure 4.14 is a representation of the Brønsted acidity results of the Pu system as a function of Ru addition on the Mn modified alumina catalysts. Results indicate a shift of the propylene

peak from high temperatures to lower temperatures as a function of Ru addition, and the broad peaks which were introduced by Mn modification at higher temperatures are completely removed. This implies that Ru is basic and it prefers to sit on the strongest acid sites. Table 4.11 is a summary of the trends observed for the Pu support system (Figure 4.14), where a decrease in the total amount of BAS is observed as a function of Mn addition and further Ru addition.

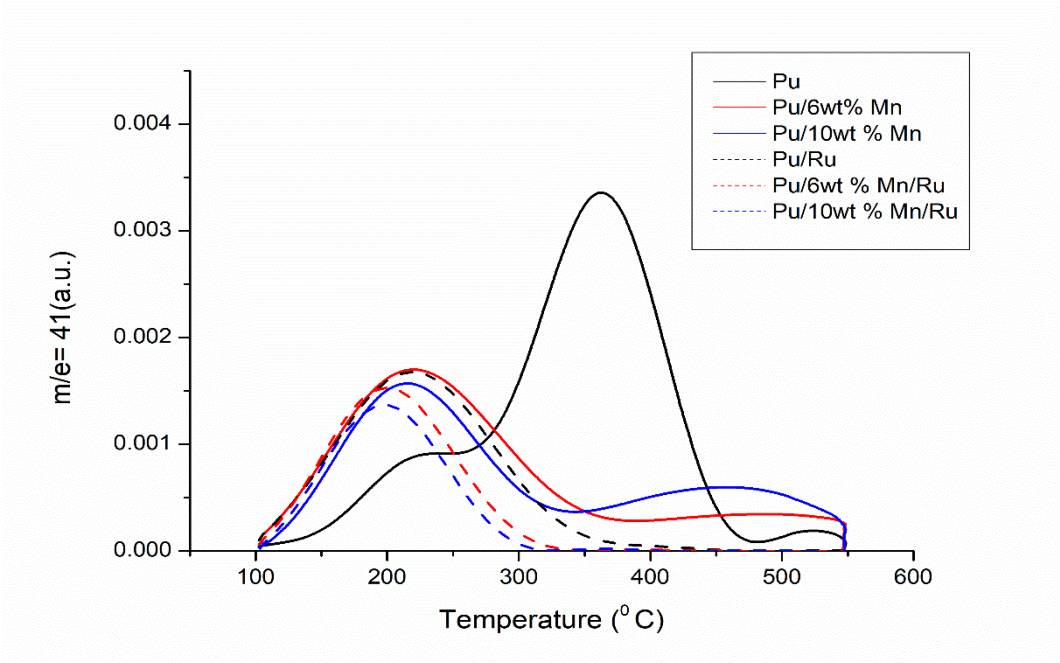



**Figure 4. 14** MS data of evolved propylene on Pu support system

**Table 4. 11** Summary of BAS of Ru on Mn modified catalysts for Pu system

| Pu system | LT-Brønsted acid sites (µmol/g) | HT-Brønsted acid sites (µmol/g) | Total-Brønsted acid sites (µmol/g) | Surface Area $m^2/g$ | Brønsted* acid sites (µmol/$m^2$) |
|---|---|---|---|---|---|
| **Pu** | 0.91 | 3.36 | 4.27 | 167 | 0.026 |
| **Pu/6wt% Mn** | 1.7 | 0.48 | 2.17 | 147 | 0.015 |
| **Pu/10wt% Mn** | 1.6 | 0.45 | 2.05 | 146 | 0.014 |
| **Pu/Ru** | - | - | 1.68 | 156 | 0.011 |
| **Pu/6wt% Mn/Ru** | - | - | 1.53 | 148 | 0.010 |
| **Pu/10wt% Mn/Ru** | - | - | 1.37 | 139 | 0.009 |

**Brønsted acid sites per surface area= Total Brønsted acid sites ÷ Surface area*

From the PuCal catalyst system, the BAS results do not seem to have any clear trend as a function of Ru addition (Figure 4.15 and Table 4.12). The PuCal/6wt% Mn/Ru catalysts has the highest basicity of the three catalysts, whereas the PuCal/4wt% Mn/Ru indicate two peaks instead of one peak. There is no clear explanation of the differences in these profiles but the two peaks do not seem to influence the total amount of BAS on this catalyst compared to the samples with only one peak. Comparing the two catalysts systems which are the Pu and the PuCal, there are no similarities with regards to the amounts of BAS per surface area as a function of Ru addition as was observed initially after Mn modification.

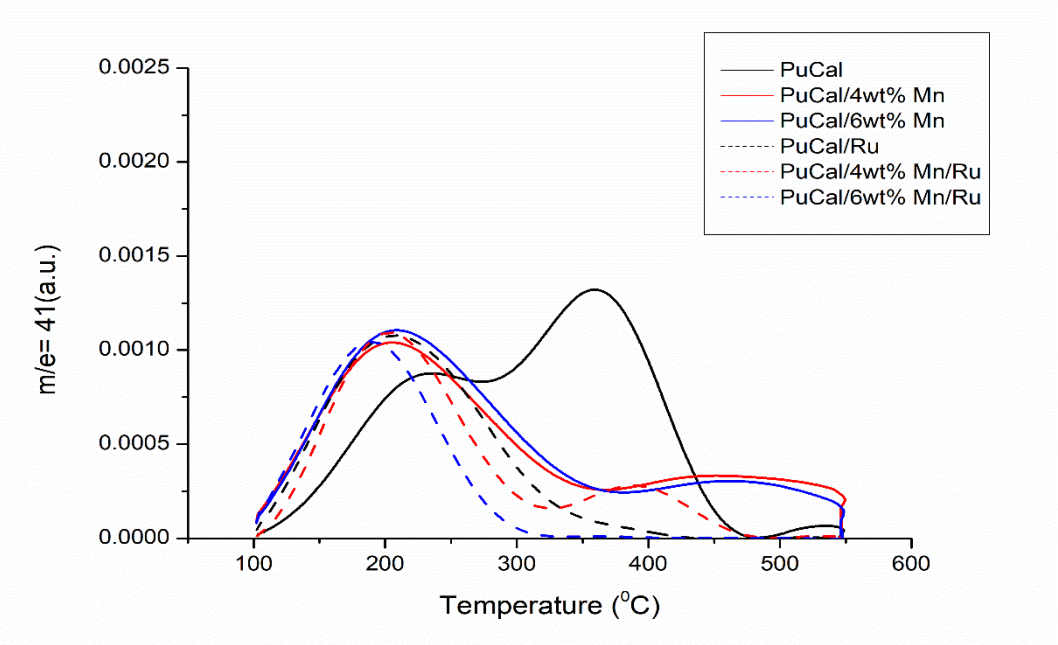



**Figure 4. 15** MS data of evolved propylene on PuCal and Pu support

**Table 4. 12** Summary of BAS of Ru on Mn modified catalysts for PuCal system

| PuCal system | LT-Brønsted acid sites (µmol/g) | HT-Brønsted acid sites (µmol/g) | Total-Brønsted acid sites (µmol/g) | Surface Area ($m^2/g$) | Brønsted* acid sites (µmol/$m^2$) |
|---|---|---|---|---|---|
| **PuCal** | 0.88 | 1.32 | 2.19 | 97 | 0.023 |
| **PuCal/4wt% Mn** | 1.11 | 0.30 | 1.41 | 96 | 0.015 |
| **PuCal/6wt% Mn** | 1.09 | 0.28 | 1.37 | 95 | 0.014 |
| **PuCal/Ru** | - | - | 1.80 | 102 | 0.0176 |
| **PuCal/4wt% Mn/Ru** | 1.09 | 0.28 | 1.37 | 99 | 0.0138 |
| **PuCal/6wt% Mn/Ru** | - | - | 1.04 | 38 | 0.0274 |

**Brønsted acid sites per surface area= Total Brønsted acid sites ÷ Surface area*

### 4.4.5 $CO_2$-Temperature programmed desorption

Basicity results in Figure 4.16 and Table 4.13 for the Pu system after Ru addition are represented below. Results indicate that Ru/Pu catalyst has more basic sites compared to the Pu support confirming the basic nature of ruthenium. Addition of Ru to Pu/6wt %Mn modified support caused a decrease in the basic sites however on the Pu/10wt%Mn support, the addition of Ru increased the basic sites. Thus on the catalysts prepared there is no particular trend that is observed. A similar trend is observed for the PuCal catalyst system, where a drop in basicity is observed for Ru addition on the PuCal/4wt%Mn support and an increased basicity with Ru addition on the PuCal/6wt%Mn support. The results are represented in Figure 4.17 and Table 4.14 and from the calculation done there are no similarities looking at the amount of basic sites per surface area.

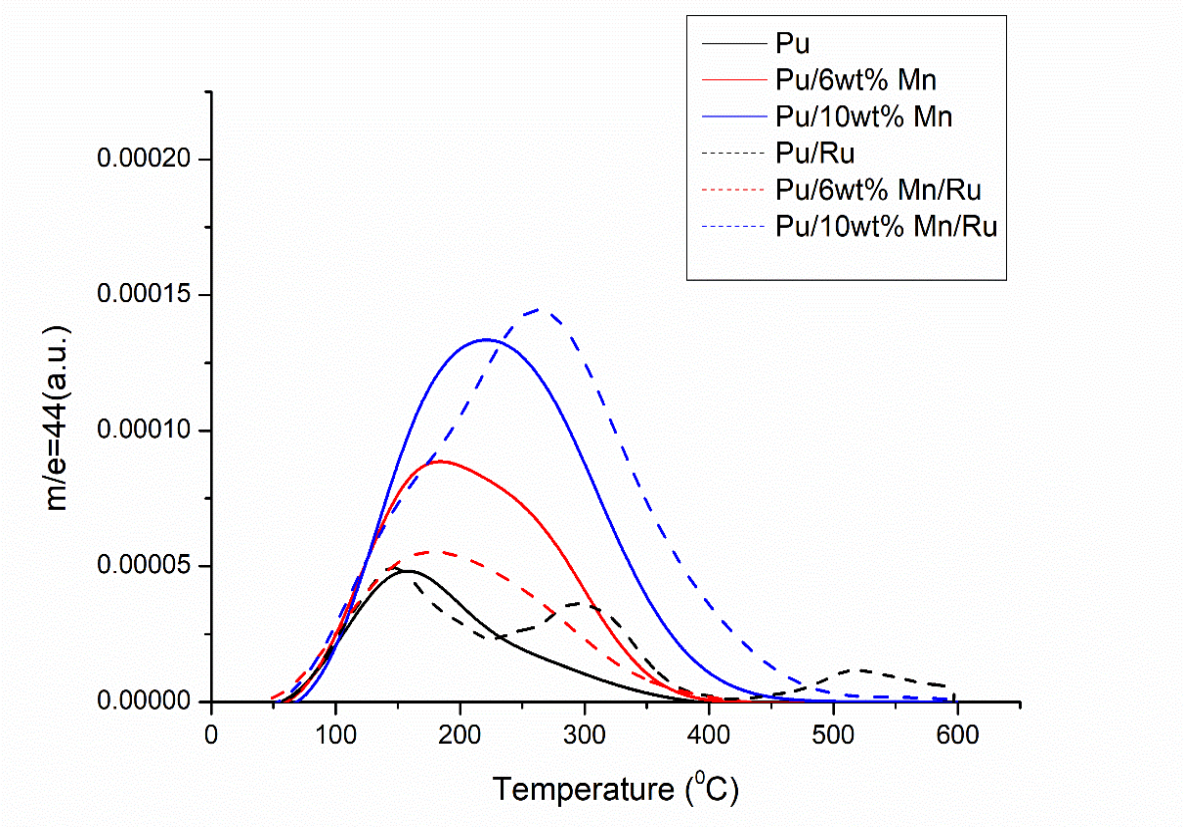



**Figure 4. 16** MS data of evolved $CO_2$ on Pu catalysts system

**Table 4. 13** Summary of Basicity of Ru on Mn modified catalysts for Pu system

| Pu system | LT-Basic sites (µmol/g) | HT-Basic sites (µmol/g) | Total-Basic sites (µmol/g) | Surface Area ($m^2$/g) | Basic* sites (µmol/$m^2$) |
|---|---|---|---|---|---|
| **Pu** | - | - | 0.048 | 167 | 0.00029 |
| **Pu/6wt% Mn** | - | - | 0.089 | 147 | 0.00059 |
| **Pu/10wt% Mn** | - | - | 0.133 | 146 | 0.00091 |
| **Pu/Ru** | 0.049 | 0.036 | 0.086 | 156 | 0.00055 |
| **Pu/6wt% Mn/Ru** | - | - | 0.055 | 148 | 0.00037 |
| **Pu/10wt% Mn/Ru** | - | - | 0.145 | 139 | 0.001 |

***Basicity sites per surface area= Total basic sites ÷ Surface area***

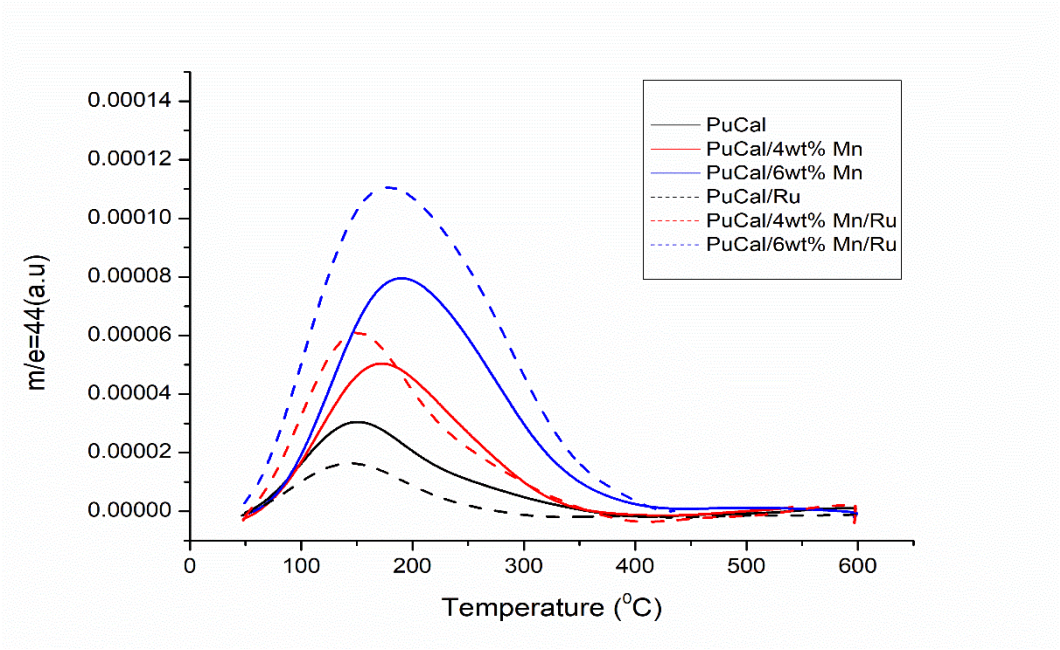



**Figure 4. 17** MS data of evolved $CO_2$ on PuCal catalysts system

**Table 4. 14** Summary of Basicity of Ru on Mn modified catalysts for PuCal system

| PuCal system | Total-Basic sites (µmol/g) | Surface Area $m^2$/g | Basic* sites (µmol/$m^2$) |
|---|---|---|---|
| **PuCal** | 0.030 | 97 | 0.00031 |
| **PuCal/4wt% Mn** | 0.050 | 96 | 0.00053 |
| **PuCal/6wt% Mn** | 0.079 | 95 | 0.00084 |
| **PuCal/Ru** | 0.016 | 102 | 0.0016 |
| **PuCal/4wt% Mn/Ru** | 0.061 | 99 | 0.0006 |
| **PuCal/6wt% Mn/Ru** | 0.111 | 38 | 0.0029 |

** Basicity sites per surface area= Total basic sites ÷ Surface area*

### 4.4.6 TEM-Elemental mapping

TEM results with elemental mapping was done to observe the distribution and site occupancy of both Mn and Ru on the catalysts surface. Figure 4.18(a) is TEM images of an oxidised PuCal/6wt%Mn/Ru catalyst and Figure 4.18(b) is TEM images of oxidised Pu/10wt%Mn/Ru catalyst. From the results it was observed that Mn has big crystallite sizes compared to the Ru crystals. The crystallite size of Mn was more pronounced for the 10 wt% Mn loading compared to the 6 wt% Mn loading. Although Mn and Ru are in close proximity with each other, visually they seem to occupy different positions on the catalyst surface.

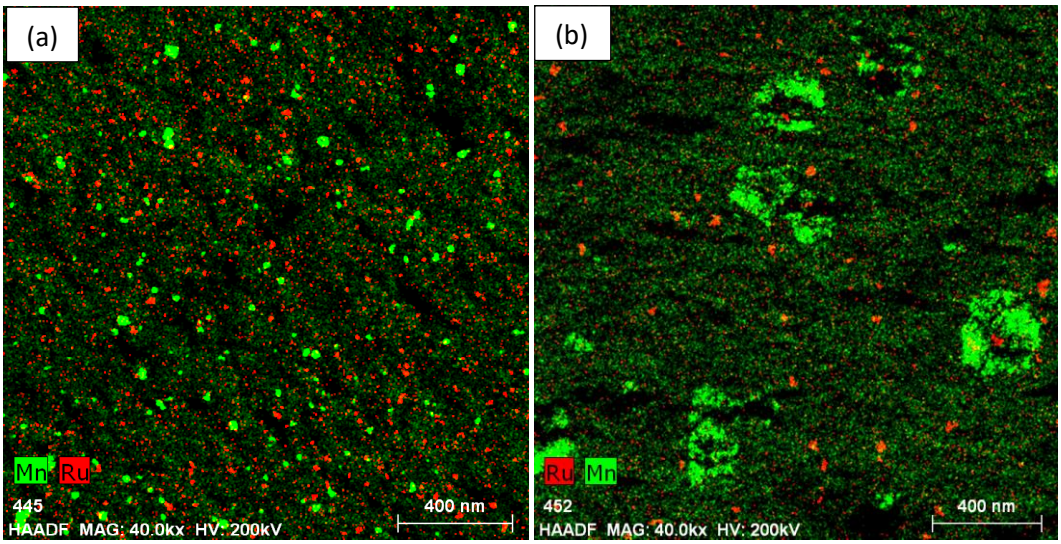



**Figure 4. 18** (a) PuCal/6wt%Mn/Ru; (b) Pu/10wt%Mn/Ru before reduction

To understand the promotional effect of Mn in the Ru catalyst system, it is important to understand the location of both metals and their interaction to give better insight of the results. Since FT activity testing happens after the catalysts is activated and not with the oxidised sample, it was then suggested to reduce the catalysts, and observe the interaction of Mn and Ru on the surface. Figure 4.19(a) and Figure 4.19(b) are the TEM images before and after reduction respectively. After reduction, a decrease in the crystallite size of Mn is observed, which indicate re-dispersion of Mn under reducing conditions. Migration of Mn is also observed as Mn and Ru become co-localised. It is suspected that the presence of these Mn compounds near the $Ru^0$ influences the electronic properties of these sites, and the FTS testing of these catalysts will have a better influence on this interaction.

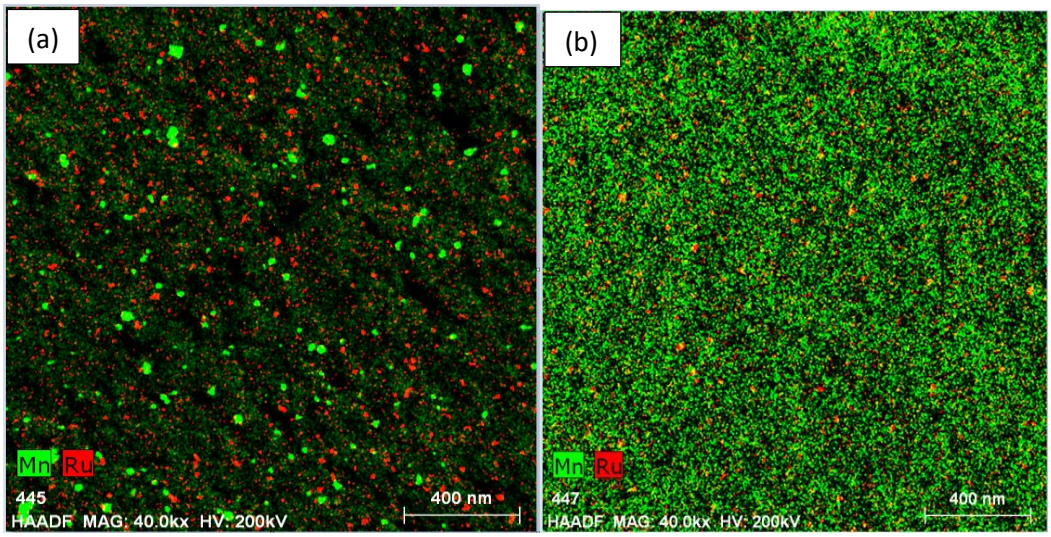



**Figure 4. 19** (a) PuCal/6%Mn/Ru before reduction; (b) PuCal/6%Mn/Ru after reduction

### 4.4.7 Temperature Programed Reduction of catalysts (TPR) & In-Situ XRD

$H_2$-TPR technique was employed to investigate the optimum temperature where ruthenium reduces as well as the effect of Mn addition on the reduction behaviour of the catalysts. The TPR profiles of the $H_2$ absorption results are presented in Fig. 4.20 and Figure 4.21.

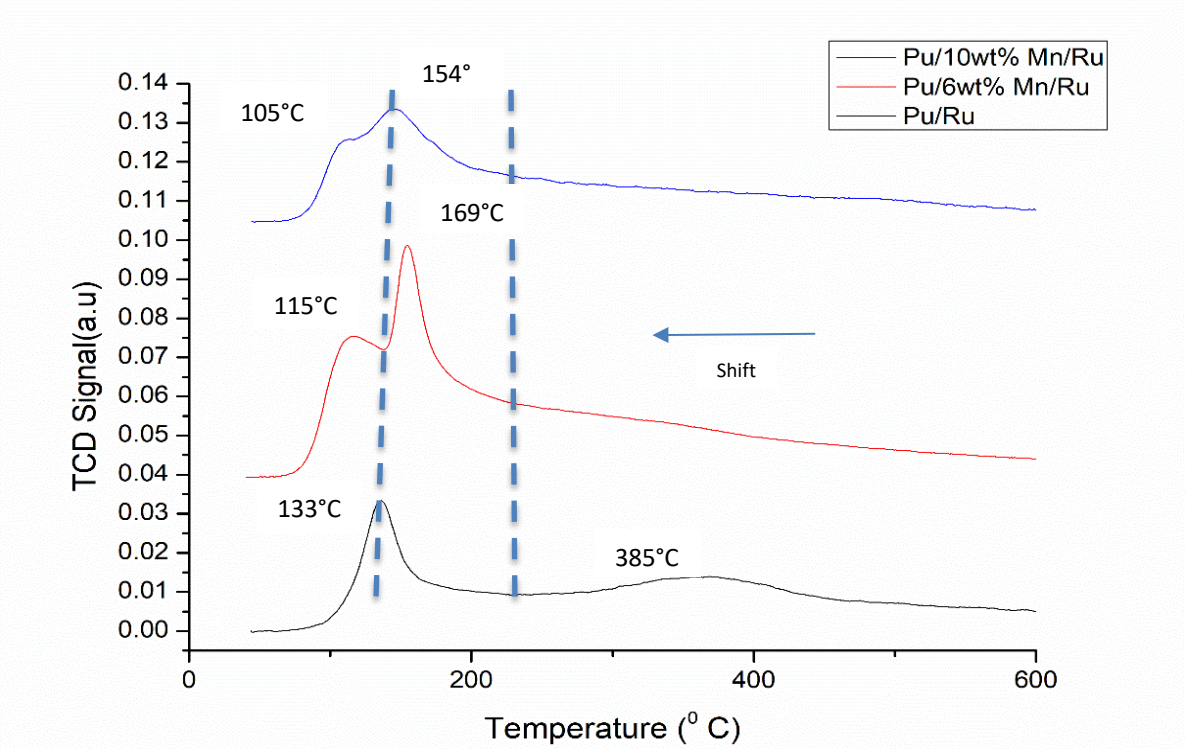



**Figure 4. 20** TPR profiles of the Pu system

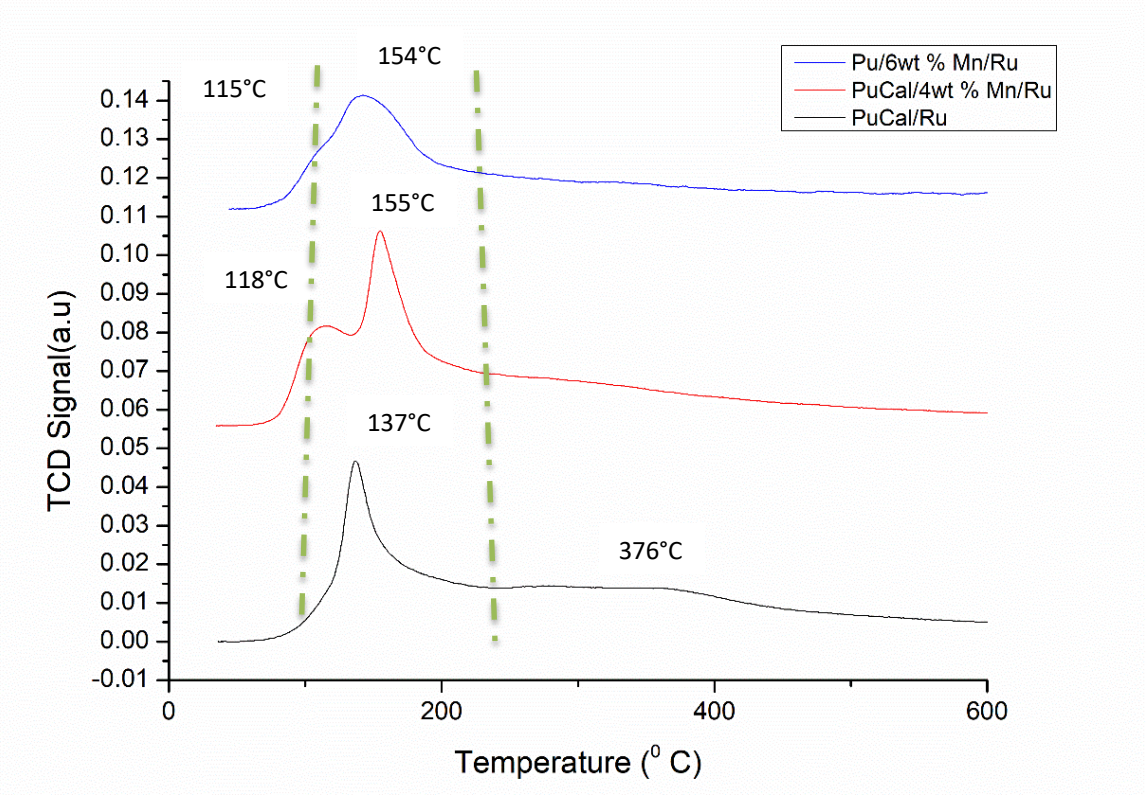



**Figure 4. 21** TPR profiles of the PuCal system

From literature, Ru based catalysts indicated either a one-step reduction reaction or two step reduction as represented by Equation 4.1 and 4.2 below[6].

$$RuO_2 + H_2 \longrightarrow RuO + H_2O$$
$$RuO + H_2 \longrightarrow Ru + H_2O \quad \text{.....Eq4.1}$$

$$RuO_2 + H_2 \longrightarrow Ru + H_2O \quad \text{.....Eq4.2}$$

Narunnabi *et al*. attributes the difference in the peak profiles as a function of the Ru precursor used for catalysts synthesis as well as the kind of support used[7,8]. In their studies Narunnabi *et al*. saw a one reduction peak for unpromoted $Ru/Al_2O_3$ catalysts and two reduction peaks for their Mn promoted catalysts system. The reduction at higher temperatures is always attributed to the transition from $RuO_2$ to $Ru^0$. When two peaks are observed as in the study of the effect of ruthenium precursors on $Ru/Mn/Al_2O_3$ and $Ru/Al_2O_3$ catalysts, the first shoulder peak observed in their TPR profiles is attributed to possible reduction of incompletely decomposed $Ru(C_5H_7O_2)_3$. Based on their work, a similar trend is also observed for all TPR

profiles in this study and In-situ XRD results in Figures 4.22 and 4.23 supports the observation made.

Pu/Ru and PuCal/Ru catalysts indicate one reduction peak at 133 °C and 137 °C respectively, which is attributed to the reduction of $RuO_2$ to metallic $Ru^0$. The broader peak observed at higher temperatures (±380 °C), is attributed to strong metal support interaction of Ru and alumina. In the Mn modified catalysts systems, two reduction peaks are observed. The first peak at lower temperatures is attributed to incompletely decomposed $Ru(C_5H_7O_2)_3$ as also reported by Narunnabi *et al*. The second reduction peaks observed at ±160 °C, is attributed to the reduction of $RuO_2$ to $Ru^0$. On the influence of Mn addition, the presence of Mn seems to retard reduction as a delay in the reduction peak is observed in both the Pu and the PuCal system. A similar trend was observed in Narunnabi *et al.*'s work, where delayed reduction peaks of the $Ru/Mn/Al_2O_3$ catalyst with respect to the $Ru/Al_2O_3$ was observed: The delay is attributed to the Mn-species interaction with the Ru which forces the $RuO_2$ phase to be reduced at a higher temperature. This observation was also supported by the TEM results, where after reduction, Ru-Mn appear co-localised.

Since it was stated above that reduction can either occur in a single step or occur in two steps, in-situ x-ray diffraction was performed on the Pu/Ru and PuCal/6wt%Mn/Ru catalyst to establish the correct reduction reaction for the prepared catalyst system. Results indicate that the starting phase of ruthenium is $RuO_2$ represented in 100 °C plot in Figure 4.22. With increase in temperatures, $RuO_2$ reduces to Ru in a single step as the RuO phase could not be identified, this is observed in the 300 °C plot in Figure 4.22. Similar to what is observed in Figure 4.22, the transition of $RuO_2$ in plot 100 °C to Ru in 300°C was observed in Figure 4.23. For Figure 4.2.3, the differences are observed clearly when the two plots are overlaid. This then confirms the stoichiometry of the reduction system to be 1:1. There was no need to perform a phase identification analysis in this regards as this was not the purpose of perfuming in situ x-ray diffraction analysis on these samples.

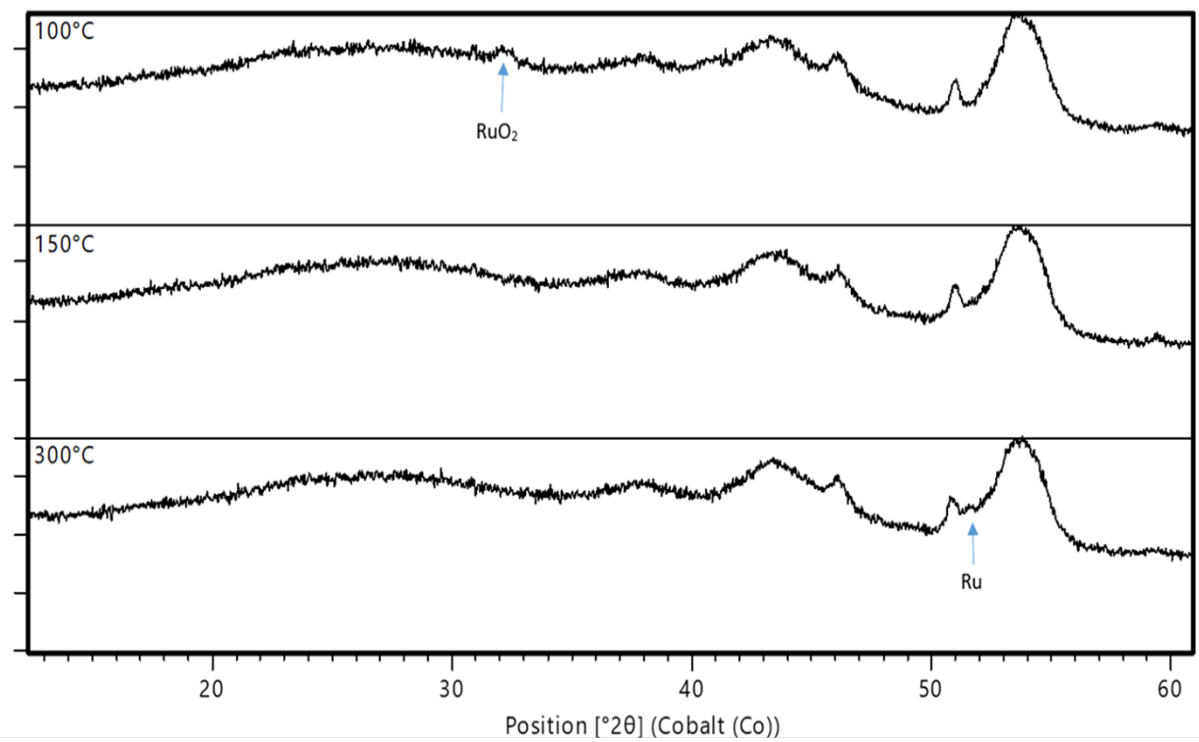



**Figure 4. 22** In-situ XRD results of Pu/Ru catalysts system

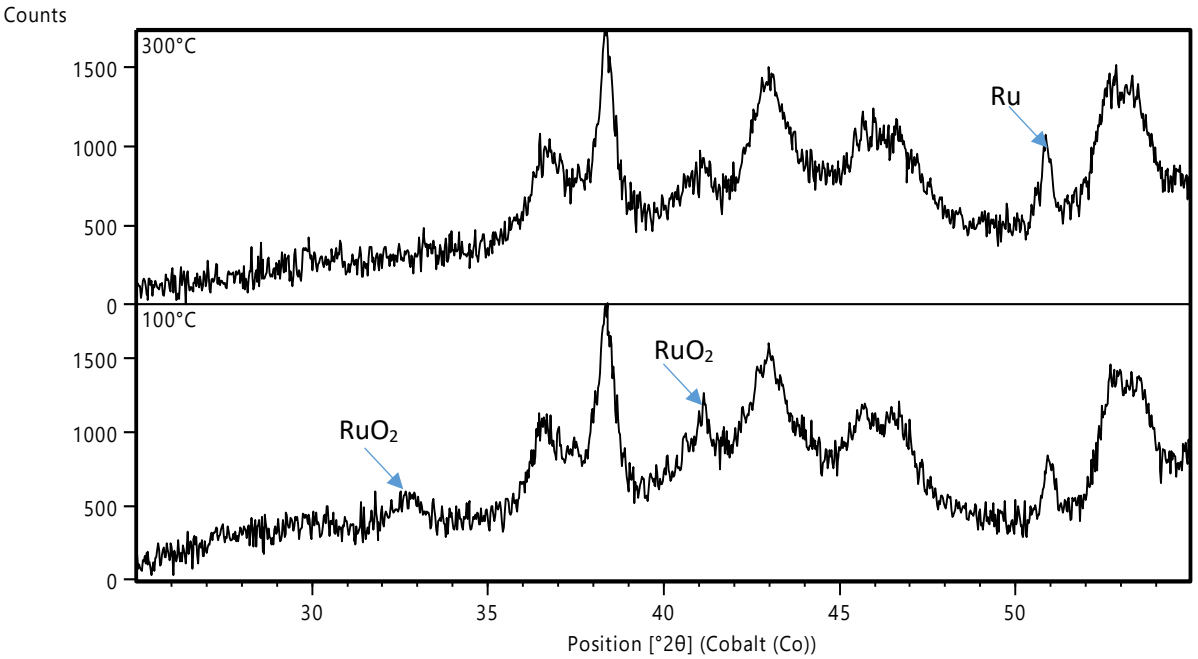



**Figure 4. 23** In-situ XRD results of PuCal/6wt% Mn/Ru catalysts system

### 4.4.8 $H_2$-chemisorption

The results of the $H_2$-chemisorption study for all the catalysts are listed in Table 4.15. $H_2$-chemisorption analysis was done to determine the active metal surface area, the percentage dispersion as well as the crystallite size of metallic Ru. Prior to the $H_2$-chemisorption the calcined (250 °C) catalysts were reduced in pure hydrogen at 425 °C for 4 hours.

**Table 4. 15** $H_2$-chemisorption results of the prepared catalysts systems

| Sample | Metal loading (W %) | DOR (%) | MSA ($m^2/g_{cat}$) | d (nm) | D (%) |
|---|---|---|---|---|---|
| Pu/Ru | 2.2 | 45 | 0.98 | 9.9 | 13.4 |
| Pu/6wt%Mn/Ru | 2.5 | 51 | 2.2 | 4.5 | 29.6 |
| Pu/10wt% Mn/Ru | 1.7 | 61 | 2.8 | 3.5 | 38.4 |
| PuCal/Ru | 1.8 | 71 | 0.91 | 10.7 | 12.4 |
| PuCal/4wt%Mn/Ru | 2.4 | 45 | 1.8 | 5.5 | 23.9 |
| PuCal/6wt%Mn/Ru | 1.8 | 63 | 1.8 | 5.4 | 24.6 |

$H_2$-chemisorption results indicate an increase in the degree of reduction for the Pu catalysts system as a function of increased Mn addition. However for the PuCal catalyst system, no clear trend is observed. A decreased in the crystallite size of the Ru is observed as a function of increase Mn addition and also looking at the dispersion, there is an improvement of the metal dispersion as Mn increases which means that Mn becomes an anchor of Ru. The average crystallite diameter obtained for ruthenium was largest for PuCal/Ru on the calcined system (10.7 nm) with the lowest dispersion and the highest degree of reduction. In all samples tested, metal dispersion (H / Ru) and average particle size of Ru are determined from irreversible $H_2$ uptakes measured at 100 ° C, assuming a stoichiometry of chemisorption H/Ru = 1:1 which is also confirmed by XRD results in-situ.

### 4.4.9 Summary of the characterization results of the calcined and uncalcined Ru-based FTS catalyst

The model ruthenium based catalysts were successfully prepared using the slurry impregnation method as shown by various characterization results obtained. Characterization results from XRF, $N_2$-physisorption, XRD, TPD, TEM, TPR, in-situ XRD & $H_2$-chemisorption results were discussed and the following can be concluded from the results.

XRF confirmed the desired amount of Mn addition and Ru was achieved although the techniques is semi-quantitative. $N_2$-physisorption results indicated a decrease in surface area

and pore volume as a function of both the Mn and Ru addition. An average pore diameter of 8 nm and 11 nm was observed for the Pu and PuCal catalysts systems respectively. XRD indicated a relative abundance of 2 % of the $RuO_2$ for all catalysts, and an inconsistent trend in the crystallite size of Ru was also observed. IPA-TPD results indicated that Ru preferably sits on stronger Brønsted acid sites but no clear trend is observed on the catalysts systems. Similar results are observed in the $CO_2$-TPD, where an increase in basicity is observed. The addition of Mn to a Pu-PuCal/Ru-based causes a decrease in the reducibility of $RuO_2$ as reported by TPR data while in-situ XRD results confirms the stoichiometry to be 1:1. However $H_2$-chemisorption results indicate that Mn does aid in increasing the metal dispersion and a decrease in the crystallite size of Ru as a function of increased Mn addition for both Pu and PuCal catalysts systems.

# *References*


(1) Phung, T. K.; Herrera, C.; Larrubia, M. Á.; García-Diéguez, M.; Finocchio, E.; Alemany, L. J.; Busca, G. Surface and Catalytic Properties of Some γ-Al2O 3 Powders. *Appl. Catal. A Gen.* **2014**, *483*, 41–51.

(2) Komeili, S.; Takht Ravanchi, M.; Taeb, A. Influence of Calcination Parameters on the Properties of Alumina as a Catalyst Support. *Sci. Iran.* **2017**, *23* (3), 1128–1135.

(3) Yang, X.; Sun, Z.; Wang, D.; Forsling, W. Surface Acid-Base Properties and Hydration/Dehydration Mechanisms of Aluminum (Hydr)Oxides. *J. Colloid Interface Sci.* **2007**, *308* (2), 395–404.

(4) Site, A.; Al, H. Y. S. APPLICATION NOTE 147 A Pulse Chemisorption and TPD Application. 3–4.

(5) Naturwissenschaften, D. Der. Characterization of Acidic and Basic Properties of Heterogeneous Catalysts by Test Reactions. **2004**.

(6) Betancourt, P.; Rives, A.; Hubaut, R.; Scott, C. E.; Goldwasser, J. A Study of the Ruthenium ± Alumina System. **1998**, *170*.

(7) Urunnabi, M. N.; Urata, K. M.; Kabe, K. O.; Anaoka, T. H. Effects of Ruthenium Precursors on Ru / Mn / Al 2 O 3 and Ru / Al 2 O 3 Catalysts for Fischer-Tropsch Synthesis. **2010**, *53* (2), 75–82.

(8) Nurunnabi, M.; Murata, K.; Hanaoka, T. Effects of Manganese Salts on Ru/Mn/Al Sub (2) O Sub (3) Catalytic Activity and Stability for Fischer-Tropsch Synthesis. *J. Japan Pet. Inst.* **2011**, *54* (1), 36–44.

# Chapter 5

## *Fischer-Tropsch synthesis performance of the model catalysts*

In this chapter, the Ru-based catalysts were evaluated for Fischer-Tropsch Synthesis (FTS), in a Continuous Stirred-Tank Reactor (CSTR), to determine the effect of acid-base properties on their activity and selectivity. Important parameters that were looked at were the FTS rate, $CH_4$ selectivity as well as the paraffin to olefin ratios. Mn has been used, as a promoter, in Fe, Ru and Co based catalysis, and its influence in the FTS process, has been documented[1,2,3,4]. For the Ru based catalyst, Nurunnabi *et al* investigated the influence of Mn addition on catalyst activity and resistance to deactivation. Studies indicated that the Ru/Mn/$\gamma$-$Al_2O_3$ catalyst exhibited good catalytic activity and resistance to catalyst deactivation, while the Ru/$\gamma$-$Al_2O_3$ catalyst deactivated with time on stream. They attributed the result to an increase in the density of Ru active atoms on the surface as a function of Mn addition.[1] In Co based catalysts, Morales *et al* indicated that the addition of Mn to a Co/$TiO_2$-based FTS catalyst caused a decrease in the reducibility of $Co_3O_4$, which resulted in less metallic active sites. However, the promotional effect of Mn aided in the suppression of $CH_4$ formation, increased the $C_{5+}$ selectivity, and enhancement of the cobalt-time yield[5].

In this study, the effect of acid- base properties of Ru based catalysts on the FTS activity and selectivity as a function of Mn addition was investigated. The six prepared catalysts that were tested were labeled using the following naming convention of Pu and PuCal and were compared per catalyst system.

Catalyst codes are as follows:

1. Pu catalyst system:
    - Pu/Ru
    - Pu/6wt%Mn/Ru
    - Pu/10wt% Mn/Ru
2. PuCal catalysts system:
    - PuCal/Ru

- PuCal/4wt%Mn/Ru
- PuCal/6wt%Mn/Ru

### 5.1. FTS behaviour of model catalysts

The changes in the FTS reaction rate or catalyst activity (expressed as (mole CO/g-cat/s)) with time-on-line (TOL) are shown in Figure 5.1. The increase in intensity of the blue markers represents the increase of Mn levels from 0 wt% to 10 wt%. In the figure, results indicate that the presence of Mn does not have any promotional effect, but rather has a poisoning effect. An increase in the Mn addition from 6 wt% to 10 wt% doesn't seem to have any further influence on catalyst activity as these two runs have a comparable FTS activity rate. The characterization studies of Nurunnabi *et al.* on the effects on Mn loading indicated that a suitable ratio of Mn: Al in $Ru/Mn/Al_2O_3$ increases the concentration of active Ru metal. High levels of Mn had a negative effect on catalyst, which was observed in their TPR results, where increased Mn led to difficulty in the reducibility of the catalyst[6]. Similar results were also observed in the TPR data obtained from the current study, where Mn impedes the reduction of Ru as a delay in reduction peaks was observed. TEM results after reduction indicated a migration of the Mn species towards Ru, where Mn was found to be closely associated with Ru. This might have resulted in a surface enrichment of Mn, consequently giving a geometric blocking of the Ru metal. $H_2$-chemisorption data indicated that the presence of Mn resulted in an increased dispersion as well and a decrease in the average crystallite size. Thus a decrease in activity of the Pu catalyst system as a function of increased Mn, is found to be highly structure-sensitive when Ru < 5 nm. Carballo *et al* in a study on the catalytic effects of ruthenium particle size in FTS, reported that in a range where Ru crystallite size is <10 nm, the turnover frequency of CO consumption increases as the particle size increases, reaching a constant value for Ru particles which is larger than 10 nm. The lower TOF observed by Ru clusters <10 nm were related to the stronger CO adsorption and concomitant partial blocking of active sites, as suggested by the decreased CO surface residence time as the Ru cluster size increases in the range below 10 nm[7]. $CO_2$-TPD technique indicate that Mn increases the basicity of the catalyst, which speaks to an increase in the oxygenated products observed in the selectivity data. This could mean that increased basicity has a negative impact with regards to catalyst activity. Less Brønsted acid sites are observed as a function of Mn addition as reported by IPA-TPD.

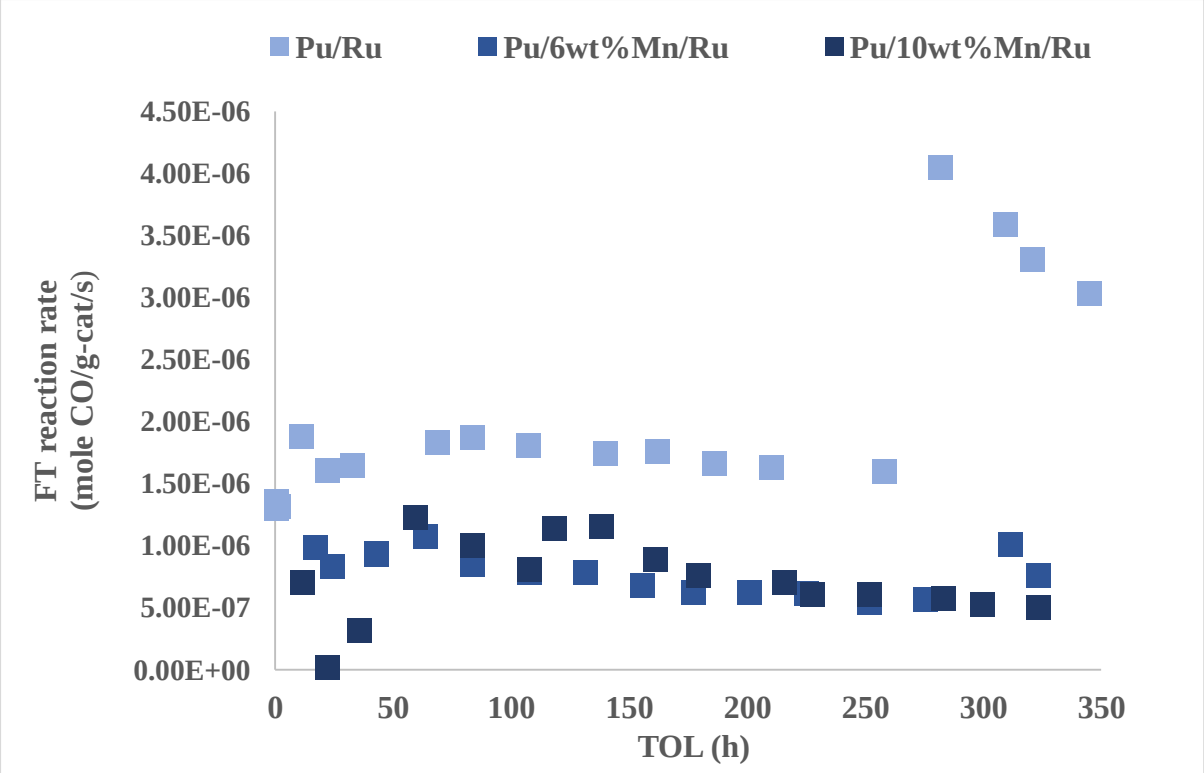



**Figure 5. 1** FTS Activity (mole CO/g-cat/s) with TOL of Pu system

It was observed that the Pu/Ru catalyst started to deactivate after 200 hrs TOL. In a study by Carballo *et al* on "Insights into the deactivation and reactivation of $Ru/TiO_2$ during Fischer–Tropsch synthesis",[8]different $H_2$ treatment were explored to recover the initial catalytic performance. Experiments by Raman and in situ FTIR showed the presence of carbonaceous deposits on the surface of the spent catalyst, believed to serve as poisoning species by hindering the adsorption of reactants. A treatment phase for $H_2$ however assisted in the slight recovery of catalytic activity, followed by static air treatment. The partial recovery of the catalytic activity is due to $H_2$ thermal therapy, which does not remove the carbonaceous deposits completely. A $H_2$ treatment step was applied after 200 hrs TOL in this study to see if an improvement in catalytic activity can be obtained. The treatment seemed to only have a positive influence on the Pu/Ru catalysts as an increase in activity is observed and the catalysts with Mn do not seem to respond to the treatment. All the catalysts runs were given a $H_2$ treatment approximately after 200 hrs online to rejuvenate the catalyst activity by cleaning the catalyst surface from known poisons (e.g. carbonaceous deposits). Therefore for these catalysts the main parameters that resulted in the lower catalytic activity is the presence of Mn which increases dispersion resulting in <5 nm Ru crystallites which are structure sensitive, furthermore Mn could migrate onto these smaller crystallites and become poison for the active sites of Ru.

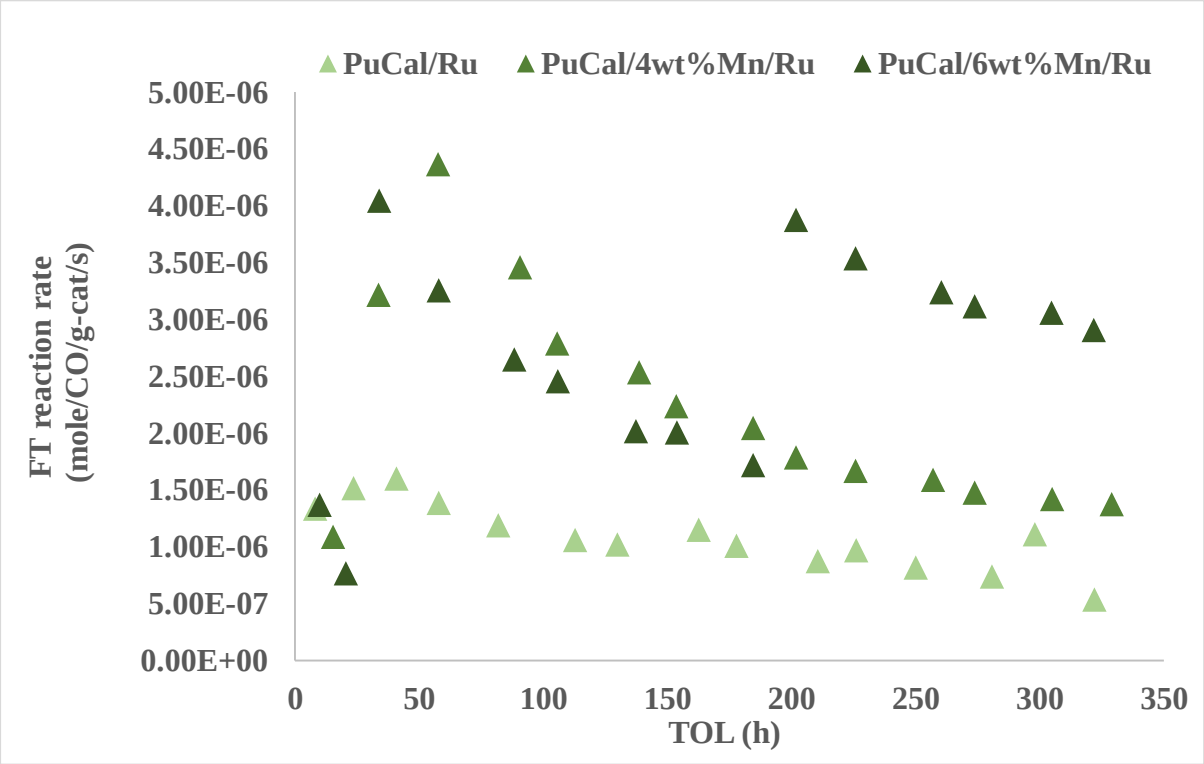



**Figure 5. 2** FTS Activity (mole CO/g-cat/s) with TOL of PuCal system

Figure 5.2 represents the changes in the FTS reaction rate or catalyst activity with time-on-line of the PuCal catalysts system. It is noticeable that the addition of manganese to the catalyst has a marked effect on the FTS reaction rate. The increase in the intensity of the colour of the green markers is also an indication of the increase in Mn levels from 0 to 6 wt%. In this catalyst system an increase in Mn from 0 % to 6 wt% results in an increase in the FTS reaction rate. The low activity observed for the PuCal/Ru catalyst could be attributed to a decrease in surface area as confirmed by the $N_2$ physisorption results and the presence of predominantly theta alumina as reported by XRD. The $H_2$ treatment after 200 hrs TOL indicated a change in the order of activity as a function of increased Mn levels from 0 wt% Mn to 6 wt% Mn with PuCal/6wt%Mn/Ru being the most active catalyst. Another factor that may result in good catalyst activity is a good metal dispersion which gives rise to higher active metal surface area. $H_2$-chemisorption indicated that Mn had a good influence with regards to the metal dispersion (%D) and the crystallite size, which resulted in an increase in activity as a result of an increase in Mn which means Mn has been shown to act as a structural promoter by increasing the Ru dispersion. The improved activity of the catalysts is correlated to Ru metal active sites with a particle size ranging from 5-10 nm which is known to be a typical particle size range for

Fischer-Tropsch synthesis[9]. The results confirm that good metal dispersion and smaller average ruthenium crystallite size are important for the catalyst system (dissociation, insertion and hydrogenation) to obtain a high activity. The results indicate that the high number of exposed active sites that are responsible for dissociative adsorption of CO and $H_2$ of the syngas is responsible for these results as a function of Mn addition.

A summary of FTS reaction rate of all the catalysts is captured in Figure 5.3 and the FTS reaction rate at around 100 hrs TOL vs MSA and crystallite size from $H_2$-chemisorption in Table 5.1.

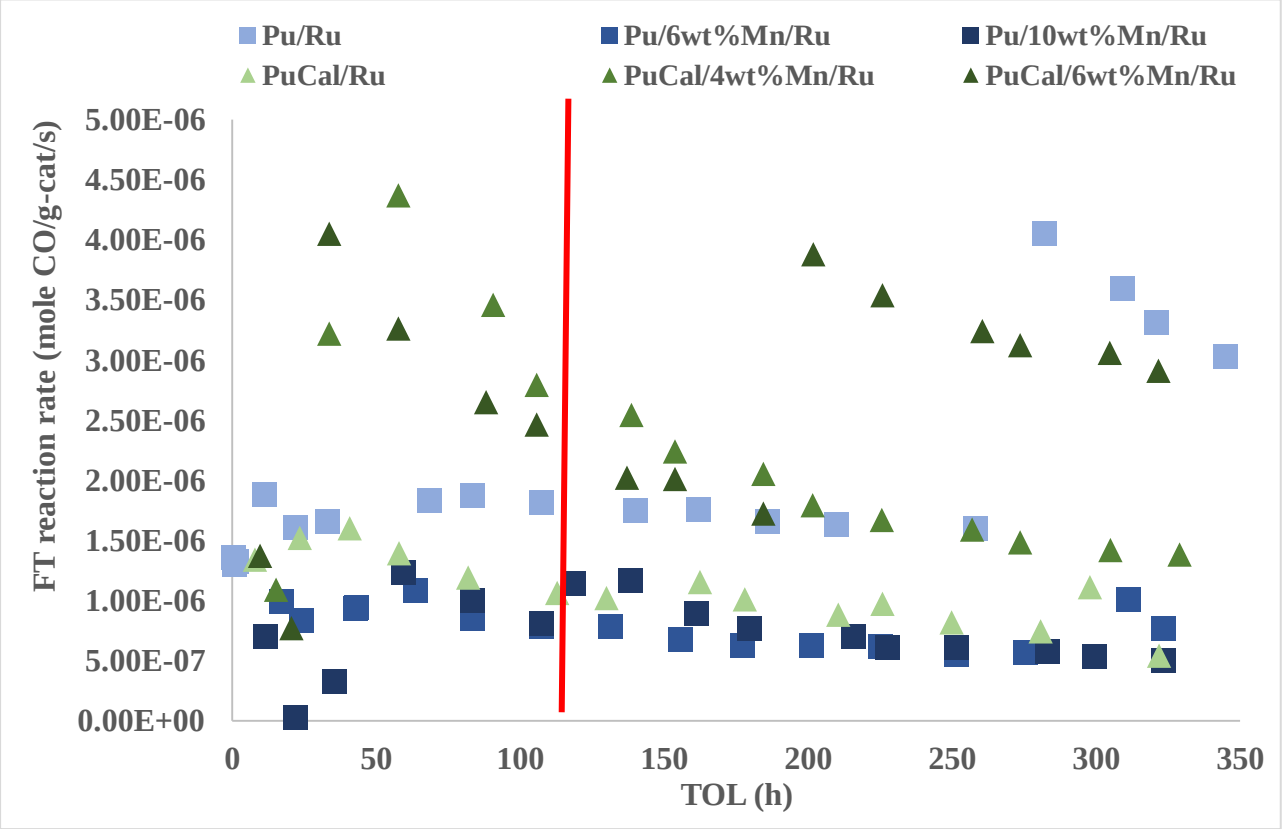



**Figure 5. 3** A summary of FTS Activity (mole CO/g-cat/s) with TOL for all the catalysts

It is generally known in catalysis that in order to increase catalytic activity, one approach is to improve the active phase surface area by decreasing the size of the particles that make up the active phase[10]. It is however said that increasing the number of exposed surface sites works well for structure-insensitive reactions. Results in Table 5.1 indicate that this phenomenon was applicable for the PuCal catalysts system whereas it did not seem to apply for the Pu catalyst

system. It was observed from the PuCal catalysts system that a decrease in the crystallite size from~10 nm to~5 nm improved the MSA and further resulted in an increase in the FTS reaction rate. From the Pu catalysts system, the decrease in crystallite size from ~10 nm to ~4 nm resulted in an improved MSA however a decrease in the FTS reaction rate. Kang's work[11], indicated that the TOF and product selectivities of the FTS reaction are strongly dependent on the particle size of the Ru-based catalyst. In their work using carbon nanotube-supported Ru-based catalysts with a mean Ru particle size of ~7 nm display the highest activity and selectivity toward long chain hydrocarbons. Carballo *et al*[7] studied $Ru/Al_2O_3$ catalysts with different metal particle sizes and found that the TOF of the FTS reaction increases with Ru particle size, reaching a constant value for Ru nanoparticles larger than 10 nm; this is similar to what has been observed for Co based catalysts.

Results reported in this study suggests that although an decrease in crystallite size results in an improved MSA, there is however an optimum crystallite size necessary to obtain a high FTS reaction rate for this system which seem to be around 5 nm.

**Table 5. 1** A summary of acid-base properties of prepared catalysts

| **Catalysts ID** | **FT Reaction Rate (E-06) @ 100 TOL** | **MSA ($m^2/g_{cat}$)** | **d (nm)** |
|---|---|---|---|
| Pu/Ru | 1.81 | 0.98 | 9.9 |
| Pu/6wt% Mn/Ru | 0.78 | 2.2 | 4.5 |
| Pu/10wt% Mn/Ru | 0.81 | 2.8 | 3.5 |
| PuCal/Ru | 1.06 | 0.91 | 10.7 |
| PuCal/4wt% Mn/Ru | 2.79 | 1.8 | 5.5 |
| PuCal/6wt% Mn/Ru | 2.46 | 1.8 | 5.4 |

### 5.2. Selectivities of model catalysts

Figure 5.4 indicates the methane selectivities of all the prepared catalyst discussed. From a selectivity point of view, a low methane selectivity is normally desired, combined with a high $C_{5+}$ selectivity or a high chain growth probability ($\alpha$)[12]. Results indicated low methane selectivity for catalysts that had higher FTS reaction rate activity.

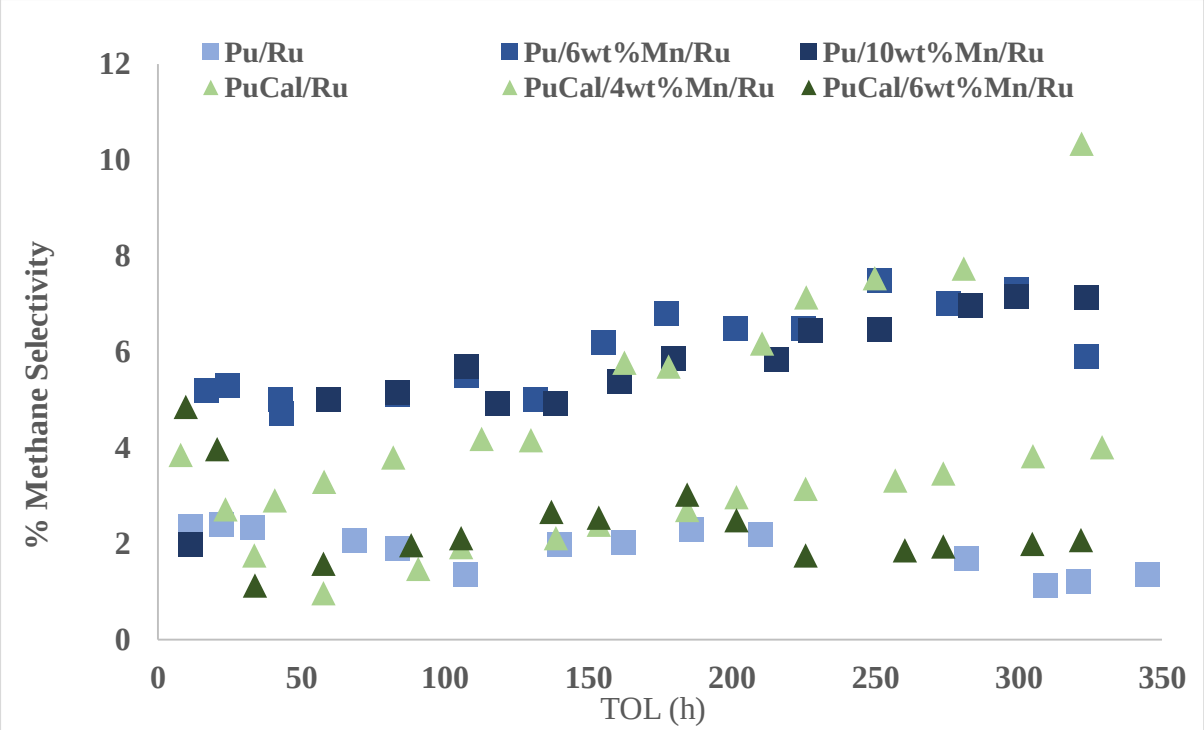



**Figure 5. 4** Methane selectivity with TOL for all the catalysts

Table 5.2 is a summary of the results obtained from $CO_2$-TPD and IPA-TPD, which gives an insight into the acid-base properties of the support systems in this study as function of Mn addition. From the results a correlation was established between Brønsted acidity and basicity where an increase in basicity as a function of Mn addition resulted in a decrease in Brønsted acidity of the supports.

**Table 5. 2** A summary of acid-base properties of Mn-modified supports

| **Catalysts ID** | **Brønsted acid sites (µmol/m2)** | **Basic sites (µmol/m2)** |
|---|---|---|
| Pu | 0.026 | 0.00029 |
| Pu/6wt% Mn | 0.015 | 0.00059 |
| Pu/10wt% Mn | 0.014 | 0.00091 |
| PuCal | 0.023 | 0.00031 |
| PuCal/4wt% Mn | 0.015 | 0.00053 |
| PuCal/6wt% Mn | 0.014 | 0.00084 |

Figure 5.5 and Table 5.3 shows the, FTS reaction rate, $CH_4$ selectivity, $C_2$- alcohols and $C_3$-$C_5$ olefins of the six catalysts prepared together with their reactor partial pressures. The results presented indicate that catalyst selectivity increased significantly towards alcohol and olefinic products as a result of increased manganese loadings/increased basicity as reported in Table 5.2. Highly active catalyst PuCal/6wt%Mn/Ru, had high yields of $C_2$-alcohols, and $C_2$-olefins as opposed to the rest of the other catalysts. An increase in these selectivities is observed as a function of increased Mn levels in the catalysts. Although Pu/Ru catalyst was also one of the high performing catalyst with regards to FTS reaction rate, the absence of Mn in this catalyst clearly distinguishes the role of Mn as a selectivity promoter rather than an activity promoter. The distinct selectivities show that the catalysts likely followed different polymerization mechanisms which can be related to the $H_2$/CO ratio on the Ru metal surface. The application of Mn in ruthenium based catalysts yields increased amounts of unsaturated species and shifts the product distribution towards longer chains.

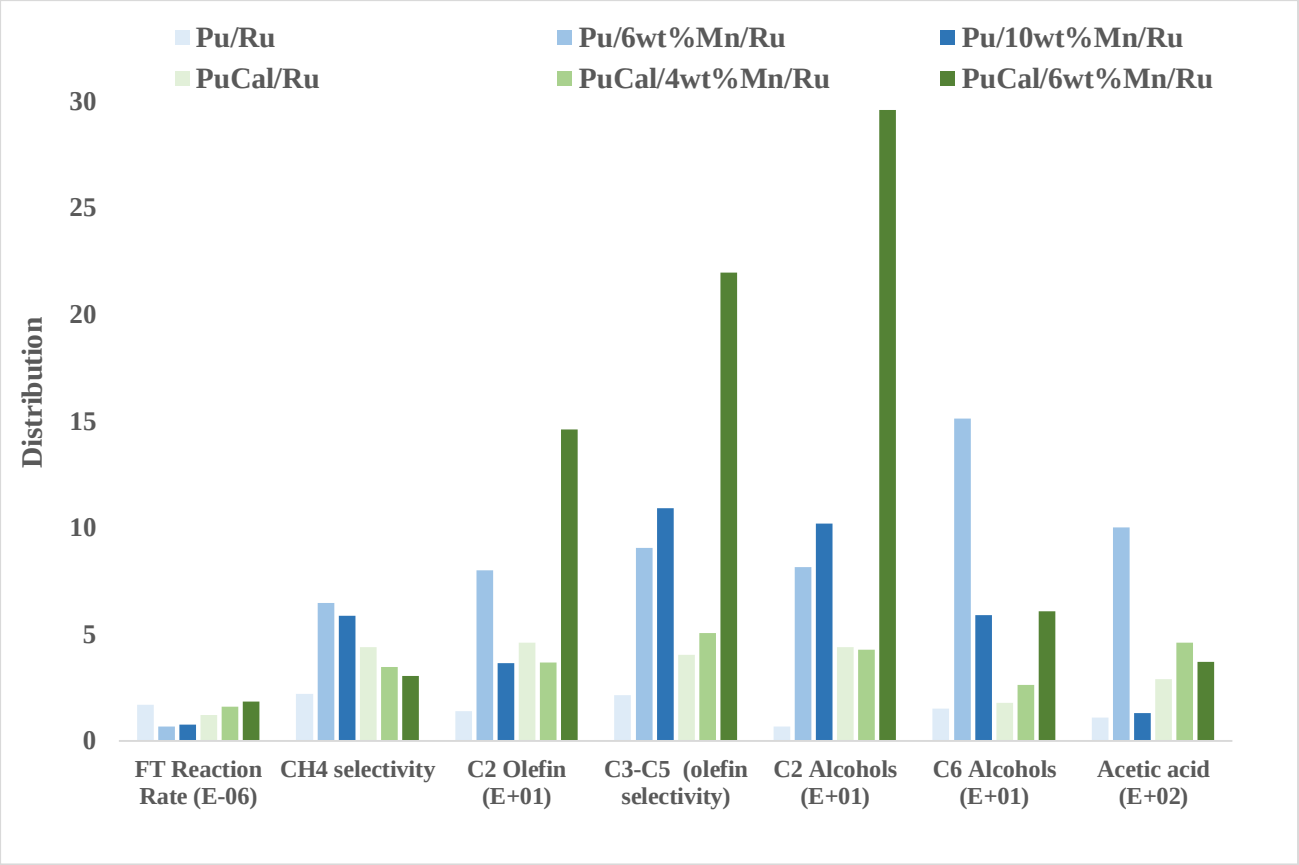



**Figure 5. 5** Summary of FTS reaction performances for all the catalysts at approx. 200 h TOL

**Table 5. 3** Summary of FTS reaction performances for all the catalysts at approx. 200 hrs TOL

| **Catalysts ID** | **Pu/Ru** | **Pu/6wt%Mn/Ru** | **Pu/10wt%Mn/Ru** | **PuCal/Ru** | **PuCal/4wt%Mn/Ru** | **Ru/6wt%Mn/Ru** |
|---|---|---|---|---|---|---|
| ***Reactor P ($H_2$) Bar*** | 13.13 | 13.73 | 14.27 | 13.65 | 13.30 | 13.00 |
| ***Reactor P (CO) Bar*** | 6.54 | 6.39 | 7.15 | 6.88 | 6.62 | 6.61 |
| ***Reactor P ($H_2O$) Bar*** | 2.00 | 0.57 | 0.79 | 1.27 | 1.90 | 2.05 |
| ***Reactor P ($CO_2$) Bar*** | 0.007 | 0.959 | 0.009 | 0.060 | 0.033 | 0.029 |
| ***Reactor P(Syngas) Bar*** | 19.68 | 20.12 | 21.43 | 20.53 | 19.91 | 19.60 |
| ***CO + $CO_2$ Conversion (%)*** | 23.47 | 7.22 | 10.04 | 16.06 | 22.46 | 23.85 |
| ***FT Reaction Rate (E06)(mole CO/g-cat/s)*** | 1.7 | 0.67 | 0.75 | 1.2 | 1.6 | 1.83 |
| ***$CH_4$ selec (%)*** | 2.19 | 6.47 | 5.87 | 4.37 | 3.46 | 3.03 |
| ***C2 Olefin (%)*** | 0.14 | 0.80 | 0.36 | 0.46 | 0.37 | 1.46 |
| ***C3-C5 Olefin (%)*** | 2.15 | 9.05 | 10.90 | 4.03 | 5.06 | 21.95 |
| ***C2 Alcohols (%)*** | 0.07 | 0.82 | 1.02 | 0.44 | 0.43 | 2.96 |
| ***C6 Alcohols (%)*** | 0.15 | 1.51 | 0.59 | 0.18 | 0.26 | 0.61 |
| ***Acetic acid (E+02) (%)*** | 1.1 | 10 | 1.3 | 2.9 | 4.6 | 3.7 |

### 5.3 GC-GC results

From the selectivity results presented it was observed that Mn was able to demonstrate good activity and a high selectivity to oxygenated and olefinic species for the PuCal system, whereas for the Pu system Mn only promoted selectivity towards oxygenated and olefinic species However since there is considerable overlap in these products it was necessary to develop a method of analysing via GC x GC since with a conventional GC, it is difficult to separate or classify the oxygenated products. From the GC x GC results presented in Figures 5.6 and 5.7 respectively, results are a comparison between a catalyst with Mn and a catalyst without Mn. Pu/Ru and PuCal/6wt%Mn/Ru are the only samples that could be analysed. From the results it is observed that Mn leads to an increase in the formation of oxygenates (acids, alcohols, aldehydes, ketones and esters)[2]. It appears as if the PuCal/6wt%Mn/Ru led to formation of cyclic paraffins which are not so discernable when looking at the components formed when using the Pu/Ru catalyst. The Pu/Ru catalyst seems to have more paraffins relative to the PuCal/6wt%Mn/Ru catalyst. Both catalysts give similar paraffin and olefin distributions of roughly $C_4$ to $C_{23}$.

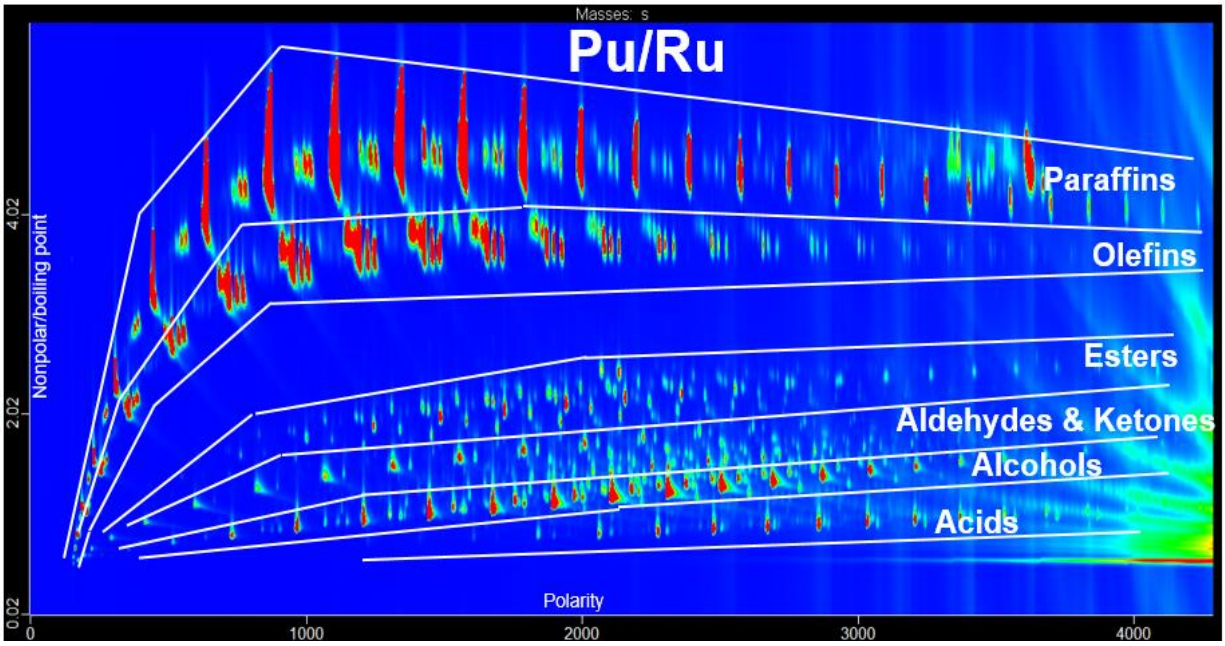



**Figure 5. 6** GCXGC spectra of Pu/Ru catalyst

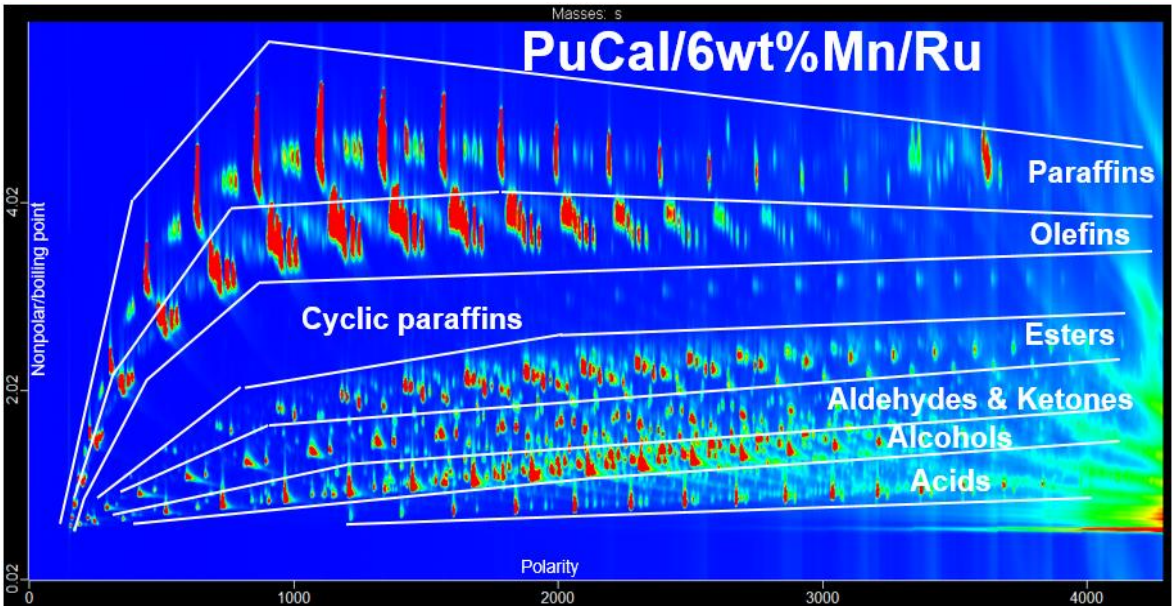



**Figure 5. 7** GCXGC spectra of PuCal/6wt%Mn/Ru catalyst

### 5.4. Concluding remarks

Acid-base properties as a function of Mn addition were investigated on Ruthenium based Alumina catalysts for Fischer-Tropsch synthesis. Two systems of catalysts were compared against each other as a function of calcination of the alumina support, the Pu catalyst system and the PuCal catalysts system.

- In the Pu catalyst system, Mn addition did not have any promotional effect with regards to activity thus Mn functions as a poison regardless of Mn level by blocking the active site of Ru. Mn may also result in very good Ru dispersion on this high SA system, resulting in too small Ru crystallites (<5 nm) which exhibit lower activity due to structure sensitivity.
- However in the PuCal system, Mn enhances activity, with PuCal/6wt%Mn/Ru being the most active catalyst of the system. Thus, there should also be an optimum Mn loading.
- Higher activity rate correlated to lower methane selectivity in all catalysts systems.
- Mn addition indicated to be selective towards oxygenates as expected based on literature.

# *References*


(1) Nurunnabi, M.; Murata, K.; Okabe, K.; Inaba, M.; Takahara, I. Effect of Mn Addition on Activity and Resistance to Catalyst Deactivation for Fischer-Tropsch Synthesis over Ru/Al2O3 and Ru/SiO2 Catalysts. *Catal. Commun.* **2007**, *8* (10), 1531–1537.

(2) Paterson, A. J.; Peacock, M.; Purves, R.; Sullivan, K.; Wilson, J.; Paterson, J.; Peacock, M.; Purves, R.; Partington, R.; Sullivan, K.; et al. Accepted Article.

(3) Østbye, E.; Svenum, I.; Blekkan, E. A. Mn Promoted Co Catalysts for Fischer-Tropsch Production of Light Olefins – An Experimental and Theoretical Study. *J. Catal.* **2018**, *361*, 23–32.

(4) Feltes, T. E.; Espinosa-alonso, L.; Smit, E. De; Souza, L. D.; Meyer, R. J.; Weckhuysen, B. M.; Regalbuto, J. R. Selective Adsorption of Manganese onto Cobalt for Optimized Mn / Co / TiO 2 Fischer – Tropsch Catalysts. *J. Catal.* **2010**, *270* (1), 95–102.

(5) Morales, F.; Groot, F. M. F. De; Gijzeman, O. L. J.; Mens, A.; Stephan, O. Mn Promotion Effects in Co / TiO 2 Fischer – Tropsch Catalysts as Investigated by XPS and STEM-EELS. **2005**, *230*, 301–308.

(6) Nurunnabi, M.; Murata, K.; Hanaoka, T. Effects of Manganese Salts on Ru/Mn/Al Sub (2) O Sub (3) Catalytic Activity and Stability for Fischer-Tropsch Synthesis. *J. Japan Pet. Inst.* **2011**, *54* (1), 36–44.

(7) Carballo, J. M. G.; Yang, J.; Holmen, A.; García-Rodríguez, S.; Rojas, S.; Ojeda, M.; Fierro, J. L. G. Catalytic Effects of Ruthenium Particle Size on the Fischer-Tropsch Synthesis. *J. Catal.* **2011**, *284* (1), 102–108.

(8) Carballo, J. M. G.; Finocchio, E.; García-Rodriguez, S.; Ojeda, M.; Fierro, J. L. G.; Busca, G.; Rojas, S. Insights into the Deactivation and Reactivation of Ru/TiO2 during Fischer-Tropsch Synthesis. *Catal. Today* **2013**, *214*, 2–11.

(9) Bezemer, G. L.; Bitter, J. H.; Kuipers, H. P. C. E.; Oosterbeek, H.; Holewijn, J. E.; Xu, X.; Kapteijn, F.; Dillen, A. J. Van; Jong, K. P. De. Cobalt Particle Size Effects in the Fischer - Tropsch Reaction Studied with Carbon Nanofiber Supported Catalysts. **2006**, No. 6, 11568–11569.

(10) Liu, J.; Wang, P.; Xu, W.; Hensen, E. J. M. Particle Size and Crystal Phase Effects in Fischer-Tropsch Catalysts. *Engineering* **2017**, *3* (4), 467–476.

(11) Kang, J.; Zhang, S.; Zhang, Q.; Wang, Y. Ruthenium Nanoparticles Supported on Carbon Nanotubes as Efficient Catalysts for Selective Conversion of Synthesis Gas to Diesel Fuel **. **2009**, 2565–2568.

(12) Van de Loosdrecht, J.; Botes, F. G.; Ciobica, I. M.; Ferreira, A.; Gibson, P.; Moodley, D. J.; Saib, A. M.; Visagie, J. L.; Weststrate, C. J.; Niemantsverdriet, J. W. *Fischer-Tropsch Synthesis: Catalysts and Chemistry*; Elsevier Ltd., 2013; Vol. 7.

# Chapter 6

## Conclusions and Summary

The aim of the study was to investigate the acid-base properties of ruthenium based FTS catalysts as influenced by (i) calcination temperatures of the alumina support, (ii) support modification with manganese addition, and (iii) ruthenium impregnation on the modified support. The support and catalyst materials were successfully synthesised and characterized using techniques such as TGA, BET, TPD, SEM-EDX, XRF, TPR, TEM, XRD and $H_2$-chemisorption. The following conclusions are drawn from these studies:

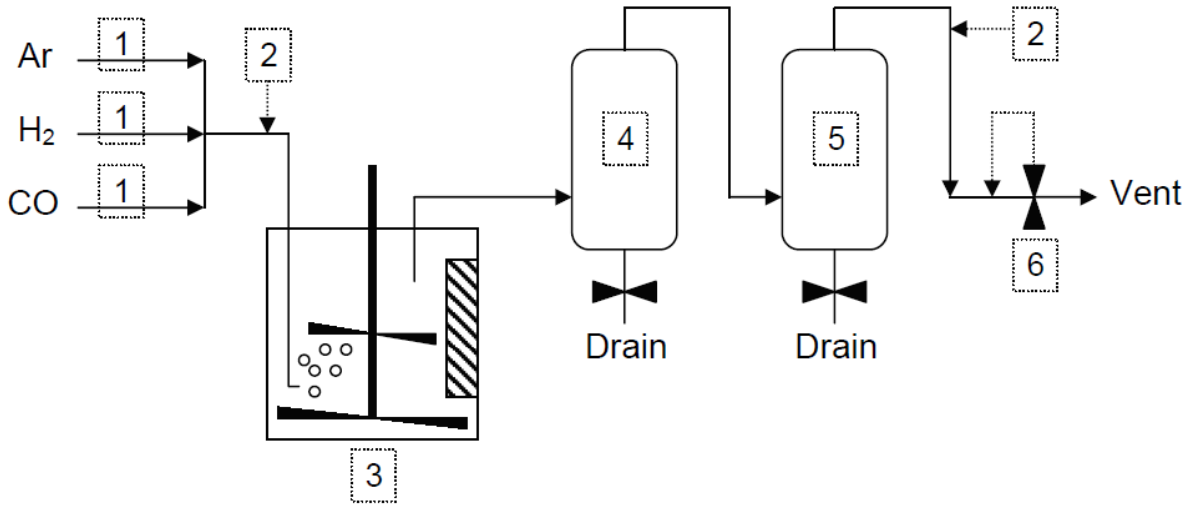
Characterization results from $N_2$-physisorption, indicated a decrease in the surface area and the pore volume as a function of increased calcination temperature while XRD results showed and confirmed the changes in the phase of alumina as a function of increased temperature. SEM-EDX showed that the Mn-modified supports had an even distribution of Mn on the surface. With regards to surface probing techniques, IPA-TPD saw a shift of peaks from higher to lower temperatures which indicated that Mn prefers to occupy the stronger acid sites on the alumina surface. However, from calculation it was observed that the amount of Mn per surface area was equal for Pu vs PuCal systems. $CO_2$-TPD showed increased amount of basic sites as a function of a loss in hydroxyl groups of the alumina. The amount of basic sites per surface area for the two systems were comparable. Thus $CO_2$-TPD results complements the IPA-TPD results as Mn addition saw an increase in intensity of the basicity peak on both Pu and the PuCal systems and the actual amount of both basic and acidic sites were comparable.

XRF confirmed the desired amount of Mn addition and Ru was achieved although the technique is semi-quantitative. $N_2$-physisorption results indicated a decrease in surface area and pore volume as a function of both the Mn and Ru addition. An average pore diameter of 8 nm and 11 nm was observed for the Pu and PuCal catalysts systems respectively. XRD indicated a relative abundance of 2 % of the $RuO_2$ for all catalysts, and an inconsistent trend in the crystallite size of Ru was also observed. IPA-TPD results indicated that Ru preferably sits

on stronger brønsted acid sites but no clear trend is observed on the catalysts systems. Similar results are observed in the $CO_2$-TPD, where an increase in basicity is observed. The addition of Mn to a Pu-PuCal/Ru-based causes a decrease in the reducibility of $RuO_2$ as reported by TPR data and In-situ XRD results confirms the stoichiometry to be 1:1. However $H_2$-chemisorption results indicate that Mn does aid in increasing the metal dispersion and a decrease in the crystallite size of Ru is also observed as a function of increased Mn addition for both Pu and PuCal catalysts systems.

Comparison of Fischer Tropsch activity, Mn had a promotional effect on PuCal catalyst but operated as a poison for the Pu system. High FTS reaction activity led to lower methane selectivity. Mn is selective towards oxygenates, as Mn containing catalysts exhibited a pronounced distribution of oxygenates.

## Appendix A: CSTR Reactor scheme




1. Gas supply lines
2. Gas sample points
3. Slurry reactor with gas supply, impeller system and baffles shown
4. Hot knock-out pot
5. Cold knock-out pot
6. Back-pressure regulator

**Figure A.1** Schematic diagram of reactor rig layout used FTS testing

## Appendix B: SEM-Backscatter of modified Mn supports

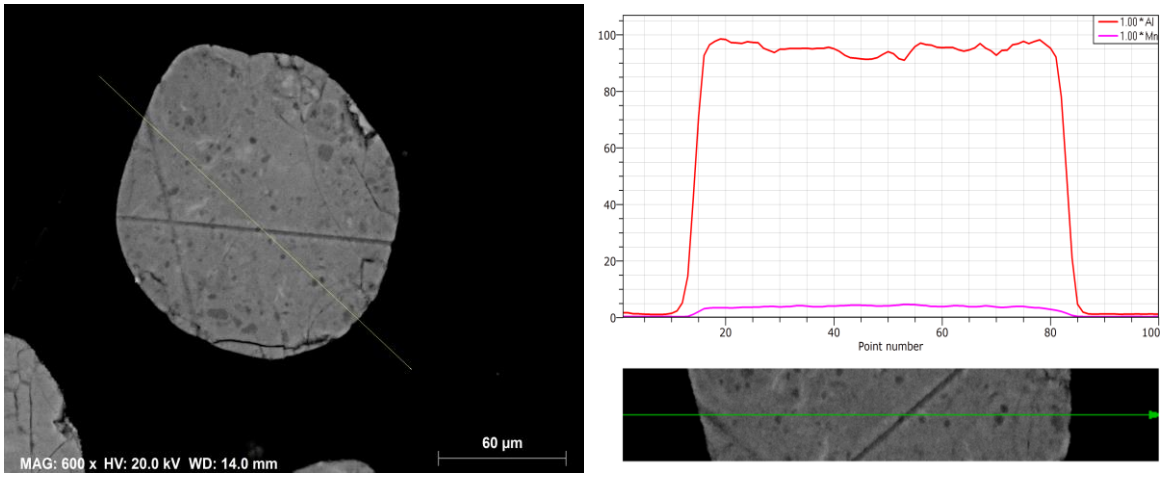



**Figure B.1** SEM-Backscatter 6wt% Mn/Pu support

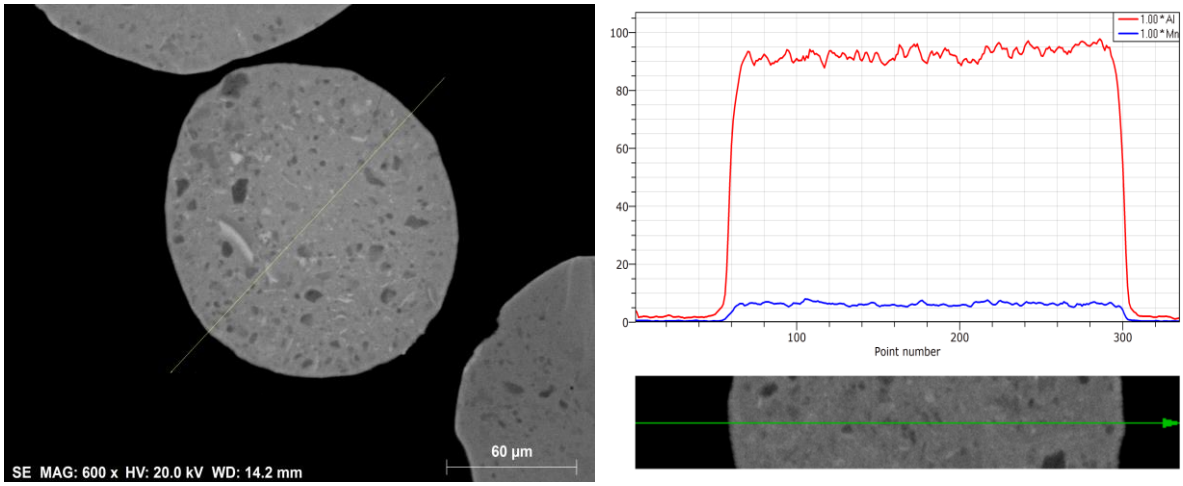



**Figure B.2** SEM-Backscatter 10wt% Mn/Pu support

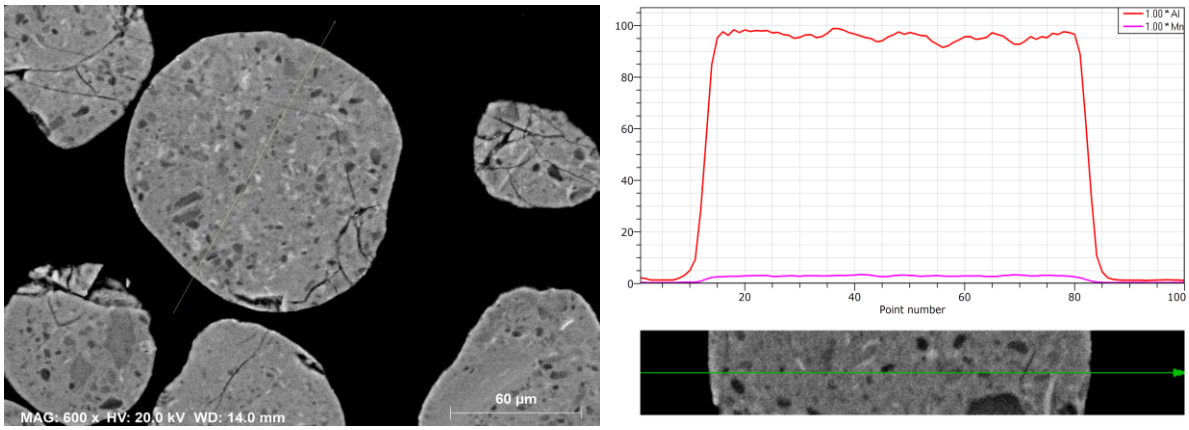



**Figure B.3** SEM-Backscatter 4wt% Mn/PuCal support

## Appendix C: SEM-Backscatter of Pu and PuCal catalysts

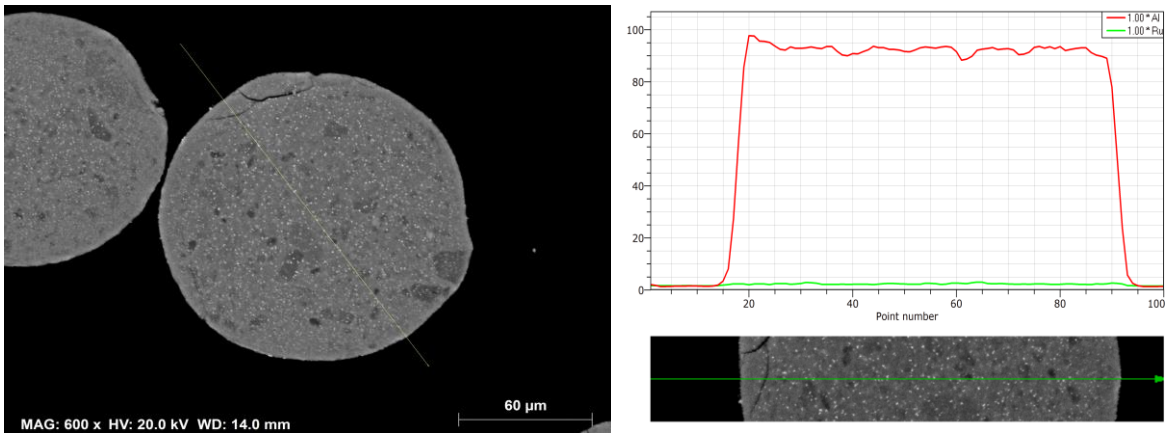



**Figure C.1** SEM-Backscatter Ru/Pu catalyst

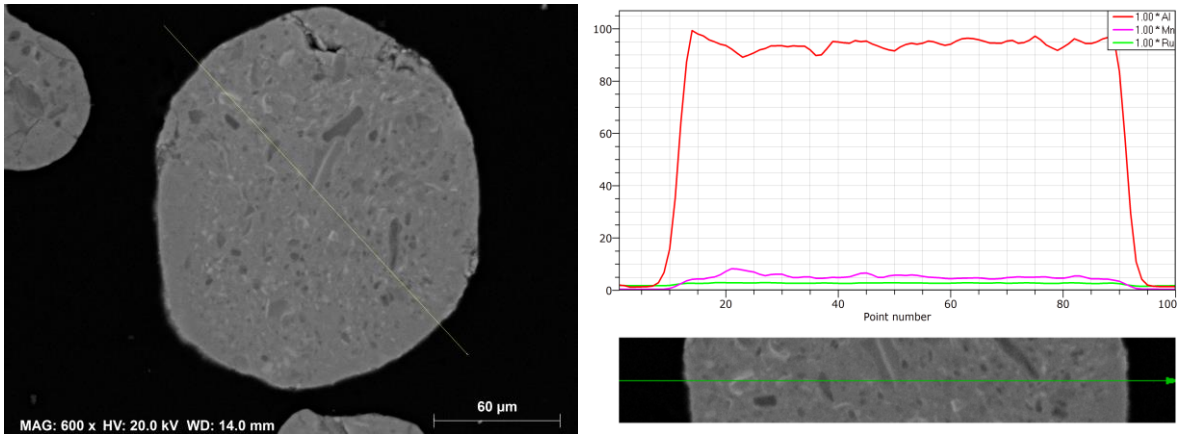



**Figure C.2** SEM-EDX Ru/6wt%/Pu catalyst

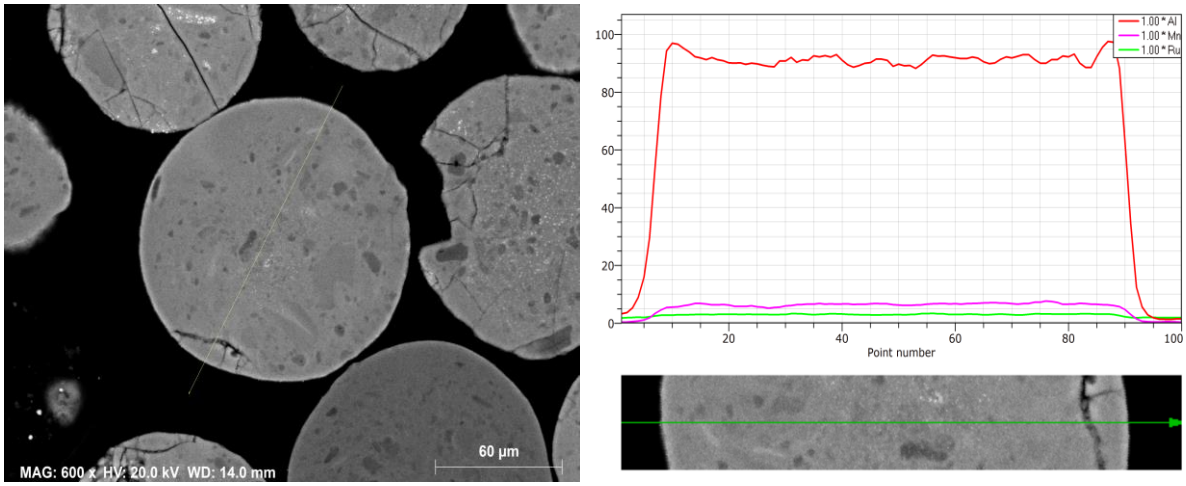



**Figure C.3** SEM-EDX Ru/10wt%/Pu catalyst

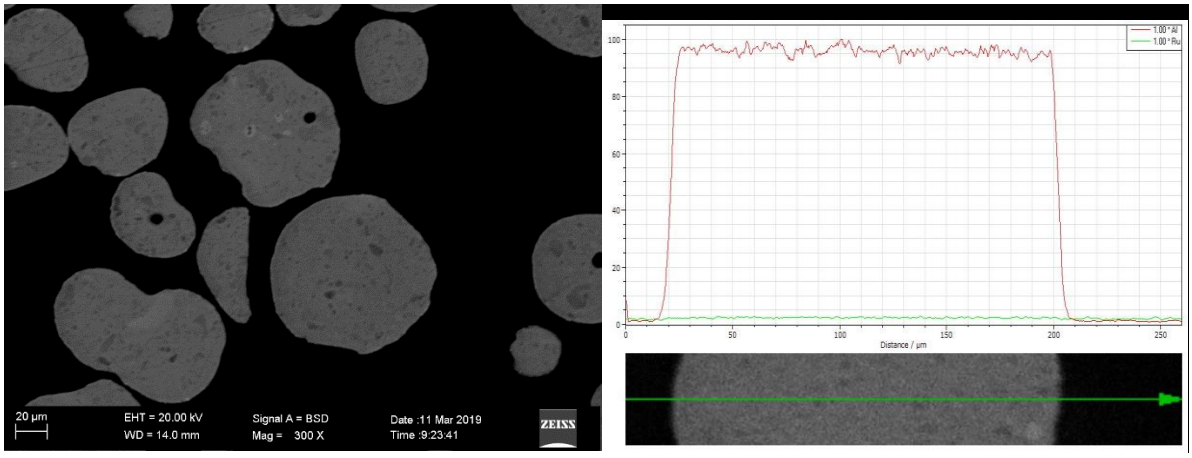



**Figure C.4** SEM-Backscatter Ru/PuCal catalyst

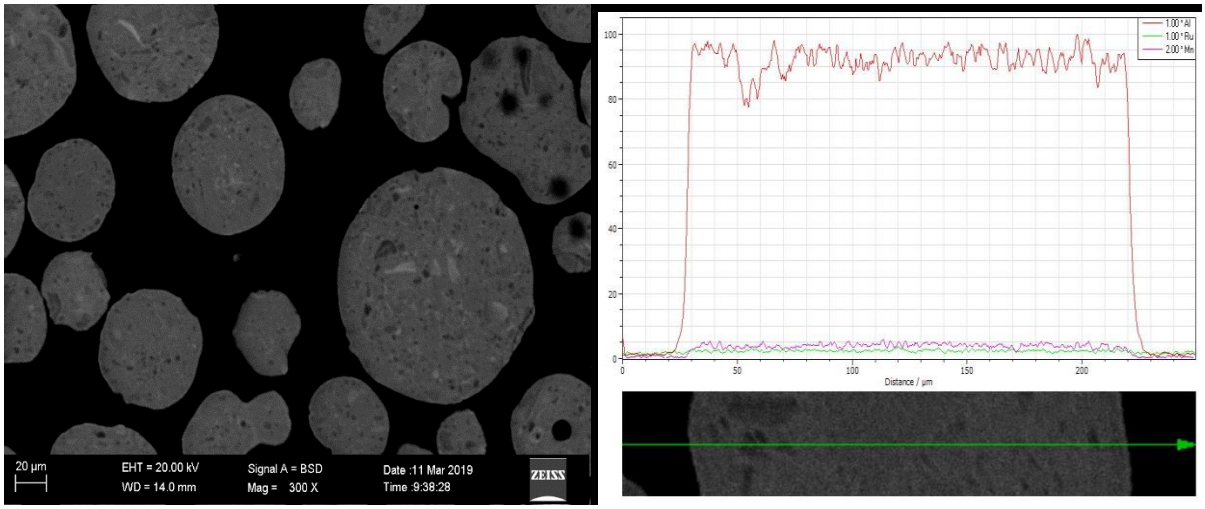



**Figure C.5** SEM-Backscatter Ru/4wt%/PuCal catalyst

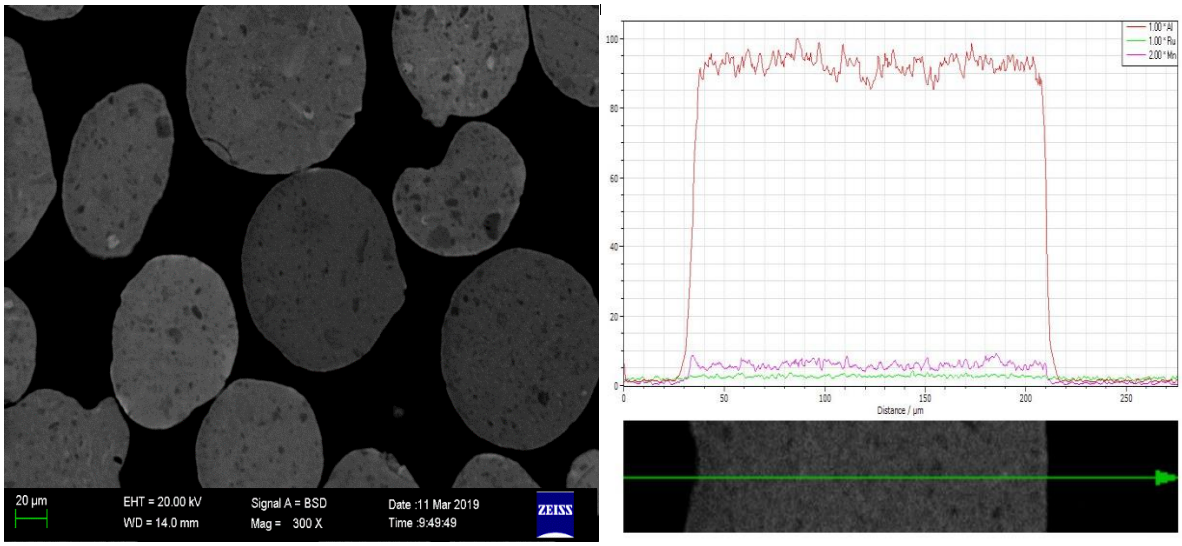



**Figure C.6** SEM-backscatter Ru/6wt%/PuCal catalyst

## Appendix D: TEM

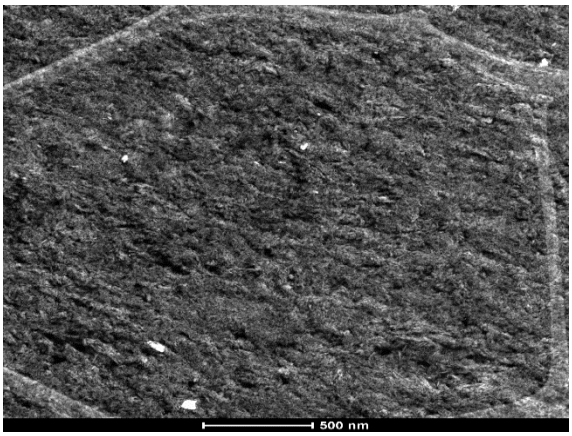



**Figure D.1** HAADF TEM Ru/Pu catalyst

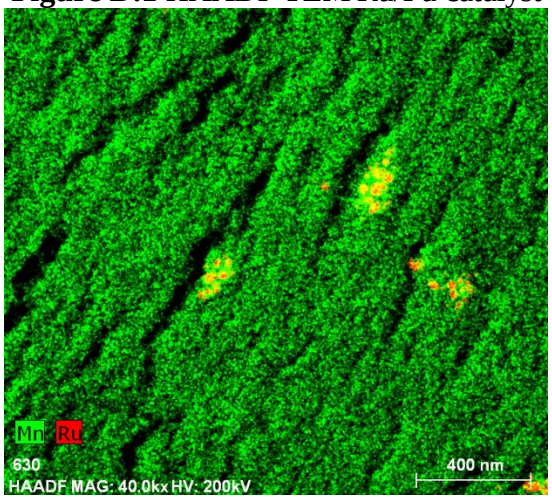



**Figure D. 2** TEM Ru/6wt%Mn/Pu

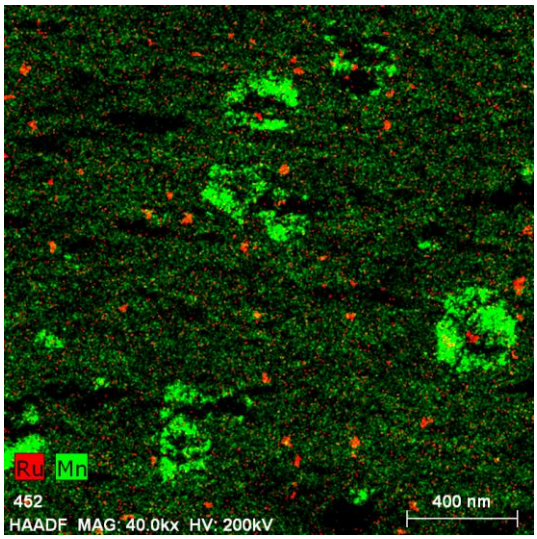



**Figure D. 3** TEM Ru/10wt%Mn/Pu

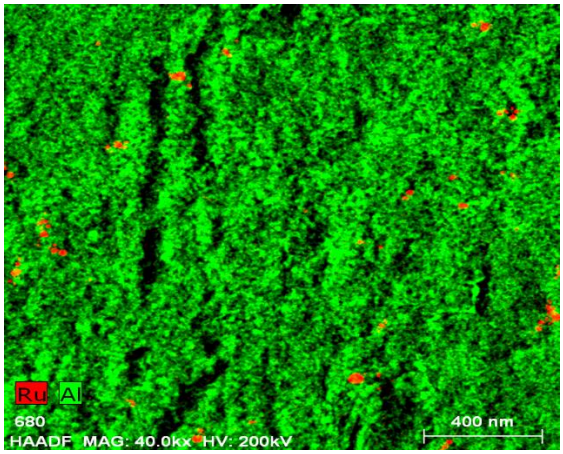



**Figure D. 4** TEM Ru/PuCal

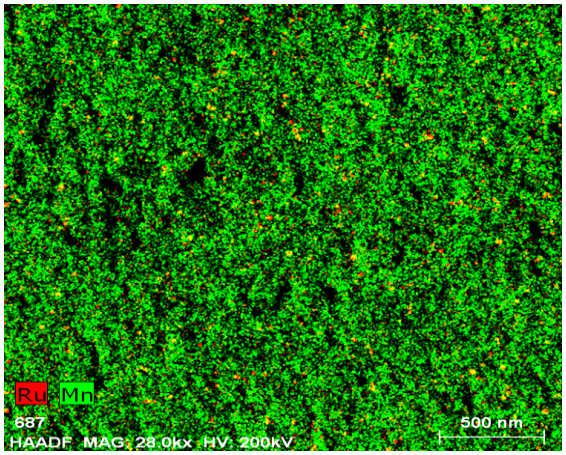



**Figure D. 5** TEM Ru/4wt%/PuCal

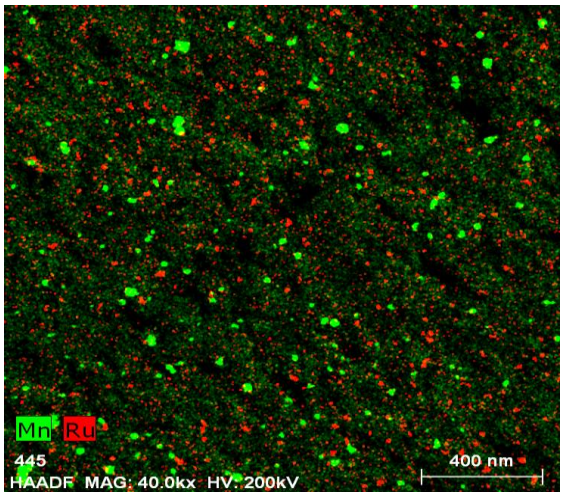



**Figure D. 6** TEM Ru/6wt%PuCal

## Appendix E: XRD Datasets

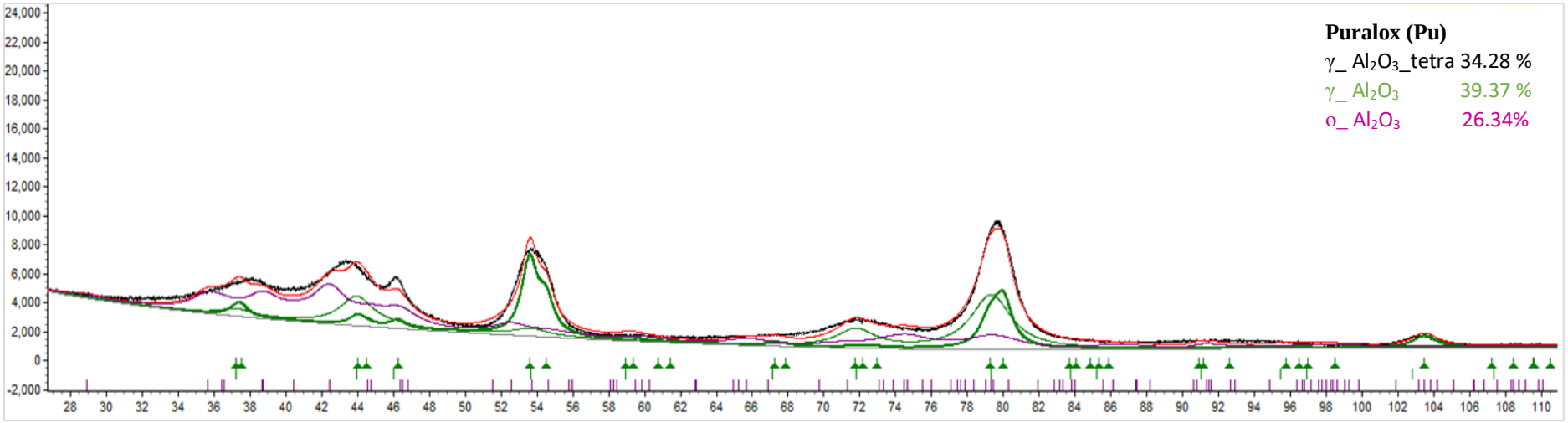



**Figure E. 1** Rietveld refinement for Puralox (Pu) support

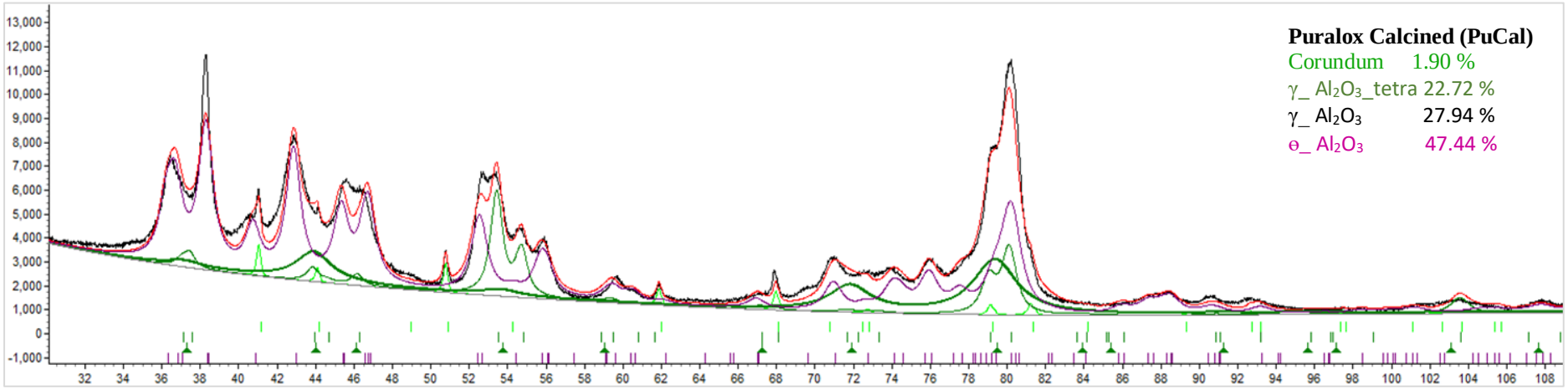



**Figure E. 2** Rietveld refinement for Puralox Calcined (PuCal) support

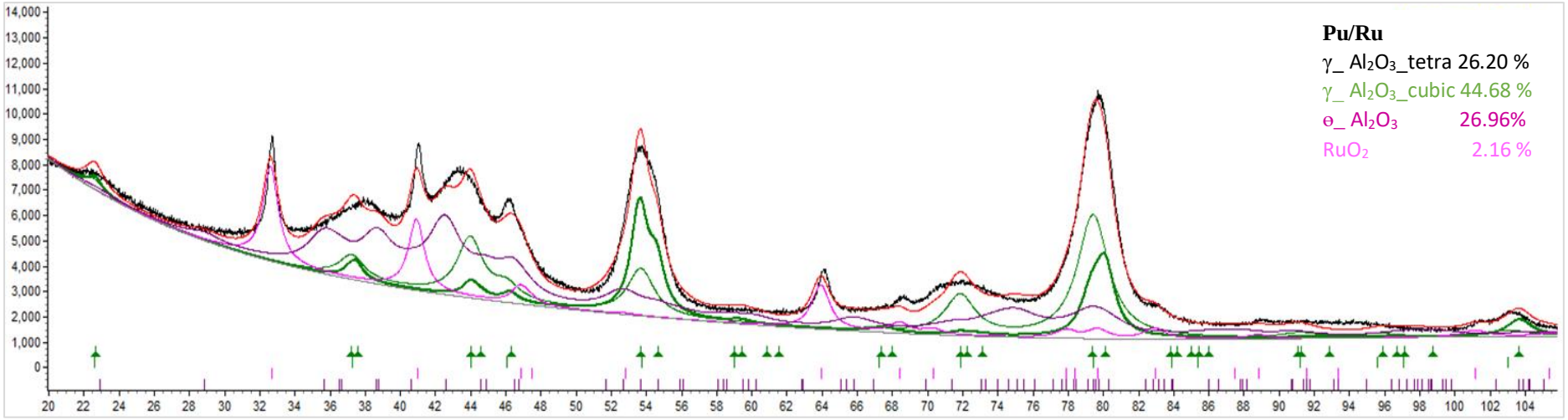



**Figure E. 3** Rietveld refinement for Pu/Ru catalyst

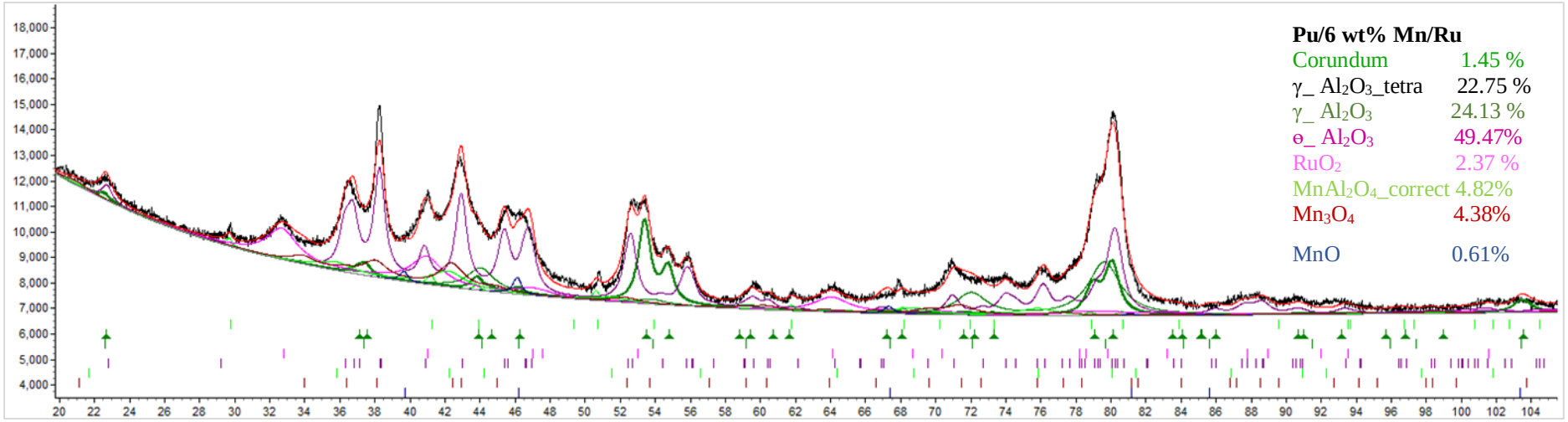



**Figure E. 4** Rietveld refinement for Pu/6 wt% Mn/Ru catalyst

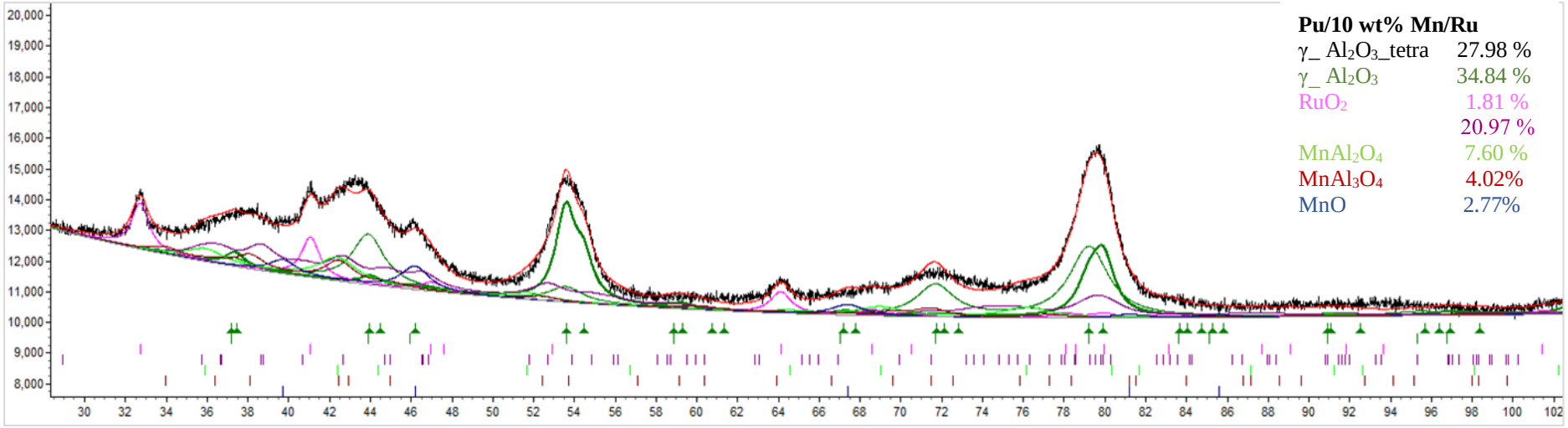



**Figure E. 5** Rietveld refinement for Pu/10 wt% Mn/Ru catalyst

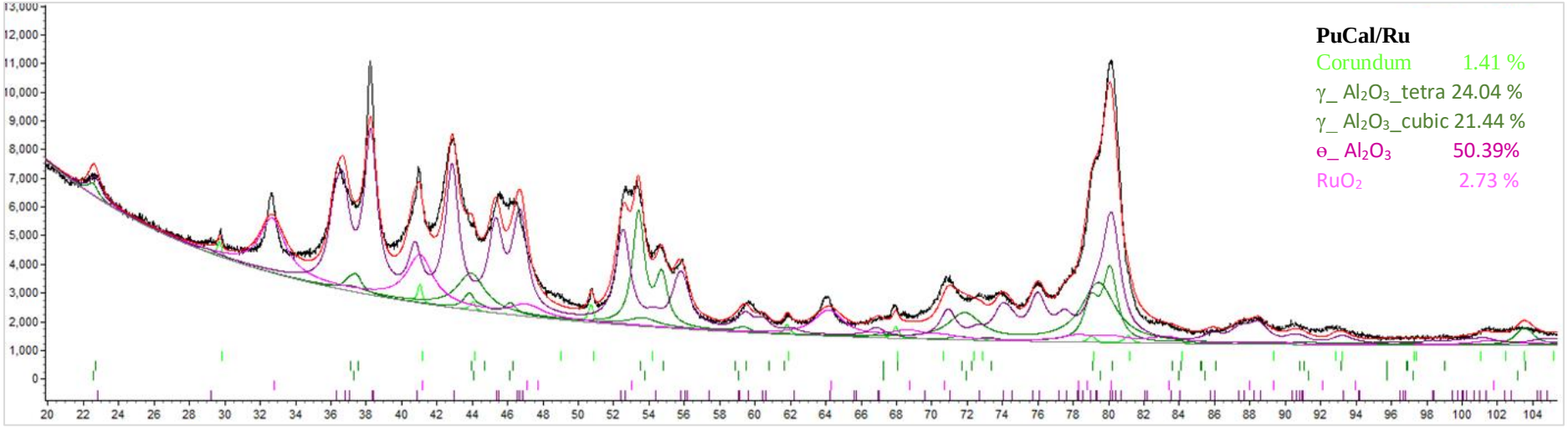



**Figure E. 6** Rietveld refinement for PuCal/Ru catalyst

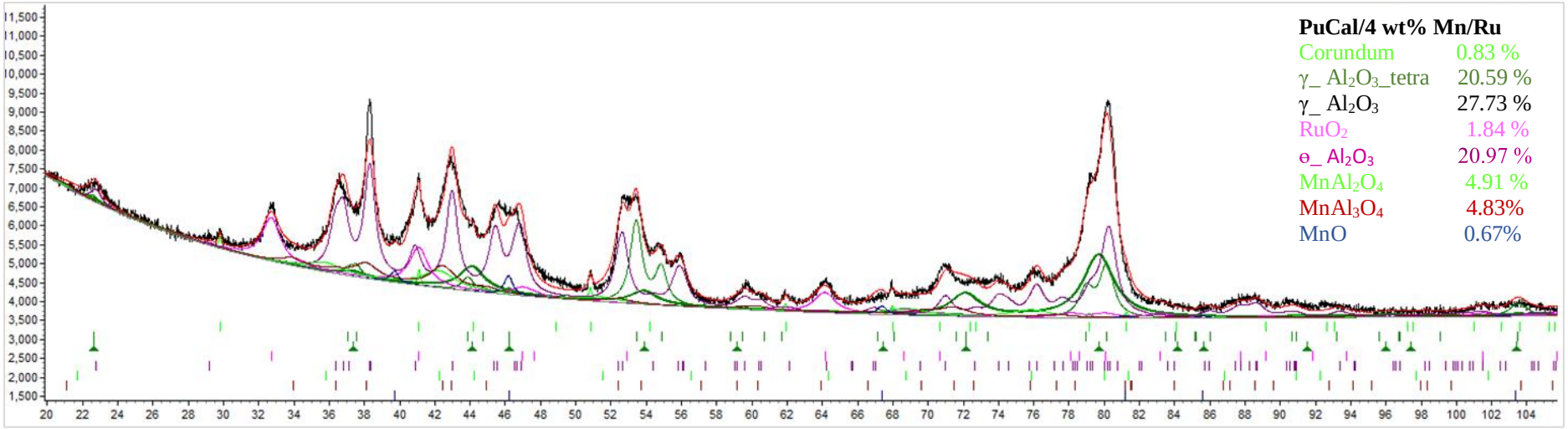



**Figure E. 7** Rietveld refinement for PuCal/4 wt% Mn/Ru catalyst

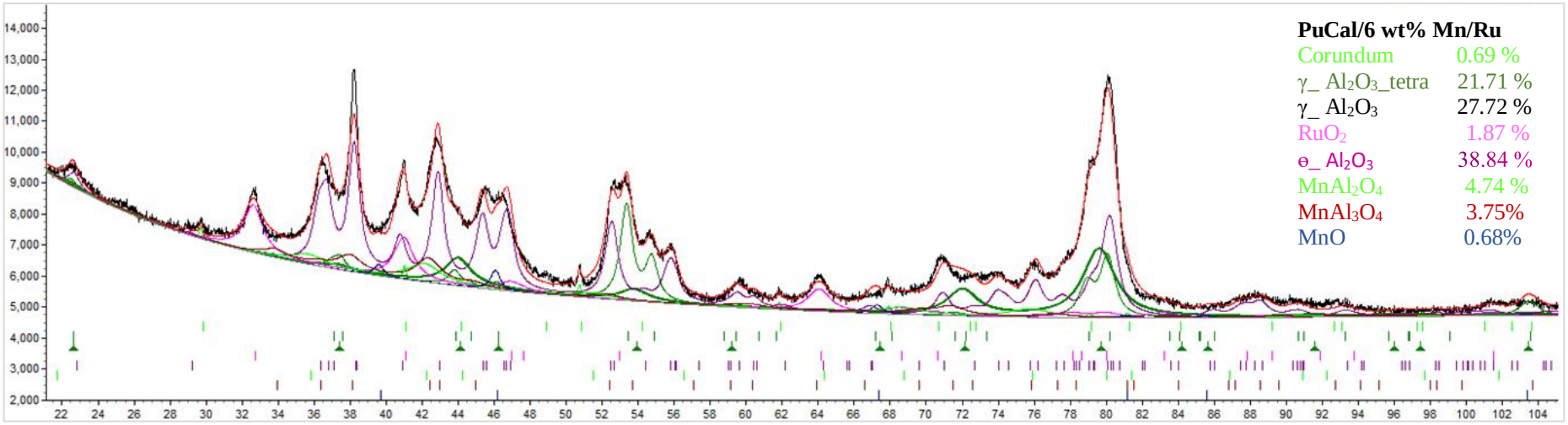



**Figure E. 8** Rietveld refinement for Pu/6 wt% Mn/Ru catalyst